The Polyspecific Organic Cation Transporters: Role in Cancer Drug Targeting, Xenobiotic Disposition, and Drug-drug Interactions

Letícia Salvador Vieira

A dissertation

submitted in partial fulfillment of the

requirements for the degree of

Doctor of Philosophy

University of Washington

2023

Reading Committee:

Joanne Wang, Chair

Kenneth E. Thummel

Libin Xu

Program Authorized to Offer Degree:

Pharmaceutics

Letícia Salvador Vieira

University of Washington

Abstract

The Polyspecific Organic Cation Transporters: Role in Cancer Drug Targeting, Xenobiotic Disposition, and Drug-drug Interactions

Letícia Salvador Vieira

Chair of the Supervisory Committee:

Joanne Wang

Department of Pharmaceutics

The polyspecific organic cation transporters (pOCTs) include the organic cation transporters (OCT1-3), the multidrug and toxin extrusion proteins (MATE1/2K) and the plasma membrane monoamine transporter (PMAT). These transporters have been implicated in the absorption, distribution and excretion of many drugs and xenobiotics, and are considered major determinants in the pharmacokinetics, pharmacodynamics, and toxicity of its substrates. Additionally, the OCT2 and MATE1/2K renal transporters are considered important sites for transporter-mediated drug-drug interactions (DDIs), capable of impacting systemic and intrarenal concentrations of xenobiotics. There are still many gaps in our knowledge of pOCTs, including their role in cancer-drug targeting, their contribution to the disposition and toxicity of environmental xenobiotics, and how to improve the in vitro to in vivo prediction of renal

transporter-mediated DDIs. The overall goal of this dissertation research is to fill in some of these gaps by: (1) investigating the expression of pOCTs in neuroblastoma and their potential role in tumor disposition of the theranostic agent meta-iodobenzylguanidine (mIBG), (2) characterizing the interactions and uptake kinetics of pOCTs with benzalkonium chlorides (BACs) and their role in tissue accumulation of these environmental compounds, and (3) exploring the use of a double-transfected system to improve prediction of OCT2/MATE1-mediated renal DDIs.

Neuroblastoma is a childhood cancer with poor survival rates in high-risk patients. 131-iodine labeled mIBG (^{131}I-mIBG) kills tumor cells by exposure to radiation and has emerged as a promising therapy for high-risk neuroblastoma. mIBG enters neuroblastoma cells via the norepinephrine transporter (NET), however expression of NET alone cannot predict clinical response to mIBG. Previously, our lab identified that mIBG is an excellent substrate of OCTs and MATEs, and thus the expression of pOCTs in neuroblastoma could impact tumor disposition and response to ^{131}I-mIBG. As part of this dissertation research, I investigated the expression of pOCTs and other monoamine transporters in neuroblastoma cell lines, in local tumor samples, and using neuroblastoma genomic data available at the NCI TARGET database. Our results revealed that PMAT is a previously unrecognized transporter highly expressed in neuroblastoma and that its expression level is positively associated with overall survival of high-risk patients without MYCN oncogene amplification. Additionally, we showed that PMAT efficiently transports mIBG, is mainly localized in mitochondria of neuroblastoma cells and mediates mitochondrial uptake of mIBG. Together, these results support a role of PMAT in intracellular disposition of mIBG in neuroblastoma, potentially impacting tumor exposure and response to ^{131}I-mIBG therapy.

The pOCTs have the potential to impact not only human exposure to drugs, but also our exposure to environmental xenobiotics. BACs are quaternary ammonium compounds used as

disinfectants and as preservatives in several consumer products. However, multiple studies report that BACs are cytotoxic and may be involved in biochemical interactions, and thus their safety has been questioned by the FDA. Humans are chronically exposed to BACs, and these compounds have been found to broadly distribute and accumulate in tissues with known expression of pOCTs such as the kidneys. To characterize the interaction of BAC of varying alkyl chain length (C8, C10, C12 and C14) with the human OCT1-3 and MATE1/2K, we conducted in vitro uptake and inhibition assays in HEK293 cells transfected with the transporters. We showed that all investigated BACs are inhibitors OCTs and MATEs, and that C8 and C10 are substrates of these transporters. We further demonstrated that BAC C8 and C10 are transported across a OCT2/MATE1 double-transfected MDCK monolayer, and that intracellular accumulation of these compounds is much higher in OCT2/MATE1-expressing cells in comparison to vector-transfected cells, suggesting a role of these transporters in the intrarenal accumulation of short chain BACs. We propose that OCTs and MATEs mediate tissue distribution and accumulation of short chain BACs and thus may represent important determinants of organ susceptibility to BAC toxicity in humans as a result of chronic environmental exposure.

The research presented in this dissertation highlights that many xenobiotics can interact with pOCTs as substrates and/or inhibitors, raising the concern for transporter-mediated DDIs. Accurately predicting clinical DDI potential based on in vitro data is challenging and this is especially evident for MATE inhibitors, for which the use of plasma unbound maximal inhibitor concentration ($I_{max,u}$) and IC_{50} values determined in single transporter-transfected cells often lead to false or overprediction of DDI potential. With the goal of improving DDI risk assessment, I explored the use of OCT2/MATE1 double-transfected MDCK cells in a Transwell system as a new in vitro tool to assess the inhibitory potential of compounds. Our results revealed that some

potent in vitro inhibitors of MATE1 (hydroxychloroquine, brigatinib and famotidine) failed to inhibit the transepithelial flux of metformin in the double-transfected system. In contrast, the classical OCT2/MATE1 inhibitors pyrimethamine and cimetidine dose-dependently inhibited metformin transepithelial flux. We hypothesize that the different behaviors of these MATE1 inhibitors in the double-transfected system vs single-transfected model could be explained by their different abilities to gain intracellular access and reach MATE1 site of inhibition. Additionally, we propose a new parameter reflecting inhibitory potential on overall OCT2/MATE1-mediated secretion ($IC_{50,flux}$), and concluded that the $IC_{50,flux}$ performs better than individual transporter IC_{50} values when predicting in vivo DDIs using a static model. Together, our findings suggest that the use of OCT2/MATE1 double-transfected cells in DDI risk assessment is promising and has the potential to reduce the burden of unnecessary clinical DDI investigations by identifying in vitro MATE1 inhibitors unlikely to result in DDIs in vivo.

In summary, this dissertation research has contributed significantly to our knowledge of the clinical significance of pOCTs, exploring their role in mIBG disposition in neuroblastoma, their contribution to the tissue-disposition and toxicity of BACs, and providing new tools to improve in vitro to in vivo prediction of OCT2/MATE1-mediated renal DDIs.

TABALE OF CONTENTS

LIST OF FIGURES

LIST OF TABLES

DEDICATION

To my parents, Mariângela and João,

who have repeatedly shown me that their love and encouragement recognize no barriers –

Eu amo vocês

To my grandparents, Vô Antônio, Vó Thereza, and Vó Izaura,

who gave me some of my happiest childhood memories and whose love continues to embrace me from both earthly and heavenly realms

To my husband, Anthony,

who is a constant source of joy in my life and who supported me unconditionally through this journey

ACKNOWLEDGEMENTS

My PhD journey was one that pushed me academically and emotionally, highlighting different facets of my personality and propelling me to grow immensely throughout this process. I would not have been able to get to this moment without the support of so many kind and incredible people that were by my side along the way.

First, I want to express my gratitude to my advisor, Dr. Joanne Wang, for her guidance, mentorship, and ultimately her friendship throughout these years. I learned from her not only about science and work ethics, but also about patience and the importance of communication. Joanne cheered me on during the peaks of my accomplishments and encouraged me during the challenging valleys of graduate school. Thank you, Joanne – I am forever grateful for your teachings and for how you shaped me into a more capable and confident scientist.

I would also like to thank my committee members, Dr. Ken Thummel, Dr. Libin Xu, Dr. Jash Unadkat, Dr. Rodney Ho, and Dr. Rheem Totah. All through our committee meetings, you helped me dive in and think critically about my work, while also making sure I didn't lose sight of the big picture. A special thank you to my reading committee members, Ken and Libin, for all their time and effort carefully reading this work. Ken – I appreciate our conversations and will always cherish the memory of when you opened the door of your office to me so I could have a private space to talk to my parents over Zoom, I owe you a birdwatching tour in Brazil. Libin – Thank you for giving me the opportunity to collaborate with you in the work that became the Chapter 3 of this dissertation, I learned so much from you and I deeply appreciate your support and encouragement.

To the members of the Wang Lab: You are the best and I'm so grateful for experiencing such a supportive lab environment. In particular, I want to thank Yuchen, Antonio, Austin and Tim – thank you for welcoming me with open arms, for teaching me so much, and for being great academic siblings. The memories of our lab dinners, game nights and trips together hold a special place in my heart. I also want to thank the previous members of the Wang lab, as well as all the collaborators I had the privilege to work with over the past five years – the work presented here owes much to your dedication and contributions.

Thank you to the friends I made along the way, inside and outside of the Department of Pharmaceutics. Moving to a different county was not easy, and you made sure to embrace me and make me feel like I belong. To my friends back in Brazil and throughout the world – thank you for always checking in on me and for making the vast physical distance between us seem like nothing more than a small detail in the tapestry of our friendship.

Thank you to my amazing and loving husband, Anthony. Our story evolved in parallel with graduate school and words feel insufficient to express how grateful I am for you. At many moments I doubted myself and let my overthinking nature take the best of me. You believed in me even (and especially) when I did not. You are the most encouraging partner I could have ever asked for, and you constantly inspire me to be more resilient. The love and joy you bring into my life were the fuel for this accomplishment.

One of the most important and significant acknowledgements I want to give is to my parents, Mariângela and João, and to my brother, Guilherme:

Gui – I am proud to be your sister and it is no secret that I look up to you. Thank you for not only being my big brother but also my best friend, for always playing devil's advocate and for helping me see things from another (much brighter) perspective.

Mom and dad – I feel immensely grateful for the unwavering love, the nurturing environment and for the countless opportunities you provided me throughout my life. From the moment I first mentioned my interest in pursuing a PhD internationally, you supported and encouraged me despite knowing the inevitable challenges posed by the distance between us. You are my pillars. Your sacrifices for both me and Gui have not gone unnoticed, and my heart is flooded with gratitude. I love you, you inspire me, and I could never have reached this point without you.

Mamãe e papai – Eu sou tão grata pelo amor inabalável, pelo carinho, e pelas inúmeras oportunidades que vocês me proporcionaram ao longo da minha vida. Desde a primeira vez que eu mencionei meu interesse em fazer um doutorado fora do país, vocês me apoiaram e me encorajaram mesmo sabendo o quão desafiador seria viver tão longe uns dos outros. Vocês são meu alicerce. Seus sacrificios por mim e pelo Gui não passaram despercebidos, e meu coração está repleto de graditão. Eu amo vocês, vocês me inspiram, e eu nunca conseguiria chegar tão longe sem vocês.

Writing this acknowledgement has been an amazing exercise in looking back and recognizing what really matters the most. Thank you to all of those who contributed to my journey until here.

Chapter 1. INTRODUCTION

Part of this chapter was published in:
Vieira L.S., Wang J. Brain Plasma Membrane Monoamine Transporter in Health and Disease. Handb Exp Pharmacol. 2021;266:253-280. doi: 10.1007/164_2021_446. PMID: 33751232.

1.1 The Importance of Transporters in Drug Development and Toxicology

Most drugs intend to act on targets within specific tissues, and while some targets are on the external surface of tissues, other targets reside intracellularly. Concentration in the target tissue is what drives pharmacological effect, and concentration in off-target sites may lead to toxic effects. Ability to cross membranes is fundamental in how drugs and xenobiotics may distribute and accumulate in different tissues, and while lipophilic compounds rely on passive permeability to cross membranes, the uptake of hydrophilic compounds into tissues may often involve facilitated mechanisms mediated by membrane transporters.

The expression and localization of these transporters throughout the human body can greatly impact not only the pharmacokinetics of its substrates but also its distribution to target tissues (thus impacting pharmacodynamics) and overall tissue accumulation, which may result in off-target effects and toxicity (International Transporter Consortium *et al.*, 2010; Giacomini and Huang, 2013; Wagner *et al.*, 2016). As tissue concentrations are challenging to measure in the clinic, plasma concentrations are commonly used as a surrogate for tissue concentrations, and while that may be acceptable for compounds with high passive diffusion, the action of membrane transporters can generate intracellular drug concentrations much higher (by the action of uptake transporters) or lower (by the action of efflux transporters) than plasma concentrations, and thus transporters can have a major impact on local concentrations of its substrates (Zhang *et al.*, 2019).

The clinical significance of drug transporters as a source of interindividual variability in drug response and toxicity, as well as their involvement in drug-drug interactions (DDIs) is increasingly acknowledged (International Transporter Consortium *et al.*, 2010; Yin and Wang, 2016; Koepsell, 2021; Kamath *et al.*, 2022). Thus, several regulatory agencies, including the U.S. Food and Drug Administration (FDA), the European Medicines Agency (EMA), and the Pharmaceuticals and Medical Devices Agency (PMDA) have included assessment of new molecular entities (NMEs) as substrates and inhibitors of transporters during the drug-development process (EMA Guidance, 2012; PMDA Guidance, 2018; FDA Guidance, 2020).

This thesis focuses on a special group of solute carrier (SLC) transporters – the polyspecific organic cation transporters (pOCTs), which include the organic cation transporters (OCT1-3), the multidrug and toxin extrusion proteins (MATE1/2K) and the plasma membrane monoamine transporter (PMAT). These transporters are expressed in a variety of human tissues and mediate the cell uptake and efflux of a wide range of compounds, impacting tissue distribution and systemic elimination of many drugs, toxins, and endogenous compounds (**Figure 1.1**). The human tissue expression and function of each pOCT transporter are discussed in more detail below.

1.2 THE POLYSPECIFIC ORGANIC CATION TRANSPORTERS (POCTS)

1.2.1 *Organic Cation Transporters (OCTs)*

The human organic cation transporters (OCTs) consist of three closely related members encoded by the *SLC22* gene family: OCT1 (*SLC22A1*), OCT2 (*SLC22A2*) and OCT3 (*SLC22A3*), sharing between 50-70% of protein identity (Sala-Rabanal *et al.*, 2013; Koepsell, 2020). OCTs can transport a wide range of structurally diverse compounds (Koepsell, 2020), and function as electrogenic transporters utilizing the physiological inside-negative membrane potential as a driving force to mediate cellular uptake of its substrates (Koepsell, 2004; Wagner *et al.*, 2016).

While many functional similarities are observed between OCT1, OCT2, and OCT3 isoforms, their tissue distribution varies greatly.

In humans, OCT1 is the major OCT isoform expressed in the liver. Localized to the basolateral membrane of hepatocytes, OCT1 mediates the uptake of substrates from the plasma and can greatly influence liver intracellular concentrations and pharmacodynamics of drugs such as the antidiabetic drug metformin (Shu *et al.*, 2007). Additionally, uptake by OCT1 can be the rate-limiting step before hepatic metabolism mediated by hepatic enzymes, and thus OCT1 deficiency can significantly impact the systemic exposure of drugs such as the $beta_2$ agonist fenoterol (Zamek-Gliszczynski *et al.*, 2018).

OCT2 is the major isoform expressed in the human kidney, and together with the multidrug and toxin extrusion proteins (MATEs), constitute the renal organic cation secretion system (Morrissey *et al.*, 2013; Yin and Wang, 2016). Expressed in the basolateral membrane of renal proximal tubule epithelial cells (PTECs), OCT2 mediates the first step of renal tubular secretion of organic cations – i.e., the uptake of substrates from the plasma into the intracellular space – and is implicated in the renal elimination of several drugs including metformin, atenolol, lamivudine and oxaliplatin (Nies *et al.*, 2011; Yin *et al.*, 2015; Yin and Wang, 2016).

Compared to OCT1 and OCT2, OCT3 has a broader tissue distribution in the human body, with high expression levels reported in many organs such as the brain, heart, salivary glands, placenta, skeletal muscle, lungs, and small intestine (Wagner *et al.*, 2016; Koepsell, 2020). Due to its ubiquitous expression, OCT3 has been implicated in the distribution of drugs to various tissues, including the placenta and salivary glands where it mediates the secretion of metformin to the fetus and saliva, respectively (Lee *et al.*, 2014, 2018), and the cardiac uptake of doxorubicin (Huang *et al.*, 2021).

In addition to healthy tissue expression, tumor expression of OCTs can influence tumor-targeting of anti-cancer drugs, and thus the degree of OCT expression in tumors has also been reported as an important determinant in chemotherapy response (Li and Shu, 2014; Tatsumi *et al.*, 2014; Gu *et al.*, 2019). For instance, expression of OCTs in colorectal tumors has been implicated in tumor response to oxaliplatin, a first line chemotherapy treatment (Yokoo *et al.*, 2008; Tatsumi *et al.*, 2014; Gu *et al.*, 2019). The ability of OCTs to drive tumor uptake and retention of chemotherapeutics suggest that further investigation of pOCTs expression in tumors could aid in treatment selection and in the prediction of anti-cancer drug response.

1.2.2 *Multidrug and Toxin Extrusion Proteins (MATEs)*

The human multidrug and toxin extrusion proteins (MATEs) are encoded by the *SLC47* gene family and include two functional members: MATE1 (*SLC47A1*) and MATE2K (*SLC47A2*) (Yin and Wang, 2016; Koepsell, 2020). In contrast to OCTs, MATEs function as organic cation/proton exchangers, using the transmembrane proton gradient as the driving force and with proton binding happening on the opposite side from substrate binding (Otsuka *et al.*, 2005; Masuda *et al.*, 2006; Yin and Wang, 2016).

Characterized as an efflux transporter of organic cations, MATE1 is mainly expressed in human kidney, liver, and skeletal muscle and localized to the apical membrane of PTECs and hepatocytes, while MATE2K is a kidney-specific isoform restricted to the apical membrane of PTECs (Otsuka *et al.*, 2005; Masuda *et al.*, 2006). Additionally, MATE1 has also been reported to be highly expressed in tumor tissues such as lung adenocarcinoma, in which its expression was correlated with chemosensitivity to a potent platinum–acridine hybrid anticancer agent (Yao *et al.*, 2020).

In the kidneys, the slightly acidic physiological pH of urine (pH 6.0-6.8) provides the ideal driving force for MATE-mediated organic cation efflux, and in conjunction with OCT2-mediated organic cation uptake in PTECs, the OCT2/MATE1-2K pathway is a major secretion system in the clearance of organic cations (International Transporter Consortium *et al.*, 2010; Yin and Wang, 2016). As MATEs mediate the final step of organic cation renal secretion (i.e., the efflux of substrates from the intracellular space into the proximal tubule lumen), DDIs involving these transporters can significantly impact the intracellular accumulation of compounds, raising concerns over nephrotoxicity. This issue is discussed in further detail in section 1.5.2.

1.2.3 *Plasma Membrane Monoamine Transporter (PMAT)*

The plasma membrane monoamine transporter (PMAT) is encoded by the *SLC29* gene family (Wang, 2016). This SLC family primarily encodes the equilibrative nucleoside transporters (ENTs), and thus this transporter was initially named ENT4 (*SLC29A4*). Despite the transporter's sequence similarity to the ENTs, extensive screening work did not detect significant transport activities for nucleosides, nucleobases, and related analogs (Engel *et al.*, 2004). Instead, our laboratory has identified that this transporter mediates the uptake of a variety of endogenous monoamines (e.g., dopamine, norepinephrine, epinephrine, 5-hydroxytryptamine 5-HT) and thus this transporter was renamed to PMAT to reflect its true substrate profile (Engel *et al.*, 2004).

Besides monoamines, PMAT also transports a variety of structurally diverse organic cations and shares a remarkable functional resemblance to the OCTs, and thus it is considered a new member of the pOCTs (Engel and Wang, 2005). Like the OCTs, PMAT functions as an electrogenic transporter and utilizes the physiological membrane potential as the driving force to mediate the uptake of its substrates (Itagaki *et al.*, 2012). Additionally, an acidic pH can further

stimulate PMAT-mediated transport activity (Zhou *et al.*, 2010; Itagaki *et al.*, 2012). Although the precise mechanism underlying this observation remains unclear, this effect is hypothesized to occur via either direct coupling of protons with organic cations or through a pH-induced change to PMAT's protein ionization and folding state impacting its intrinsic transport activity (Wang, 2016; Vieira and Wang, 2021).

The main site of expression of PMAT is in the brain, where it represents a major low-affinity and high-capacity transporter for monoamine neurotransmitters (Vieira and Wang, 2021). PMAT is expressed in multiple brain regions (Engel *et al.*, 2004; Duan and Wang, 2010, 2013), with immunoblotting and immunostaining studies further confirming protein expression in human cerebellum and choroid plexus tissue samples (Dahlin *et al.*, 2007; Duan and Wang, 2013). In addition to the brain, PMAT is also expressed in other human tissues such as intestine, kidney, and heart (Barnes *et al.*, 2006; Zhou *et al.*, 2007; Xia *et al.*, 2009), as well as in certain tumors, including breast cancer, desmoplastic small round cell tumor, and neuroblastoma (Li *et al.*, 2008; Orentas *et al.*, 2012; Makhtar, 2017). The broad substrate profile and tissue expression of PMAT suggest that besides endogenous monoamine transport, this transporter may also play an important role in the disposition of a variety of xenobiotics. However, PMAT's role in the disposition of drugs across epithelial barrier tissues and in cancer cells has remained understudied, and further studies are necessary to characterize the clinical significance of PMAT in drug disposition.

1.2.4 *Knowledge Gaps in the Field of pOCTs Research*

Since the discovery of the pOCTs, great advances have been made in understanding their molecular features, mechanisms of transport, and tissue distribution and in the characterization of substrates and inhibitors. While the general role of pOCTs in drug disposition and response is

well appreciated, the pharmacological and clinical significance of these transporters has only been studied with a handful of clinically used drugs, especially with the anti-diabetic drug metformin (Shu *et al.*, 2007; Lee *et al.*, 2014, 2018; Yin and Wang, 2016; Liang and Kathleen M. Giacomini, 2017). However, the impact of these transporters on the tissue-specific disposition, pharmacokinetics, pharmacodynamics and toxicology remains largely unknown for the vast majority of xenobiotic substrates. In particular, very little is known regarding the role of pOCTs in tumor disposition of cationic drugs and theranostic agents used in cancer management. Further, besides therapeutic agents, humans are chronically exposed to a variety of environmental xenobiotics which may also interact with these transporters. Research conducted in this thesis aims to address some of these gaps by elucidating the role of pOCTs in the tumor disposition of a cancer theranostic agent (i.e. *meta*-iodobenzylguanidine – mIBG) (Chapter 2) and in the tissue disposition of xenobiotic cations of environmental origin (i.e. benzalkonium chlorides – BACs) (Chapter 3).

Another major gap is the accurate prediction of transporter-mediated renal DDIs in clinical practice based on in vitro data. The research presented in this thesis revealed that many drugs and environmental compounds are likely to be substrates or inhibitors of pOCTs, raising the concern of renal DDIs involving the OCT2/MATE1-2K pathway. In vitro data is routinely used during drug development to inform and predict DDI risk in the clinic (FDA Guidance, 2020). However, there are significant challenges in translating in vitro data to in vivo inhibition, especially for MATE inhibitors, leading to a high number of false positive predictions and to unnecessary clinical evaluations (Mathialagan *et al.*, 2021; Krishnan *et al.*, 2022). New tools to improve DDI risk assessment are greatly needed, and thus Chapter 4 proposes innovative and promising method to improve the prediction of OCT2/MATE1-mediated renal DDIs.

The background rationales for each of the following chapters are described below.

1.3 Role of Transporters in the Disposition of the Theranostic Agent meta-Iodobenzulguanidine (mIBG)

1.3.1 *Clinical Uses of mIBG*

Radiolabeled *meta*-iodobenzylguanidine (mIBG) is a metabolically stable structural analog of norepinephrine currently used as a theranostic agent – that is, a compound with both therapeutic and diagnostic capabilities. This radiopharmaceutical was first developed in the late 1970s as a non-invasive imaging agent with the goal of detecting irregularities in the medulla of adrenal glands such as adrenal medullary hyperplasia and related tumors (Wieland *et al.*, 1980). mIBG can be labeled with either ^{131}I or ^{123}I isotopes, and in addition to its adrenergic imaging capabilities $^{123/131}$I-mIBG is also successful in cardiac imaging and as targeted radiotherapy for neuroendocrine tumors (Nakajima *et al.*, 2018; O'Brien and Pryma, 2022).

^{123}I-mIBG scintigraphy is routinely used in the clinic to diagnose and monitor neuroendocrine cancers such as pheochromocytoma, paraganglioma, and neuroblastoma (Van Berkel *et al.*, 2015; Parisi *et al.*, 2016; Desai *et al.*, 2019). While ^{123}I-mIBG (AdreView™) leads to better imaging resolution and is better suited for imaging with conventional gamma cameras, ^{131}I-mIBG (AZEDRA®) emits particulate radiation (β radiation) which can result in DNA damage and cell death, and thus ^{131}I-mIBG is favorable as a targeted radiotherapy alternative for neuroendocrine tumors. In 2018, the FDA approved the use of high-dose ^{131}I-mIBG in the treatment of advanced pheochromocytoma and paraganglioma, two forms of neuroendocrine cancers most prevalent in adults (Eisenhofer *et al.*, 2011; Ilanchezhian *et al.*, 2020). Its use in high-risk neuroblastoma – a neuroendocrine tumor most prevalent in children – is currently under

investigation in multiple clinical trials (Wilson *et al.*, 2014a; Parisi *et al.*, 2016; Suh *et al.*, 2020). However therapeutic response to ^{131}I-mIBG in neuroblastoma is highly variable and cannot be predicted by mIBG tumor avidity alone (Wilson *et al.*, 2014a). The mechanisms driving the uptake and retention of mIBG in these tumor tissues are further described in section 1.3.3.

1.3.2 *mIBG Disposition in Healthy Tissue and Clearance*

After being administered intravenously, $^{123/131}$I-mIBG whole-body scintigraphy shows that – in addition to its uptake in neuroendocrine tumors and in the heart – mIBG rapidly distributes to a variety of healthy tissues, including the salivary glands, liver, urinary bladder, intestines, and adrenal glands (Coleman *et al.*, 2009; Chin *et al.*, 2014). Following high-dose ^{131}I-mIBG therapy, the accumulation and distribution of mIBG to these healthy tissues are associated with several adverse reactions including sialadenitis (i.e. painful swelling of salivary glands), cardiac, liver and gastrointestinal toxicities (Modak *et al.*, 2008; Bleeker *et al.*, 2013; Parisi *et al.*, 2016). A majority of the mIBG administered dose (> 90%) is excreted unchanged in the urine with 50% of the dose excreted within 24 hours (Lashford *et al.*, 1988; Blake *et al.*, 1989; López Quiñones *et al.*, 2022), and mIBG renal clearance is ~2.5-fold higher than the glomerular filtration rate (GFR), indicating a significant component of renal tubular secretion (Blake *et al.*, 1989; López Quiñones *et al.*, 2020).

Previous work conducted in our laboratory has identified mIBG as an excellent substrate of OCT1-3 and MATE1/2K (López Quiñones *et al.*, 2020). This finding suggests that OCT1 and OCT3 transporters may play important roles in the extensive tissue distribution of mIBG in humans, and more specifically in its uptake in the liver, salivary glands, and heart (López Quiñones *et al.*, 2020, 2022). Additionally, the efficient transport of mIBG by OCT2 and MATE1/2K, as

well as its 20-fold higher transepithelial permeability (basolateral-to-apical) across OCT2/MATE1 double-transfected cells in comparison to control cells suggests that the renal organic cation secretion system is a major elimination pathway mediating tubular secretion of mIBG (López Quiñones *et al.*, 2020).

The identification of mIBG as a substrate of these transporters raises concerns regarding the potential for transporter-mediated drug-drug interactions (DDIs). For instance, inhibition of OCT2 could impact renal clearance and lead to significant increases in systemic exposure to radiolabeled mIBG. On the other hand, inhibition of MATE-mediated efflux may also increase intrarenal accumulation of mIBG, leading to an increased risk of nephrotoxicity (Yin and Wang, 2016; López Quiñones *et al.*, 2020, 2022). Thus, DDIs involving these renal transporters can have significant implications for patient safety, and coadministration of mIBG with potential OCT2/MATEs inhibitors should be avoided. Contrastingly, inhibition of OCT1 and OCT3-mediated uptake of mIBG in healthy tissue may be desirable, as uptake in normal tissue may compete with tumor uptake, interfere with tumor imaging, and lead to radiation-induced toxicities (Bayer *et al.*, 2016; López Quiñones *et al.*, 2022). However, a detailed understanding of the mechanisms driving mIBG uptake and retention in neuroendocrine tumors is also necessary when developing strategies aimed to reduce mIBG healthy tissue uptake without compromising its tumor exposure.

1.3.3 *mIBG Tumor Disposition*

As previously mentioned, high-dose ^{131}I-mIBG (AZEDRA®) is approved by the FDA for the treatment of pheochromocytoma and paraganglioma. It has also been used to treat relapsed and refractory neuroblastoma and is currently under investigation as frontline therapy in the treatment

of high-risk neuroblastoma (Wilson *et al.*, 2014a; Parisi *et al.*, 2016; Suh *et al.*, 2020). ^{131}I-mIBG kills tumor cells by exposure to radiation (β particles), and consequently tumor uptake and retention are important determinants of its clinical efficacy.

The norepinephrine transporter (NET) is highly expressed in the majority of neuroendocrine tumors and is known to mediate the initial uptake of mIBG and to correlate with mIBG tumor avidity (Eisenhofer, 2001; DuBois *et al.*, 2012, 2017; Streby *et al.*, 2015). Although the initial uptake by NET is a major determinant in mIBG avidity, retention of mIBG is also an important determinant in tumor exposure. In pheochromocytoma and paragangliomas (the two adult forms of neuroendocrine tumors), the vesicular monoamine transporters (VMATs) have been suggested to mediate mIBG transport into intracellular storage vesicles (Eisenhofer, 2001; Blanchet *et al.*, 2012), contributing to the intracellular retention of mIBG. Neuroblastoma, however, contains lower amounts of storage vesicles in comparison to pheochromocytomas and paragangliomas (Montaldo *et al.*, 1991; Streby *et al.*, 2015), and the use of the VMAT inhibitor reserpine had minimal impact on mIBG retention in neuroblastoma-derived cell lines (Smets *et al.*, 1990; Mairs *et al.*, 1991). Importantly, electron spectroscopy imaging revealed that majority of mIBG is concentrated in the mitochondria of neuroblastoma cells (Gaze *et al.*, 1991), and multiple studies reported that in neuroblastoma, mIBG is stored and retained intracellularly via mechanisms independent from its cellular uptake (Lashford *et al.*, 1991; Montaldo *et al.*, 1991; Iavarone *et al.*, 1993).

1.3.4 *Knowledge Gaps*

Although the vast majority of neuroblastoma tumors (>90%) are mIBG avid (Streby *et al.*, 2015; Parisi *et al.*, 2016), therapeutic response of neuroblastoma to ^{131}I-mIBG treatment remains

highly variable and cannot be predicted by NET expression alone (Wilson *et al.*, 2014a; Streby *et al.*, 2015; Parisi *et al.*, 2016), and the mechanisms involved in mIBG mitochondrial uptake and retention in neuroblastoma remain poorly understood. The identification of mIBG as a substrate of OCTs and MATEs (López Quiñones *et al.*, 2020) raises the question of whether transporters other than NET could be involved in tumor disposition of mIBG in neuroblastoma. PMAT is a pOCT and monoamine transporter that was identified as one of the top 25 candidate genes as immunotherapy targets in neuroblastoma (Orentas *et al.*, 2012). Additionally, the substrate profile of PMAT largely overlaps with those from OCTs, suggesting that PMAT could represent a pOCT transporter expressed in neuroblastoma with the potential to transport mIBG.

In Chapter 2 of this thesis, we evaluated the expression of pOCTs and monoamine transporters functionally related to NET in neuroblastoma tumor samples and cell lines, and explored the association between the expression of these transporters and the overall survival of high-risk neuroblastoma patients. Further, we investigated the subcellular localization of PMAT in neuroblastoma and its potential role in the intracellular disposition of mIBG.

1.4 Emerging Concerns on Benzalkonium Chlorides (BACs)

1.4.1 *Uses, Regulatory Status and Human Exposure*

Benzalkonium chlorides (BACs) are a class of quaternary ammonium compounds often commercialized as a mixture of homologous compounds with alkyl chain length ranging from 8 to 18 carbons (C8 to C18), with higher antimicrobial activity reported for BAC C12-C16 (Jono *et al.*, 1986; Pereira and Tagkopoulos, 2019; Pena *et al.*, 2023). Due to their broad-spectrum antimicrobial properties, BACs have widespread applications and are used as disinfectants or

preservatives in cleaning, pharmaceutical, and personal care products (Kim *et al.*, 2018; Pereira and Tagkopoulos, 2019).

The Environmental Protection Agency (EPA) and the FDA share the role of regulating the use of BACs in the United States. These agencies determine the maximum allowed concentrations in commercial products, and such regulations should be regularly updated based on current scientific data. The EPA reports the NOAEL (no observed adverse effect level) of BACs to be 44 mg/kg/day, with a maximum acceptable chronic oral dose of 0.44 mg/kg/day. These values, however, were determined based on observable effects only (e.g., changes to body weight), and not on detailed biochemical studies (EPA, 2006).

Although BACs have been generally recognized as safe by the FDA, the toxic effects of these compounds on a wide range of biological systems are being increasingly acknowledged. For instance, BACs are toxic to aquatic life (e.g.: LC_{50} to fish between 0.5 to 5 ppm) (Kümmerer *et al.*, 1997; Nałecz-Jawecki *et al.*, 2003a) and toxic to enteric and ganglion neuronal cells at micromolar concentrations (Herman and Bass, 1989a; Sarkar *et al.*, 2012a). Additionally, BACs have been characterized as potent inhibitors of the last step of cholesterol biosynthesis (Herron *et al.*, 2016), disrupting lipid homeostasis in neuronal cell lines and in mouse neonatal brain even at nanomolar concentrations (Hines *et al.*, 2017; Herron *et al.*, 2019). Toxicological studies with mice reported that exposure to a mixture of quaternary ammonium compounds containing BACs led to a reduction in mice fertility and to an increased incidence of neural tube defects in embryos (Melin *et al.*, 2014, 2016; Hrubec *et al.*, 2017). These findings highlight that even low levels of exposure to BACs may lead to significant biochemical interactions impacting development, reproduction, and lipid homeostasis. Thus, the FDA questioned the safety of these compounds and has since

called for additional safety data concerning their usage in healthcare and consumer products to evaluate their eligibility for classification as GRAS (US FDA, 2015, 2016).

The pervasive use of BACs in cleaning, pharmaceutical, and personal care products and in the food processing industry suggests that humans are exposed to BACs via several routes, including inhalation, dermal contact, and ingestion (Arnold *et al.*, 2023). In fact, BACs have not only been detected in human blood samples, but their concentration was also correlated with toxicological endpoints such as increases in inflammatory cytokines, decreased mitochondrial function, and disruption of sterol homeostasis (Hrubec *et al.*, 2021). Further, a study analyzing human serum samples collected before and during the COVID-19 pandemic detected BACs in more than 95% of samples with over a 2-fold increase in the median BAC concentration during the pandemic when compared to pre-pandemic levels (Zheng *et al.*, 2021), suggesting that the increased use of disinfecting chemicals was reflected in the levels of systemic exposure in humans.

1.4.2 *Metabolism, Tissue Distribution, and Toxicity of BACs*

Comprehension of the mechanisms driving the clearance and the tissue disposition of BACs is necessary to improve our understanding of the systemic exposure and toxicology of BACs. Information on the metabolism of BACs in mammals remains limited, but in vitro studies by Seguin et al. (2019) have revealed that BACs are extensively metabolized by human liver microsomes, with longer-chain BACs exhibiting enhanced metabolic stability. Additionally, a screening of recombinant human hepatic cytochrome P450 (CYP) isoforms showed that CYP2D6, CYP4F2, and CYPF12 are the major contributors to the hepatic metabolism of BACs (Seguin *et al.*, 2019), and thus known genetic polymorphisms reducing or leading to loss of function of these

enzymes may significantly impact systemic exposure to BACs, making certain individuals more susceptible to their harmful effects.

In addition to systemic exposure, understanding the tissue disposition of BACs can help predict which organs are more susceptible to BAC-induced toxic effects in humans. The majority of the current knowledge on BACs' tissue distribution comes from biodistribution studies in rodents. These studies show that following oral or intravenous administration, BACs can quickly distribute to several tissues, including the heart, liver, lungs, spleen, and kidneys (Xue *et al.*, 2002; Kera *et al.*, 2021). Importantly, the kidneys are consistently reported as a major organ of BAC distribution, reaching tissue concentrations much higher than plasma levels (Xue *et al.*, 2002, 2004; Kera *et al.*, 2021). Additionally, studies in pregnant mice revealed that BAC-C12 and -C14 can cross the blood-placental barrier and reach the neonatal brain, potentially impairing neurodevelopment (Herron *et al.*, 2019).

While most biodistribution studies dosed BACs as a mixture of homologues and quantified either total BACs or a single BAC homologue as a surrogate, a study by Kera et al. (2021) investigated how the alkyl chain length of BACs influenced their tissue distribution. Their results revealed that while lungs, liver, spleen and fat samples showed higher concentrations of longer-chain BACs (C16 > C14 > C12), the opposite trend was observed in the kidneys, with preferential accumulation of short-chain BACs. Interestingly, despite the high degree of kidney accumulation, BACs concentration in urine was found to be very low.

Although no studies to date have investigated levels of BACs in human tissue samples, pathological examinations following poisoning cases provide insight into the tissues most affected following acute exposure to BACs. In reports of accidental or deliberate consumption of products containing BACs, not only the digestive tract (which is in direct contact with BACs upon oral

intake), but also the lungs, heart, liver, and kidneys are often reported as affected tissues, thus suggesting that extensive tissue distribution of BACs is also observed in humans and likely plays a significant role in its toxicological effects (van Berkel and de Wolff, 1988; Hitosugi *et al.*, 1998; Tambuzzi *et al.*, 2022).

1.4.3 *Knowledge Gaps*

The high prevalence of BACs in our environment and their broad tissue distribution is concerning. The high degree of BAC accumulation in organs such as the kidney suggest not only the potential for nephrotoxicity under chronic exposure, but also poses the question of whether these compounds could affect renal drug clearance via xenobiotic-drug interactions. Despite a growing body of literature concerning the toxicology, systemic exposure, and tissue distribution of BACs, the mechanisms driving their tissue accumulation in vivo remain unclear; hence, uncovering these mechanisms could help us better understand the overall persistence and toxicity potential of BACs in humans.

As previously mentioned, BACs are quaternary ammonium compounds containing a positive charge. Interestingly, the tissue disposition of BACs largely overlaps with tissues with significant expression of pOCTs (i.e.: OCT1 in the liver, OCT2 and MATEs in the kidneys, and OCT3 in tissues such as the heart and placenta). Although these transporters are known to interact with a variety of organic cations, including quaternary ammonium compounds (Tanihara, Masuda, Sato, Katsura, Ogawa, and K ichi Inui, 2007; Sala-Rabanal *et al.*, 2013), their potential interaction with BACs has not been explored. Thus, in Chapter 3 of this thesis, we investigated BACs of various alkyl chain lengths (C8, C10, C12, and C14) as inhibitors and substrates of the hOCT1-3

and hMATE1/2K transporters and further evaluated the potential role of hOCT2 and hMATE1 in the renal accumulation of BACs using an in vitro model of renal transepithelial transport.

1.5 Significance of OCT2 and MATE1 in Renal Drug-Drug Interactions (DDIs)

1.5.1 *Renal DDIs Involving the OCT2/MATE-pathway*

Renal clearance is a major drug elimination pathway that results from glomerular filtration, tubular secretion, and tubular reabsorption. As stated earlier, a major drug secretion system in the human kidney is the organic cation secretion system, comprised of the OCT2 and MATE1/2K transporters (International Transporter Consortium *et al.*, 2010; Yin and Wang, 2016). These SLC transporters are expressed in PTECs and work sequentially to mediate tubular secretion of its substrates, playing a role in the renal secretion of many drugs including metformin, atenolol, cimetidine, oxaliplatin and mIBG (Yonezawa *et al.*, 2006; Morrissey *et al.*, 2013; Yin *et al.*, 2015; López Quiñones *et al.*, 2020).

Polypharmacy can lead to inhibition of OCT2 and MATEs, resulting in drug-drug interactions (DDIs) that can impact both systemic and local drug concentrations. For this reason, regulatory agencies, including the FDA, EMA, and PMDA recommend all NMEs to be evaluated as potential inhibitors of these transporters during drug development (EMA Guidance, 2012; PMDA Guidance, 2018; FDA Guidance, 2020). In both in vitro and in clinical studies, metformin is often used as a probe substrate of the OCT2 and MATE1/2K transporters, as it is exclusively renally eliminated and sensitive to OCT2/MATE inhibition in vivo due to the high contribution of tubular secretion to its total clearance (FDA Table of Substrates, Inhibitors, and Inducers, 2023).

Historically, several clinically significant renal DDIs have been reported and attributed to inhibition of the OCT2 and/or MATE1/2K transporters (Yin and Wang, 2016; Koepsell, 2021). Some examples include clinical DDI studies reporting a significant reduction of metformin renal clearance and an increase in its plasma exposure following co-administration with cimetidine, pyrimethamine, and dolutegravir, known inhibitors of the OCT2 and/or MATE1/2K transporters (Somogyi *et al.*, 1987; Kusuhara *et al.*, 2011; Song *et al.*, 2016). And while there have been such discoveries, it is impractical to clinically evaluate a large number of compounds in order to investigate their DDI potential. Thus, in vitro inhibition studies are routinely used during drug development as a high-throughput screening method to assess which compounds are more likely to result in clinically significant DDIs.

1.5.2 *Impact on Renal Drug Accumulation and Nephrotoxicity*

Functioning sequentially to mediate the tubular secretion of organic cations, OCT2 is expressed at the basolateral membrane (blood-facing) of PTECs and mediate the uptake of drugs from plasma into the intracellular space, while MATEs are expressed in the apical membrane (urine-facing) and mediate the efflux of drugs from the intracellular space into the proximal tubule lumen (Otsuka *et al.*, 2005; Morrissey *et al.*, 2013). In addition to their role in the clearance and systemic exposure of drugs, OCT2 and MATEs can also greatly influence local drug levels in human PTECs. The efficiency of basolateral uptake versus apical efflux is what determines the degree of accumulation of a substrate into renal cells, and thus inhibition of basolateral OCT2 or apical MATE has opposite outcomes in regard to the intrarenal level of substrate drugs (Motohashi and Inui, 2013; Yin and Wang, 2016; Yin *et al.*, 2016). DDIs in which OCT2 is the major site of interaction can reduce drug uptake and accumulation in renal cells, thus having a nephron-

protective effect. In contrast, inhibition of apical MATEs diminishes efflux and thus can increase drug intracellular accumulation, which may result in drug-induced nephrotoxicity and kidney injury (Morrissey *et al.*, 2013; Yin and Wang, 2016).

The importance of precisely locating the site of interaction (OCT2 versus MATEs) in renal DDIs in vivo is clearly exemplified when looking at cisplatin nephrotoxicity. Cisplatin is a chemotherapeutic drug used in the treatment of various types of cancer, and cisplatin-induced nephrotoxicity is a major dose-limiting factor (Pabla and Dong, 2008; Dasari and Tchounwou, 2014). In vitro studies revealed that cisplatin is a substrate of OCT2 and MATE1/2K (Yonezawa *et al.*, 2006), and thus the roles of these transporters in the renal accumulation and nephrotoxicity of this drug in vivo have been investigated (Filipski *et al.*, 2009; Nakamura *et al.*, 2010). These studies revealed that disruption of OCT2 has a nephron-protective effect, with Oct1/Oct2-deficient mice found to be protected from severe cisplatin-induced renal tubular necrosis and with reduced nephrotoxicity observed in cancer patients carrying a variant of human OCT2 with reduced function (Filipski *et al.*, 2009). Contrastingly, disruption of MATE1 activity was shown to aggravate cisplatin nephrotoxic effects, with Mate1-deficient mice exhibiting higher renal accumulation of cisplatin in comparison to wild-type mice (Nakamura *et al.*, 2010). Additionally, co-administration of cisplatin and the selective MATE1 inhibitors pyrimethamine or ondansetron increased the nephrotoxic effects of cisplatin in mice, further demonstrating that pharmacological MATE inhibitors have the potential to increase renal accumulation and nephrotoxicity of drugs (Nakamura *et al.*, 2010; Li *et al.*, 2013). Importantly, this impact of MATE inhibitors is not restricted to cisplatin and could also influence the intrarenal accumulation of many other OCT2/MATE substrates, such as the theranostic agent ^{131}I-mIBG, potentially leading to radiation-induced renal toxicity (López Quiñones *et al.*, 2022).

Inhibitors of the organic cation secretion system are often non-specific and can interact with both OCT2 and MATEs, and thus correctly identifying the major site of interaction in vivo is critical for accurately assessing the potential hazards and consequences of an interaction. When MATEs are inhibited, the systemic exposure of substrates may not be impacted, resulting in interactions that go unnoticed in classical DDI studies. However, such invisible DDIs may still greatly impact intrarenal accumulation of drugs and the potential for drug-induced nephrotoxicity. Hence, the accurate prediction of the inhibitory potential of NMEs towards MATEs in vivo is of major importance.

1.5.3 *Gaps and Challenges in the Prediction of MATE1-mediated Renal DDIs*

Currently, all NMEs should be investigated as potential inhibitors of OCT2 and MATE1/2K transporters during drug development according to regulatory guidelines (FDA Guidance, 2020). This investigation is initially conducted in vitro, where the half-maximal inhibitory concentration (IC_{50}) towards a specific transporter is determined using single-transfected cell lines. Following the in vitro investigation, the clinical risk of DDI is assessed by dividing the inhibitor's maximal unbound plasma concentration ($I_{max,u}$) by the IC_{50} value obtained for each transporter ($I_{max,u}/IC_{50}$), and if any of the calculated ratios is above the threshold set by the regulatory authority (i.e. ≥ 0.1 for OCT2 or MATE1 by FDA), the sponsor is recommended to conduct an in vivo DDI study (FDA Guidance, 2020). While this approach is widely adopted due to its simplicity, there are challenges in translating in vitro data to successfully predict in vivo DDIs, and these challenges are especially apparent for MATEs.

While many compounds exhibit potent MATE1 inhibition in vitro – with $I_{max,u}/IC_{50}$ greatly surpassing the 0.1 threshold – they often lack translation to in vivo DDIs (Hibma *et al.*, 2016;

Mathialagan *et al.*, 2021; Ogasawara *et al.*, 2021; Krishnan *et al.*, 2022), and the high rates of false- and over-prediction of MATE1-mediated DDIs often lead to unnecessary and costly clinical evaluations (Mathialagan *et al.*, 2021; Krishnan *et al.*, 2022). A possible reason contributing to the poor in vitro to in vivo extrapolation of MATE1-mediated DDIs could be the use of plasma $I_{max,u}$ to predict the degree of MATE1-inhibition in vivo. As previously mentioned, MATEs are located at the apical membrane of PTECs – not in direct contact with the plasma – and previous evidence from our lab suggests that MATE1 is inhibited through an intracellular binding site (Yin *et al.*, 2016). Hence, intracellular inhibitor concentrations may be more relevant in assessing DDI potential towards MATE1, and these concentrations may significantly differ from $I_{max,u.}$ Additionally, while OCT2 and MATEs function sequentially to mediate tubular secretion, the current assessment of DDI potential is based on the inhibition of individual transporters and does not consider their interplay or the overall inhibitor's impact on the net secretion process.

Accurate prediction of OCT2/MATE-mediated renal DDIs based on in vitro data remains a challenge. Refinement of in vitro systems is important given that it may increase their translational value, and hence various modifications to current in vitro inhibition assays have been proposed to better mimic what is observed in vivo, including the addition of a pre-incubation step with inhibitor, inclusion of plasma proteins, estimation of inhibitor intracellular concentrations and considerations on substrate-dependent inhibition (Yin *et al.*, 2016; Arakawa *et al.*, 2017; Kikuchi *et al.*, 2017, 2019). In Chapter 4 of this thesis, I address the issue of false- and over-prediction of MATE1-mediated DDIs and evaluate the use of a simple OCT2/MATE1 double-transfected cell system as an alternative approach to assess the inhibitory potency of compounds. This strategy is innovative and promising as it allows the assessment of an inhibitor's overall impact on OCT2/MATE1-mediated secretion, and it inherently accounts for the inhibitor's intracellular

accessibility and ability to inhibit MATE1 from the intracellular side. Additionally, this in vitro system allows the evaluation of the inhibitor's impact on intracellular accumulation of the substrate, which could serve as a valuable indicator of intrarenal drug accumulation and drug-induced nephrotoxicity.

1.6 HYPOTHESIS AND SPECIFIC AIMS

The overall goal of my dissertation research is to advance our understanding of the involvement of pOCTs in the tissue-specific disposition of drugs and environmental xenobiotics, as well as in renal drug-drug interactions. More specifically, I aim to elucidate the role of pOCTs in tumor distribution of mIBG and healthy-tissue disposition of BACs and to improve in vitro to in vivo prediction of OCT2/MATE1-mediated renal DDIs. Three hypotheses and specific aims are proposed:

Hypothesis 1: PMAT is a novel previously unrecognized transporter involved in the intracellular disposition of ^{131}I-mIBG in neuroblastoma.

Specific Aim 1: A) Explore the expression level of pOCTs and monoamine transporters in neuroblastoma cell lines and tumor samples. B) Investigate the relationship between transporter expression and overall survival of high-risk neuroblastoma patients. C) Determine subcellular localization of PMAT and whether it can mediate the uptake of mIBG in mitochondria of neuroblastoma-derived cell lines.

In this Aim, we first explore the expression of monoamine transporters and pOCTs using genomic data (mRNA-seq) from a cohort of high-risk neuroblastoma patients obtained from an open-access database (TARGET NCI Database). The expression of these transporters is also

evaluated in two neuroblastoma-derived cell lines (SH-SY5Y and SK-N-BE(2)) and in local tumor samples obtained from Seattle Children's Hospital using RT-qPCR. Second, I investigate the relationship between overall survival and transporter expression level through survival analysis using gene expression array data matched to the clinical outcomes of patients from the TARGET database. Finally, after determining the substrate status of mIBG with PMAT and using immunostaining to ascertain the subcellular localization of PMAT in neuroblastoma, I determined whether a PMAT inhibitor (Decynium-22) could impact the uptake of mIBG in mitochondria isolated from SH-SY5Y and SK-N-BE(2) cells. Together, this comprehensive study shines light on novel molecular markers to help inform neuroblastoma disease prognosis and provides evidence on how the expression of transporters other than NET (i.e. PMAT) may contribute to the variable response of high-risk neuroblastoma to ^{131}I-mIBG therapy.

Hypothesis 2: BACs can interact with the OCTs and MATEs, and these transporters may contribute to the tissue disposition, accumulation, and toxicity of these xenobiotics.

Specific Aim 2: A) Determine the in vitro inhibitory potential and substrate status of BACs towards OCTs and MATEs. B) Characterize BAC transport mediated by OCTs and MATEs. C) Elucidate the potential involvement of OCT2 and MATE1 in renal accumulation of BACs.

In this Aim, I systematically characterize the detailed interactions, including inhibitory potential, substrate status, and transport kinetics of BACs of varying alkyl chain length (C8, C10, C12, and C14) with human OCT1–3 and MATE1/2-K. I also use an in vitro cell culture model (OCT2/MATE1 double-transfected MDCK cells) to investigate the role of OCT2 and MATE1 in the renal accumulation of short-chain BACs. Together, my study improves our understanding of the mechanisms driving BAC disposition in humans, which directly informs the toxicology of

these compounds as their tissue accumulation may lead to biochemical interactions and deleterious effects.

Hypothesis 3: Intracellular accessibility of inhibitors is crucial for MATE inhibition in vivo, and the use of flux studies in OCT2/MATE1 double-transfected MDCK cells has the potential to improve the prediction of in vivo renal DDIs involving the renal OCT2/MATE1 pathway.

Specific Aim 3: A) Compare the inhibition potency of compounds in single- vs. double-transporter transfected cell lines. B) Investigate the usefulness of in vitro transwell studies using OCT2/MATE1 double-transfected cells in predicting in vivo DDIs involving the OCT2/MATE1 pathway.

In this Aim, I evaluate and compare the inhibitory potential of compounds towards OCT2 and MATE1 through classic uptake inhibition studies employing single-transporter transfected HEK293 cells, as well as a novel double-transporter transfected (OCT2/MATE1) MDCK cells. I propose the calculation of a new parameter ($IC_{50,flux}$) using the double-transfected cells, which reflects inhibitory potency on overall OCT2/MATE1-mediated tubular secretion and already accounts for inhibitor intracellular accessibility bypassing the need to measure intracellular inhibitor concentrations. Additionally, the performance of $IC_{50,flux}$ versus IC_{50} values for individual transporter in the prediction of in vivo renal DDIs was evaluated using a static model. This study highlights the importance of inhibitor intracellular accessibility for accurate prediction of hMATE1-mediated renal DDIs and provides an innovative in vitro approach to identify whether NMEs are likely or not to inhibit MATE1 in vivo. The strategy proposed in Aim 3 can improve in vivo prediction of OCT2/MATE1-mediated renal DDIs using in vitro data, and thus has the potential to reduce the burden of unnecessary and costly clinical DDI investigations.

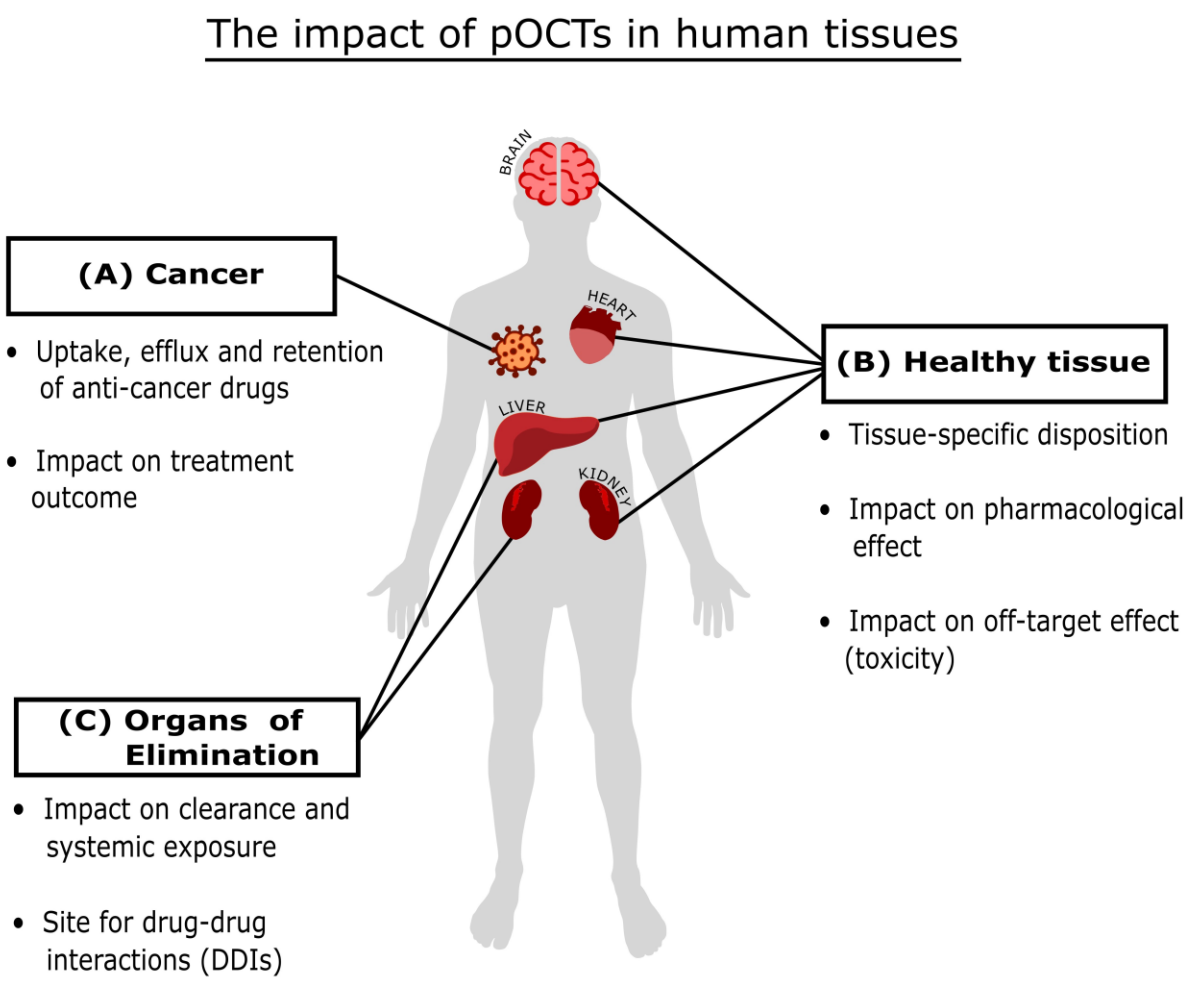

Figure 1.1. The impact of pOCTs in tissues in which these transporters are expressed.

The pOCT transporters are expressed in some types of cancers, in many healthy tissues, and in organs of elimination, and the expression of these transporters in each of these tissues have different implications on the pharmacokinetics, pharmacodynamics and toxicity of its substrates. (A) In cancer tissue, pOCTs may mediate the uptake or efflux of anti-cancer drugs, directly impacting the exposure and retention of such compounds in cancer tissues, and thus potentially influencing treatment outcomes. (B) In healthy tissues in which these transporters are highly expressed (e.g. brain, heart, liver, and kidneys), the pOCTs can facilitate entry of its substrates mediating tissue-specific disposition which may result in pharmacological effect (thus impacting

pharmacodynamics) or off-target effect (thus impacting toxicity). (C) In organs of elimination such as the liver and kidneys, the presence of these transporters can directly impact the pharmacokinetics of its substrates, and the pOCTs expressed in these tissues (i.e. OCT1, OCT2, and MATEs) are recognized as important sites for drug-drug interactions.

Chapter 2. THE PLASMA MEMBRANE MONOAMINE TRANSPORTER (PMAT) IS HIGHLY EXPRESSED IN NEUROBLASTOMA AND FUNCTIONS AS AN MIBG TRANSPORTER

Part of this chapter was published in:
Vieira L.S., Zhang Y., López Quiñones A.J., Hu T., Singh D.K., Stevens J., Prasad B., Park J.R. and Wang J. "The Plasma Membrane Monoamine Transporter (PMAT) is Highly Expressed in Neuroblastoma and Functions as an mIBG Transporter". *Journal of Pharmacology and Experimental Therapeutics* (2023) Dec;387(3):239-248. doi: 10.1124/jpet.123.001672. Epub 2023 Aug 4. PMID: 37541765
Data from this study was generated in part by Drs. Zhang, López Quiñones, Hu and Singh. The individual contribution of these authors is acknowledged in the methodology section.

2.1 ABSTRACT

Neuroblastoma (NB) is a pediatric cancer with low survival rates in high-risk patients. ^{131}I-mIBG has emerged as a promising therapy for high-risk NB and kills tumor cells by radiation. Consequently, ^{131}I-mIBG tumor uptake and retention are major determinants for its therapeutic efficacy. mIBG enters NB cells through the norepinephrine transporter (NET), and accumulates in mitochondria through unknown mechanisms. Here we evaluated the expression of monoamine and organic cation transporters in high-risk NB tumors and explored their relationship with MYCN amplification and patient survival. We found that NB mainly expresses NET, the plasma membrane monoamine transporter (PMAT), and the vesicular membrane monoamine transporter 1/2 (VMAT1/2), and that the expression of these transporters is significantly reduced in MYCN-amplified tumor samples. PMAT expression is the highest and correlates with overall survival in high-risk NB patients without MYCN amplification. Immunostaining showed that PMAT resides intracellularly in NB cells and co-localizes with mitochondria. Using cells expressing PMAT, mIBG was identified as a PMAT substrate. In mitochondria isolated from NB cell lines, mIBG

uptake was reduced by ~50% by a PMAT inhibitor. Together, our data suggest that PMAT is a previously unrecognized transporter highly expressed in NB and could impact intracellular transport and therapeutic response to ^{131}I-mIBG.

2.2 INTRODUCTION

Neuroblastoma (NB) is the most common extra-cranial solid tumor in children, and accounts for ~15% of all cancer-related pediatric deaths (Park *et al.*, 2010; Irwin and Park, 2015). NB is a neuroendocrine tumor derived from primordial neural crest cells of the sympathetic nervous system. The disease originates in adrenal glands and sympathetic ganglia but frequently metastasizes to other body areas (Park *et al.*, 2010; Parisi *et al.*, 2016). Amplification of the proto-oncogene MYCN is observed in ~25% of NB cases and strongly correlates with tumor aggressiveness and poor outcome (Huang and Weiss, 2013; Irwin and Park, 2015). Based on MYCN amplification status and other clinical factors, NB patients are stratified into low-, intermediate-, or high-risk groups to guide the choice of treatment regimens (Park *et al.*, 2013; Irwin and Park, 2015). Although the outcomes for low- and intermediate-risk NB are good, majority of NB patients at the time of diagnosis have high-risk disease with less than 50% survival rates (Borriello *et al.*, 2016; Smith and Foster, 2018; Tolbert and Matthay, 2018). Currently, new targeted therapies, including ^{131}I-mIBG radiotherapy and immunotherapy, are being developed to improve the outcome for high-risk NB (Irwin and Park, 2015; Parisi *et al.*, 2016). There is also an urgent need for novel biomarkers to help inform disease prognosis and facilitate treatment selection for high-risk patients.

Meta-iodobenzylguanidine (mIBG), a metabolic stable analog of norepinephrine, is used as a targeted radiopharmaceutical for imaging and treatment of NB. I-123 labeled mIBG (^{123}I-

mIBG or AdreView™) is used in whole-body imaging as the gold standard for diagnosis and therapeutic monitoring for NB and other neuroendocrine cancers (e.g. pheochromocytomas and paragangliomas) (Van Berkel *et al.*, 2015; Parisi *et al.*, 2016). I-131 labeled mIBG (^{131}I-mIBG or Azedra®) has been used to treat relapsed or refractory NB and is currently under numerous clinical trials as a frontline therapy for high-risk NB (Wilson *et al.*, 2014b; Parisi *et al.*, 2016; Suh *et al.*, 2020). mIBG is known to enter tumor cells via the norepinephrine transporter (NET – *SLC6A2*), expressed in ~90% NB tumors (Streby *et al.*, 2015; Parisi *et al.*, 2016). However, therapeutic response to ^{131}I-mIBG is highly variable and cannot be predicted by NET expression alone (Wilson *et al.*, 2014b; Streby *et al.*, 2015; Parisi *et al.*, 2016).

^{131}I-mIBG kills tumor cells by radiation, and hence tumor uptake and retention are major determinants for its therapeutic efficacy. After entering NB cells via NET, mIBG appears to be stored and retained intracellularly by mechanisms independent from its cellular uptake (Lashford *et al.*, 1991; Montaldo *et al.*, 1991; Iavarone *et al.*, 1993). Electron spectroscopic imaging in cultured NB cells further revealed that the majority of mIBG is retained within mitochondria, with lesser accumulation in storage vesicles (Gaze *et al.*, 1991). Numerous studies also reported that non-radiolabeled mIBG affected mitochondrial function by inhibiting the respiratory chain (Loesberg *et al.*, 1990; Cornelissen *et al.*, 1995). Although the vesicular monoamine transporter 1 and 2 (VMAT1/2 – *SLC18A1/2*) are likely to mediate the transport of mIBG into storage vesicles, the mechanisms underlying mIBG transport into mitochondria are currently unknown.

The plasma membrane monoamine transporter (PMAT – *SLC29A4*) is a monoamine and organic cation transporter first cloned and characterized in our laboratory (Engel *et al.*, 2004; Wang, 2016; Vieira and Wang, 2021). PMAT is a Na^+-independent, membrane potential-driven transporter highly expressed on the plasma membrane of neuronal cells and choroid plexus

epithelial cells in the human brain (Dahlin *et al.*, 2007; Itagaki *et al.*, 2012; Duan and Wang, 2013; Wang, 2016; Vieira and Wang, 2021). The substrate and inhibitor profiles of PMAT largely overlap with those of polyspecific organic cation transporters including the organic cation transporters (OCTs) and multidrug and toxin extrusion proteins (MATEs). We recently showed that mIBG is an excellent substrate for OCTs and MATEs and that these transporters could play a major role in mIBG disposition in normal tissues (López Quiñones *et al.*, 2020, 2022). In an exploratory study, Orentas et al. annotated gene expression in pediatric cancers and generated a list of potential immune targets based on their difference from normal tissue (Orentas *et al.*, 2012). PMAT was ranked among the top 25 candidate genes as immunotherapy targets for NB (Orentas *et al.*, 2012). Based on this evidence, we hypothesized that PMAT is expressed in NB cells and plays a role in tumor disposition of mIBG. The goals of this study are to determine the expression and cellular localization of PMAT in NB tumors, explore its relationship with disease prognosis, and evaluate its role in intracellular disposition of mIBG.

2.3 Materials and Methods

2.3.1 *Materials*

Meta-iodobenzylguanidine (mIBG), glyburide, decynium-22 (D22) and other chemicals were purchased from Sigma Aldrich (St. Louis, MO). Optima grade of acetonitrile (ACN) and formic acid were obtained from Thermo Fisher (Rockford, IL). Cell culture media and reagents were purchased from Invitrogen (Carlsbad, CA).

2.3.2 *TARGET Neuroblastoma Database*

The Therapeutically Applicable Research to Generate Effective Treatments (TARGET) neuroblastoma project (https://ocg.cancer.gov/programs/target/projects/neuroblastoma) is supported by the National Cancer Institute with the initial goal to molecularly characterize genetic changes driving the initiation and progression of neuroblastoma. The TARGET database contains gene expression data (mRNA-seq or gene array data) collected from tumor samples from patients enrolled in Children's Oncology Group biology studies and clinical trials targeting high-risk or relapsed NB. In this study, we utilized mRNA-seq data (154 NB samples) and gene expression array data with matched clinical outcome (249 NB samples). The mRNA-seq data was generated from NB tumor samples and transformed into Fragments Per Kilobase of transcripts per Million mapped reads (FPKM) according to the TARGET protocol (https://ocg.cancer.gov/programs/target/target-methods#3216). Relative expression of transporter genes was normalized to the expression of the housekeeping gene GAPDH in each sample. Matched clinical outcome information was not available for this dataset. Gene expression array data was obtained from 249 NB patient samples with matching clinical outcome information and was used in survival analysis. Data was generated using Gene Chip® Human Exon ST Array (Affymetrix) as described in the TARGET Project Experimental Methods (https://ocg.cancer.gov/programs/target/target-methods#421).

2.3.3 *Kaplan-Meier Survival Analysis*

Kaplan-Meier survival analysis was performed using the gene expression array data in the TARGET database containing 249 NB patients with matched clinical information including overall survival time and MYCN amplification status. The gene expression array data of selected

transporter genes was extracted using the RStudio program and matched to clinical information based on the alphanumeric patient identifier assigned to each sample. Demographic and clinical information of these patients is summarized in **Table 2.1**. The majority of patients in this cohort are Stage 4 high-risk NB patients. Six NB patients had MYCN status marked as "unknown" and were excluded from the survival analysis. The 243 patients used in the analysis consisted of 68 patients with MYCN amplification and 175 without MYCN amplification. The gene expression array data was divided into high-expression group (top 50%) and low-expression group (bottom 50%). After stratification based on MYCN amplification status, the proportional hazards assumption was confirmed by the Schoenlfeld residuals test using RStudio. Kaplan-Meier survival analysis was performed among patients with MYCN amplification or non-amplification using GraphPad Prism 7.

2.3.4 *Cell Lines and Cell Culture*

Flp-In human embryonic kidney (HEK) 293 cell lines (RRID:CVCL_0045) stably transfected with human PMAT, NET, or empty vector (pcDNA5/FRT) were previously generated in our laboratory (Duan and Wang, 2010, 2013; López Quiñones *et al.*, 2020). Cells were maintained in high-glucose Dulbecco's modified Eagle's medium (DMEM) supplemented with 10% fetal bovine serum, 2mM L-glutamine, 100 U/mL penicillin, 100 μg/mL streptomycin, and 150 μg/mL hygromycin B. Flasks and plates were coated with 0.1 mg/mL poly-D-lysine in Milli-Q water to promote HEK293 cell attachment. The NB cell lines SH-SY5Y (ATCC® Cat# CRL-2266, RRID:CVCL_0019) and SK-N-BE(2) (ATCC® Cat# CRL-2271, RRID:CVCL_0528) were purchased from ATCC (Manassas, VA) and cultured with 1:1 DMEM:F12 medium supplemented with 15% fetal bovine serum, 100 U/mL penicillin and 100 μg/mL streptomycin. These two cell

lines were chosen to respectively represent MYCN non-amplified and amplified NB cells. All cell lines were cultured in a humidified cell incubator at 37°C and with 5% CO_2.

2.3.5 *qPCR Analysis of Transporter Expression in NB Tumor Samples and Cell Lines*

Experiments in this section were conducted by Dr. Yuchen Zhang. Snap frozen tumor samples with clinically assigned MYCN status were obtained from Seattle Children's Hospital from 9 NB patients. Thirty mg of each frozen tumor sample were homogenized using a bead ruptor from Omni International (Kennesaw, GA), and NB cell lines (SH-SY5Y and SK-N-BE(2)) were cultured in T25 culture flask to 70-80% confluence. Total RNAs were extracted using RNeasy Purification Kit obtained from Qiagen (Holden, Germany), and reverse transcribed into cDNA by High-Capacity cDNA Reverse Transcription Kit from Applied Biosystems (Foster City, CA). Twenty ng of cDNA were used for TaqMan Real Time PCR according to the manufacturer's protocol. The primer and probe assay sets for selected genes were purchased from Applied Biosystems (Foster City, CA). Their assay IDs are: Hs00232074_m1 (MYCN), Hs00928283_m1 (PMAT), Hs00915193_m1 (VMAT1), Hs00996835_m1 (VMAT2), Hs00427552_m1 (OCT1), Hs00161893_m1 (OCT2), Hs01009571_m1 (OCT3), Hs00217320_m1 (MATE1), Hs00945652_m1 (MATE2), Hs00426573_m1 (NET), Hs00997374_m1 (SERT), Hs00984348_m1 (DAT) and Hs02786624_g1 (GAPDH).

2.3.6 *Immunolocalization and Fluorescence Imaging*

Experiments in this section were conducted by Dr. Yuchen Zhang and Dr. Tao Hu. Optimal Cutting Temperature compound embedded slides were prepared from NB patient tumor tissues from Seattle Children's Hospital. SH-SY5Y and SK-N-BE(2) cells were grown to 50%

confluency on 4-chamber glass slides from ThermoFisher (Waltham, MA). Slides were washed with PBS three times before incubation with ice-cold methanol at 4°C for 15 minutes. After washing three times with PBS, cells were blocked with 5% normal donkey serum from Sigma-Aldrich (St. Louis, MO) in PBS for 1 hour at room temperature. The block buffer was then replaced with primary antibodies in 1% normal donkey serum in PBS + 0.05% Tween 20 (PBS-T) at different ratios: Anti-PMAT: 1:80 (customized antibody previously developed and validated in our laboratory (Dahlin *et al.*, 2007; Duan and Wang, 2013)); Anti-Na^+/K^+ ATPase: 1:100 (Abcam® Cat# ab7671, RRID:AB_306023); Anti-COXIV: 1:200 (Abcam® Cat #ab33985, RRID:AB_879754); Anti-GPR94: 1:100 (Invitrogen® Cat# MA3-016, RRID:AB_2248666); Anti-VMAT1: 1:250 (Santa Cruz® Cat #sc-166391, RRID:AB_2187835). Slides were incubated in a humidified chamber at 4°C overnight before washing with PBS-T for 5 minutes three times. The secondary antibodies were diluted in 2.5% normal donkey serum in PBS-T at 1:1,000 ratio and incubated with cells at room temperature for 1 hour. After another three 5-minute washes, slides were mounted with DAPI mounting solution and stored at 4°C for at least 2 hours before imaging. Confocal imaging was conducted at the Keck Microscopy Center at the University of Washington using a Zeiss 710 Confocal microscope.

Fluorescent imaging was used to visualize the cellular uptake of IDT307 (a fluorescent substrate of PMAT) in SH-SY5Y cells. Cells were seeded onto Nunc Glass Bottom Dishes (Thermo Scientific, Rochester, NY) at a density of 1.0×10^5 cells/mL and allowed to grow overnight. After washing with uptake buffer (1X Hank's Balanced Salt Solution and 20 mM HEPES, pH 7.4), cells were incubated with IDT307 (1 μM) and Mitotracker Deep Red (Life Technologies, Eugene, OR) for 30 min. Fluorescent signals were imaged with a Zeiss LSM 510

META confocal microscope using 488 nm excitation and 520 nm emission wavelengths for IDT307 as described previously (Hu *et al.*, 2022).

2.3.7 *Whole Cell mIBG Uptake and Inhibition Assays*

Experiments in this section were conducted by Dr. Antonio Jesús Lopez Quiñones and Dr. Yuchen Zhang. Uptake and inhibition assays were conducted as previously described (Duan and Wang, 2010; López Quiñones *et al.*, 2020) in HEK293 cells stably transfected with pcDNA5/FRT (vector), human PMAT or NET, as well as in SH-SY5Y and SK-N-BE(2) cells. Briefly, cells were grown to 90% confluency and incubated in pre-warmed Krebs-Ringer-HEPES (KRH) buffer (125mM NaCl, 4.8mM KCl, $MgCl_2$ 1.2mM, $CaCl_2$ 1.2mM, glucose 5.6mM, HEPES 25mM, KH_2PO_4 1.2mM, pH = 7.4) containing mIBG. For studies in transfected HEK293 cell lines, transporter-specific uptake was calculated by subtracting the uptake in vector cells from uptake in transporter-expressing cells. PMAT-mediated mIBG uptake was determined at varying substrate concentrations, and kinetic parameters were determined in the initial linear phase of uptake. For inhibition assays, cells were incubated with KRH buffer containing mIBG at specified concentrations in the presence of varying concentrations of D22. At the end of the experiment, cells were permeabilized with acetonitrile and mIBG was quantified by LC-MS/MS as described below. Uptake was normalized to total protein in each well determined using BCA protein kit (ThermoFisher, Waltham, MA). For mIBG dose-dependent uptake studies, data was fitted to the Michaelis-Menten equation by non-linear regression (GraphPad Prism 7) to obtain the kinetics parameters. For dose-dependent inhibition by D22, uptake data was normalized to the control (absence of inhibitor) and the IC_{50} was obtained by fitting data to a four-parameter dose-dependent inhibition equation as described previously (López Quiñones *et al.*, 2020).

2.3.8 *Mitochondria Preparation and Uptake Experiments*

Mitochondrial fractions from SH-SY5Y and SK-N-BE(2) cells were prepared using a protocol adapted from Yu et al. (Yu *et al.*, 2003). SH-SY5Y and SK-N-BE(2) cells were grown to 50-60% and 70-80% confluency respectively, were harvested and rinsed with PBS at 4°C. Cell pellets were resuspended in 1 mL of ice-cold isotonic sucrose buffer (0.25 M sucrose, 10 mM HEPES, 1 mM EDTA, pH = 7.4) with freshly added protease inhibitor cocktail, and subject to 60 strokes in a Dounce homogenizer on ice. The homogenate was centrifuged at 1,000 x g for 10 minutes at 4oC to remove nuclei and unbroken cells. The supernatant was transferred to a new tube and centrifuged at 10,000 x g for 15 minutes at 4oC to obtain the mitochondrial fraction. Mitochondrial pellets were freshly isolated before each uptake experiment and kept in ice before conducting uptake experiments. The procedure of mitochondrial preparation was verified by pyruvate uptake in presence and absence of the mitochondria pyruvate carrier inhibitor α-cyano-4-hydroxycinnamate as previously described (Nancolas *et al.*, 2016). Mitochondrial uptake was carried out using a protocol adapted from Nancolas et al. (Nancolas *et al.*, 2016). Mitochondrial pellets were resuspended in 200 µL of assay buffer (KCl 125 mM, HEPES 20 mM, EDTA 1 mM, pH = 7.4) at 37ºC. Two aliquots were used for mitochondrial mIBG (2 µM) uptake in the absence or presence of D22 (100 µM) at 37 oC. After 5 min incubation, uptake was terminated by addition of D22 (final concentration 100 µM) to the reaction, followed by rapid sedimentation by centrifugation (15,000 x g for 1 minute at 4oC). Mitochondrial pellets were washed 3 times in ice-cold assay buffer and then lysed with 120 µL of 10% acetonitrile containing glyburide (internal standard). Ten microliters of lysate were used for protein quantification by BCA assay and 100 µL were ultracentrifuged and used for LC-MS/MS analysis.

2.3.9 *Quantification of mIBG by LC-MS/MS*

Nonradioactive mIBG was used in all transport studies and the compound was quantified using a LC-MS/MS method previously developed in our laboratory (López Quiñones *et al.*, 2020). Briefly, an AB-Sciex API 4000 QTrap mass spectrometer (Foster City, CA) coupled with Acquity UPLC system (Waters Corporation, Milford, MA) operated in the positive electrospray ionization mode was used to quantify mIBG. Cell and mitochondrial lysates were in 10% acetonitrile containing 50 nM glyburide as internal standard. The mass-to-charge (*m/z*) transitions used for quantification of mIBG and glyburide were 276.1 → 216.97 and 494.1 → 369, respectively. Instrument control and data processing was performed using AB-Sciex Analyst software 1.6.

2.3.10 *Proteomic Data Acquisition*

Experiments in this section were conducted by Dr. Dilip K. Singh. Cell lines were processed to isolate total membrane fraction using Mem-PER™ Plus membrane protein extraction kit (Thermo Scientific, Fair Lawn, NJ) for protein digestion using an optimized protocol (Xu *et al.*, 2018). The digested samples were analyzed for the PMAT surrogate peptide, FVLFYTTR, using an Easy Spray 1200 series nanoLC coupled Q-Exactive HF MS (Thermo Fisher Scientific, Waltham, MA) and a Thermo Scientific™ Acclaim™ PepMap™ 100 C18 HPLC column (75 μm x 250 mm). The mobile phase consisted of water with 0.1% formic acid (A) and 80% acetonitrile with 0.1% formic acid (B) and the following LC gradient (%B) was used to elute the peptides at a flow rate of 300 nL/min: 0-10% (0–2 min), 10–45% (2–27 min), 45–100% (27–28 min), and 100% (28–35 min). MS data were acquired using a parallel reaction monitoring (PRM) mode with an AGC target of 2e5 and collision energy of 27eV. The isolation of precursors was performed with a window of 1.6 m/z. Resolution for the HCD spectra was set to 30,000

at m/z 200 with maximum ion injection time of 80 ms. Xcalibur (Thermo Scientific, Version 4.3.73.11) was used for data acquisition. The data were analyzed using Skyline (University of Washington, Seattle, WA)

2.3.11 *Statistical Analysis*

Cell uptake and inhibition studies were performed in triplicate and repeated three times independently. Data are presented as mean ± S.D., unless specified otherwise. Statistical significance was determined using unpaired Student's t test with or without Bonferroni method for multiple comparison correction as specified in figure legends. For Kaplan-Meier survival analysis, statistical significance was assessed using Log-Rank test. A P-value < 0.05 was considered statistically significant. GraphPad Prism 7 (GraphPad Software Inc., San Diego, CA) was used for statistical analysis.

2.3.12 *Ethics Statements*

The TARGET neuroblastoma project is a publicly available database that provides open access to de-identified genomic and clinical data from neuroblastoma patients' tumor samples. All methods and experimental protocols were reviewed and approved by the Human Subjects Division at the University of Washington according to federal and state regulations. Snap frozen, de-identified tumor samples used were obtained from a tissue bank at the Seattle Children's Hospital. Sample collection and use was approved by the Institutional Review Board at the Seattle Children's Hospital with informed consents obtained from all participants and/or their legal guardian(s).

2.4 RESULTS

2.4.1 *PMAT mRNA is Highly Expressed in NB Patient Tumor Samples and Correlates with MYCN Amplification Status*

The mRNA expression of monoamine transporters (*SLC6A2* – NET, *SLC6A3* – DAT, *SLC6A4* – SERT, *SLC18A1/2* – VMAT1/2) and polyspecific organic cation transporters (*SLC29A4* – PMAT, *SLC22A1-3* – OCT1-3, *SLC47A1/2* – MATE1/2K) in NB was first explored using mRNA-seq data from 154 tumor samples mined from the TARGET database. Those tumor samples were obtained from patients enrolled in different studies targeting high-risk and/or relapsed NB. Among the genes analyzed, PMAT, NET, VMAT1 and VMAT2 were highly expressed in NB tumor samples, with PMAT expression level being the highest among all the transporters explored (**Figure 2.1 A**). In contrast, DAT, SERT, OCTs, and MATEs had minimal expression in NB tumor samples. Previously, two studies observed that MYCN amplified tumors had lower NET and VMAT protein expression compared to non-amplified tumors (DuBois *et al.*, 2012; Temple *et al.*, 2016). We thus analyzed if the mRNA expression of PMAT, NET, and VMAT1/2 was correlated with the clinically assigned MYCN status in the TARGET mRNA-seq database. Consistent with the clinical assignment, the MYCN mRNA level was much higher in the amplified cohort (**Figure 2.1 B**). A significant correlation between PMAT expression and MYCN status could be detected, with PMAT mRNA expression found to be significantly higher in MYCN non-amplified (N=121) than amplified samples (N=33) (**Figure 2.1 C**). Consistent with previous studies showing decreased NET and VMAT1/2 protein expression in MYCN amplified tumor, mRNA expression of those transporters is also significantly reduced in tumor samples with MYCN amplified (**Figure 2.1 D-F**).

We further investigated through RT-qPCR the expression of these transporters in local NB tumor samples from the Seattle Children's Hospital (**Figure 2.2 A**) and in two NB-derived cell lines with (SK-N-BE(2)) or without (SH-SY5Y) MYCN amplification (**Figure 2.2 B**). Our qPCR results showed that the overall mRNA expression pattern in NB local tumor samples and NB-derived cell lines was similar to that from the TARGET database. In both MYCN amplified and non-amplified samples, PMAT expression is the highest among the analyzed genes whereas expression of DAT, SERT, OCT1/2/3 and MATE1/2K is minimal. A preliminary proteomic measurement in SH-SY5Y and SK-N-BE(2) cells also detected PMAT expression at the protein level (**Figure 2.3**). Together, our data demonstrates that in addition to NET and VMAT1/2, NB tumors and cell lines highly express PMAT and that MYCN amplification decreases the expression of these transporters.

2.4.2 *Low PMAT and VMAT1/2 Expression Correlated with Poor Prognosis in NB Patients without MYCN Amplification*

Overall survival (OS) is one of the most important prognosis targets in clinical studies. The TARGET database provided gene expression array data with matched OS information for a cohort of 243 patients. Using this data, we explored the relationship between OS, MYCN amplification status, and transporter expression levels. The majority of this cohort of patients were at stage 4 NB (**Table 2.1**), and accordingly, low overall survival rates (35-42%) were observed regardless of MYCN status (**Figure 2.4 A**). In this high-risk population, MYCN amplification was found to slightly correlate with worse overall survival ($P = 0.018$). Gene expression of NET, PMAT, and VMAT1/2 was evenly divided into high- and low-expression groups, and survival analysis was performed for each gene. As shown in **Figure 2.4**, OS did not show significant

differences between the high- and the low-expression groups for NET and VMAT1. Interestingly, a significant association was observed for PMAT and VMAT2 (P=0.004 and P<0.001, respectively) with the high-expression group of these transporters correlating with better overall survival.

Given that MYCN amplification itself is a predictor for OS (**Figure 2.4 A**), we next investigated the relationship between transporter expression and patient survival after stratification by MYCN status (**Figure 2.5**). In patients with MYCN amplification (N=68), no association was observed for PMAT or VMAT1/2 whereas high expression of NET correlated with a worse outcome (P=0.006). Interestingly, in MYCN non-amplified patients (N=175), high expression of PMAT, VMAT1 and VMAT2 significantly correlated with better survival (P<0.001, P=0.004 and P=0.007, respectively). No association was observed for NET in this cohort. A similar result was also observed when the survival data was analyzed using the Cox regression model, which evaluates the effect of transporter expression as a continuous variable instead of the categorical "low" and "high" expression groups.

2.4.3 *PMAT Protein is Localized Intracellularly in NB-Derived Cell Lines and Tumor Samples*

PMAT protein is localized intracellularly in NB-derived cell lines and tumor samples. To investigate the cellular localization of PMAT, immunocytochemistry was conducted in SH-SY5Y and SK-N-BE(2) cells using an anti-PMAT antibody previously developed in our laboratory (Dahlin et al., 2007). Colocalization was performed using antibodies against cellular markers of the plasma membrane (Na+/K+ ATPase), mitochondria (COXIV), endoplasmic reticulum (GRP94), and storage vesicles (VMAT1) (**Figure 2.6**). Surprisingly, in both cell lines, PMAT immunostaining was predominately localized to intracellular compartments with little expression

on the plasma membrane (**Figure 2.6 A and E**). The PMAT immunofluorescence largely overlapped with the mitochondrial marker COXIV (**Figure 2.6 B and F**). Significant PMAT staining was also observed in endoplasmic reticulum and storage vesicles (**Figure 2.6 C, D, G and H**). Immunohistostaining was also conducted in NB tumor samples obtained from Seattle Children's Hospital. Although the cellular resolution was lower, staining of PMAT protein was observed in patient tumor samples. The immunofluorescence was primarily located intracellularly and appeared to partially co-localize with COXVI, VMAT1 and nuclei (**Figure 2.7**). To obtain additional evidence of PMAT in mitochondria in NB cells, we co-incubated SH-SY5Y cells with a mitochondria dye (MitoTracker) and IDT307, a fluorescent norepinephrine analog and substrate of PMAT (Duan *et al.*, 2015; Hu *et al.*, 2022). An extensive overlay of IDT307 fluorescence with MitoTracker was observed (**Figure 2.8**), suggesting that the fluorescent PMAT substrate accumulated in the mitochondria of the NB cells.

2.4.4 *mIBG is a Substrate of PMAT*

Although NET is considered the major transporter responsible for the uptake of mIBG into NB cells, the mechanisms involved in mIBG intracellular retention are currently unclear. The high levels of PMAT expression in NB and its unique intracellular localization in these cells raised the possibility that this transporter could play a role in tumor disposition of mIBG. Cell-based uptake assays were then performed to determine if mIBG is transported by PMAT. The time-dependent uptake in vector-transfected and PMAT-expressing HEK293 cell lines showed that mIBG uptake in PMAT-expressing cells was much greater than that in vector cells and was about 15-fold higher at plateau (**Figure 2.9 A**). Concentration-dependent initial rate studies further revealed that PMAT-mediated mIBG uptake displayed typical Michaelis-Menten kinetics with K_m and V_{max} of

151.7 ± 50.7 μM and 16.4 ± 1.8 nmol/mg protein/min, respectively (**Figure 2.9 B**). Dose-dependent inhibition studies with decynium-22 (D22) – a classic PMAT inhibitor (Engel *et al.*, 2004) – showed that D22 is capable of inhibiting mIBG uptake in both PMAT and NET-expressing HEK293 cell lines, with calculated IC_{50} values of 4.8 ± 0.6 μM for PMAT and 35.1 ± 8.7 μM for NET (**Figure 2.9 C**). These data demonstrate that mIBG transport by PMAT is efficient, saturable, and inhibitable.

2.4.5 *PMAT May Play a Role in Mitochondrial Uptake of mIBG in NB*

The high expression of PMAT in NB tumor cells (**Figure 2.1** and **Figure 2.2**) coupled with its robust mIBG transport activity (**Figure 2.9**) suggest that PMAT may play a role in mIBG disposition in NB tumor cells. We then incubated cultured SH-SY5Y and SK-N-BE(2) cells with mIBG in the presence of varying concentrations of D22. D22 dose-dependently inhibited mIBG total uptake in both NB-derived cell lines (**Figure 2.10 A and B**). However, this effect could also be due to D22 inhibition of NET-mediated initial uptake of mIBG into NB cells. To separate the effect from NET-mediated uptake at the plasma membrane, we isolated mitochondria from SH-SY5Y and SK-N-BE(2) cells and conducted mIBG uptake experiments. After a 5 minute incubation, mIBG accumulated in the mitochondria of NB-derived cell lines. D22 reduced mIBG levels by 42% and 51% in the mitochondria isolated from SK-N-BE(2) and SH-SY5Y, respectively (**Figure 2.10 C**). These results suggest that PMAT may contribute to the accumulation of mIBG in the mitochondria of NB-derived cell lines, potentially playing an important role in the retention of mIBG in NB.

2.5 DISCUSSION

High-risk NB patients face poor survival rates (Irwin and Park, 2015; Parisi *et al.*, 2016). Targeted ^{131}I-mIBG therapy has emerged as a promising therapy for high-risk NB patients, but therapeutic response is highly variable. Although NET has been well established as the mediator of initial mIBG uptake into NB tumors, clinical response to ^{131}I-mIBG cannot be predicted by NET expression alone (Streby *et al.*, 2015). Here, we determined the expression of PMAT in NB and explored its role in tumor disposition of mIBG. Our results showed that PMAT is highly expressed in NB tumor cells and its expression level was positively associated with overall survival for high-risk NB patients without MYCN amplification. In contrast to its typical localization at the plasma membrane of healthy tissues, the PMAT protein is unusually localized intracellularly in NB cells with predominant localization in mitochondria. PMAT efficiently transports mIBG and may play a role in its intracellular distribution. Our findings reveal a novel role of PMAT as a potential risk marker to predict disease prognosis in NB patients without MYCN amplification. Furthermore, our results suggest that PMAT is a previously unrecognized transporter involved in intracellular disposition of mIBG and thus may influence clinical response to ^{131}I-mIBG therapy.

The gene expression of monoamine and polyspecific organic cation transporters was profiled in 154 NB samples from the TARGET database, in 9 NB samples from Seattle Children's Hospital, and in two NB-derived cell lines (**Figure 2.1** and **Figure 2.2**). The results consistently showed that in both MYCN amplified and non-amplified NB, tumor cells mainly express PMAT, NET, and VMAT1/2 with insignificant expression of DAT, SERT, OCT1/2/3, and MATE1/2-K. Remarkably, PMAT has the highest expression level in NB tumor samples and cultured cells, in agreement with a previous report ranking PMAT among the top 25 membrane protein genes overexpressed in NB (Orentas *et al.*, 2012). Our preliminary proteomic study also confirmed

PMAT protein expression in SH-SY5Y and SK-N-BE(2) cells (**Figure 2.3**). Interestingly, expression of PMAT, NET and VMAT1/2, were reduced in NB tumors with MYCN amplification (**Figure 2.1** and **Figure 2.2**). Previous studies also observed that MYCN amplified tumors had lower NET or VMAT1/2 protein expression as compared to non-amplified tumors (DuBois *et al.*, 2012; Temple *et al.*, 2016). MYCN is a master regulator of gene transcription, acting either as a transcriptional activator or repressor of its target genes to drive tumorigenesis (Huang and Weiss, 2013; Hsu *et al.*, 2016). These results suggest that PMAT, NET, and VMAT1/2 are targets of MYCN transcriptional repression.

We next explored if the expression levels of PMAT, NET and VMAT1/2 in NB tumors were associated with overall survival using gene array data with matched clinical information from a TARGET database cohort of 243 patients. After stratification based on MYCN status, we revealed that the expression of PMAT, VMAT1 and VMAT2 positively correlated with survival of patients without MYCN amplification (**Figure 2.5**). The association between PMAT expression and survival in the MYCN non-amplified group was most striking, with an overall survival of ~60% in the high-expression group versus 25% in the low-expression group (**Figure 2.5**). The reason behind this observation is unknown. The clinical and gene expression data analyzed in this study were obtained from patients who received a variety of treatment regimens including multimodal chemotherapy with drugs that are not PMAT substrates. Hence, the observed association between PMAT expression and clinical outcome is less likely to be related to PMAT-mediated drug transport. Instead, this association may reflect an innate relationship with disease progression.

MYCN amplification is the most well-established clinical marker for NB prognosis, found in ~40% of advanced stage and high-risk NB (Irwin and Park, 2015; Otte *et al.*, 2021). A large

percentage of high-risk NB patients do not present MYCN amplification. Indeed, 70% of our survival analysis NB patient cohort did not have MYCN amplification (**Table 2.1**). There is an ongoing need for identification of novel and independent prognosis biomarkers that can better predict disease progress and guide selection of appropriate treatment strategy (Inomistova *et al.*, 2015; Otake *et al.*, 2016; Ahmed *et al.*, 2017). In this regard, PMAT shows promise as a prognosis marker for high-risk NB patients without MYCN amplification. Further studies are needed to validate PMAT's association with NB patient outcome and evaluate its potential as a novel prognosis marker in this population.

PMAT is a monoamine and organic cation transporter highly expressed in human brain, complementing the activity of high-affinity monoamine transporters such as NET (Duan and Wang, 2010; Vieira and Wang, 2021; Bowman *et al.*, 2022). In healthy tissues and transfected cell lines, PMAT is localized to the plasma membrane of cells (Engel *et al.*, 2004; Dahlin *et al.*, 2007; Duan and Wang, 2013). Intriguingly, immunolocalization studies in NB-derived cell lines (**Figure 2.6**) and NB tumor samples (**Figure 2.7**) revealed that PMAT protein is retained intracellularly in NB, with large co-localization with mitochondria. Corroborating with this finding, IDT307 – a fluorescent PMAT substrate – also accumulated within the mitochondria in SH-SY5Y cells (**Figure 2.8**). The reason why PMAT is abnormally localized intracellularly in NB cells is unknown. Protein mislocalization in cancer has been previously reported including transporters typically found in the plasma membrane (Wapnir *et al.*, 2003; Wang and Li, 2014; Guo *et al.*, 2019). For instance, the sodium iodine symporter (NIS) is localized to the basolateral membrane (blood-facing) of thyroid follicular cells and mediates iodide uptake (Dohán *et al.*, 2003). However, NIS was reported to be abnormally localized intracellularly in thyroid cancers as well as in certain extrathyroidal malignancies (Wapnir *et al.*, 2003; Micali *et al.*, 2014; Oh and

Ahn, 2021). Further studies have uncovered that the pituitary tumor-transforming gene 1 binding factor (PBF) – a proto-oncogene upregulated in thyroid cancer – directly binds to NIS and alters its subcellular localization, regulating its activity (Smith *et al.*, 2009; Bulotta *et al.*, 2016). The altered localization of transporters in cancer cells could alter cellular disposition of substrate drugs and endogenous molecules, influencing tumor response to cancer therapeutics.

Although mIBG is known to enter NB tumor cells via NET expressed in the plasma membrane of most NB cells, the mechanisms involved in its intracellular distribution and elimination or retention are poorly understood. Previously, VMATs have been suggested to mediate mIBG transport into intracellular storage vesicles, affecting mIBG retention in pheochromocytomas and paragangliomas – two adult forms of neuroendocrine tumors (Blanchet *et al.*, 2012). However, NB cells contain lower amounts of storage vesicles in comparison to these tumors (Montaldo *et al.*, 1991; Streby *et al.*, 2015), and the use of reserpine – a VMAT inhibitor – had minimal impact on mIBG retention in NB cells (Smets *et al.*, 1990; Mairs *et al.*, 1991). Importantly, electron spectroscopy imaging showed that after entering NB cells majority of mIBG is concentrated in mitochondria (Gaze *et al.*, 1991). Our results revealed PMAT's main localization in mitochondria in NB cells, suggesting that PMAT could be involved in mIBG mitochondrial uptake. This mitochondrial uptake may represent an important retention mechanism of ^{131}I-mIBG in NB, which could lead to DNA damage and cell death due to increased exposure to the ionizing radiation (β particles) emitted by iodine-131. Additionally, this mitochondrial uptake could also contribute to mitochondrial damage and cell death – analogous to the toxicity observed for antiviral drugs following mitochondrial uptake mediated by the human equilibrative nucleoside transporters 1 and 3 (Lai *et al.*, 2004; Govindarajan *et al.*, 2009).

Uptake studies in HEK293 cells expressing PMAT on the plasma membrane revealed that PMAT indeed transports mIBG (**Figure 2.9**). The K_m value of PMAT mIBG transport was 151.7 ± 50.7 µM, which is 17-fold higher than that of NET (López Quiñones *et al.*, 2020). This is consistent with PMAT functioning as a low-affinity, high-capacity monoamine transporter. Given that intracellular concentrations of mIBG are likely high due to the concentrative uptake by NET, this high K_m could be advantageous to avoid transporter saturation. To obtain functional evidence of PMAT's involvement in mIBG disposition in NB cells, we performed mIBG uptake studies in two NB-derived cell lines in the presence of the PMAT inhibitor D22 (**Figure 2.10 A and B**). Although we observed dose-dependent inhibition of mIBG uptake by D22 in NB-derived cells, D22 can inhibit both NET- and PMAT-mediated mIBG uptake (**Figure 2.9 C**). Hence, it is difficult to tease out the contribution of NET versus PMAT inhibition. Ideally, uptake studies in a NB cell line with PMAT knockout would help answer this question. However, attempts to generate such a cell line were unsuccessful due to the presence of PMAT pseudogenes (e.g., *SLC29A4P1* and *SLC29A4P2*). We thus isolated mitochondria from SH-SY5Y and SK-N-BE(2) cells and performed mIBG uptake studies in the absence or presence of D22. D22 significantly reduced mitochondrial mIBG uptake (**Figure 2.10 C**), providing functional evidence of PMAT-mediated mIBG uptake in mitochondria. As PMAT-mediated transport is driven by membrane potential (Itagaki *et al.*, 2012), the membrane potential (~ -150mV) across mitochondria inner membrane would serve as an ideal driving force for PMAT-mediated mIBG uptake. Together, our results suggest that PMAT may play a role in the distribution of mIBG into intracellular organelles after its initial uptake by NET, potentially impacting tumor retention and exposure to ^{131}I-mIBG. Thus, differences in PMAT expression in NB tumors may contribute to variable response to ^{131}I-mIBG therapy.

In summary, we identified PMAT as a new monoamine and organic cation transporter highly expressed in NB. Among high-risk NB patients without MYCN amplification, PMAT expression level is associated with overall survival. PMAT efficiently transports mIBG, but is mainly localized in mitochondria of NB cells, and mediates mitochondrial uptake of mIBG. Together, our study suggests that PMAT is a previously unrecognized transporter involved in mIBG intracellular disposition in NB, and hence may be an important determinant of tumor retention, exposure, and response to ^{131}I-mIBG therapy. As new radiolabeled mIBG analogs (e.g. ^{18}F-mFBG, ^{211}At-mABG) are being developed for cancer imaging and therapy, our findings also provide new insights on developing strategies to improve the specificity and efficacy of these analogs based on their transport and interaction with transporters in tumor cells.

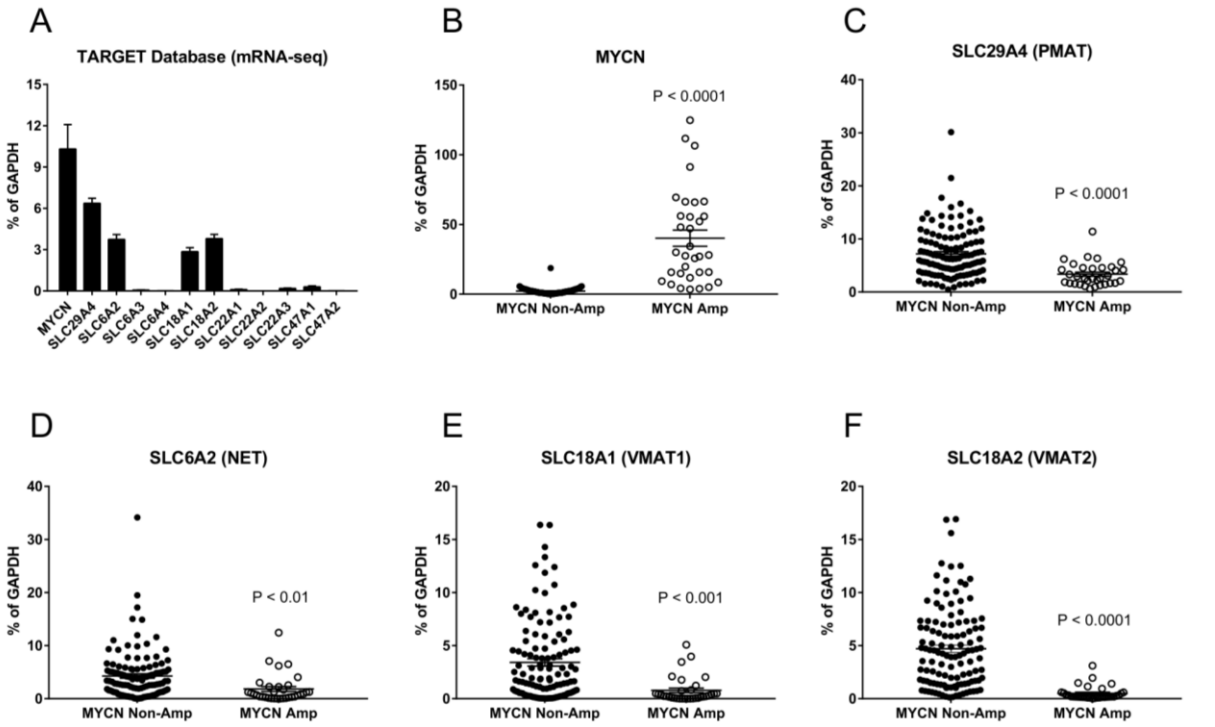

Figure 2.1. RNA expression of selected transporter genes in NB samples from TARGET database.

mRNA-seq (FPKM) data of 154 patients was acquired from TARGET neuroblastoma database. (A) The expression of selected genes was calculated relative to the expression of GAPDH in each sample. Data are presented as the mean ± S.E.M. (B-F) Scatter plots of relative expression of selected genes in MYCN amplified (N=33) versus non-amplified (N=121) samples. Dots represent individual observations and horizontal line with error bar represents the mean ± S.E.M. of the group. Statistical significance was determined using an unpaired Student's t test and the calculated p-value is shown for each gene.

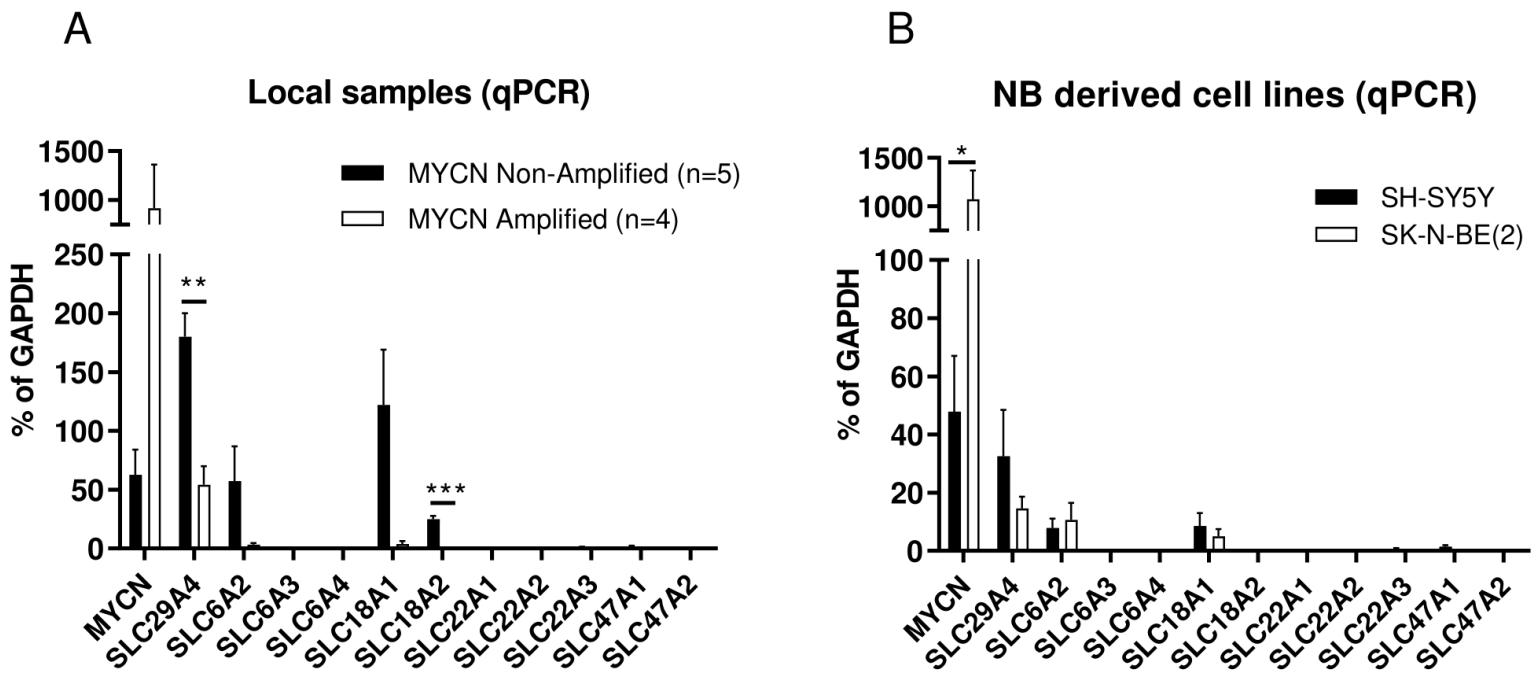

Figure 2.2. qPCR analysis of mRNA expression of selected transporter genes in local NB tumor samples and two NB-derived cell lines.

(A) qPCR results from mRNA extracted from local patient NB tissues from the Seattle Children's Hospital. (B) qPCR results from mRNA extracted from NB-derived SH-SY5Y and SK-N-BE(2) cell lines. Data are presented as the mean ± S.E.M. Expression of genes with overall high expression was compared between MYCN amplified samples versus non-amplified samples. Statistical significance was determined using an unpaired Student's t test (*P < 0.05; **P < 0.01; ***P < 0.001)

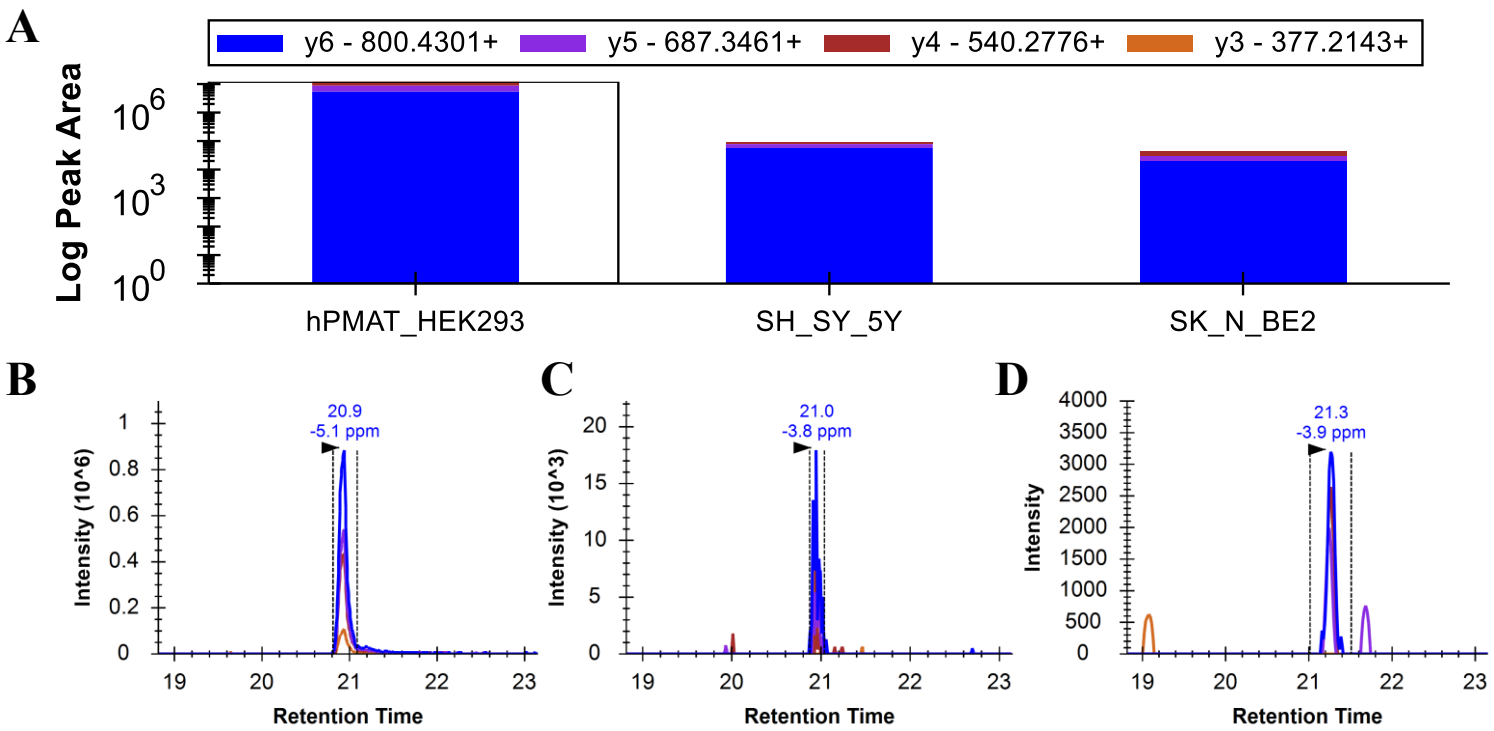

Figure 2.3. Detection of PMAT protein expression in the membrane fraction of hPMAT-overexpressing HEK293 cells, SH-SY-5Y, and SK-N-BE2 cell lines.

NanoLC coupled high-resolution-based parallel reaction monitoring (PRM) based proteomics method was employed. PMAT peptide, FVLFYTTR was used as a surrogate for protein quantification. While PMAT relative protein expression (A) in hPMAT expressing HEK293 cells (B) was much higher than the SH-SY-5Y (C) and SK-N-BE2 (D) cell lines, the PRM method confirmed using multiple MS fragments that these cell lines express PMAT at a protein level.

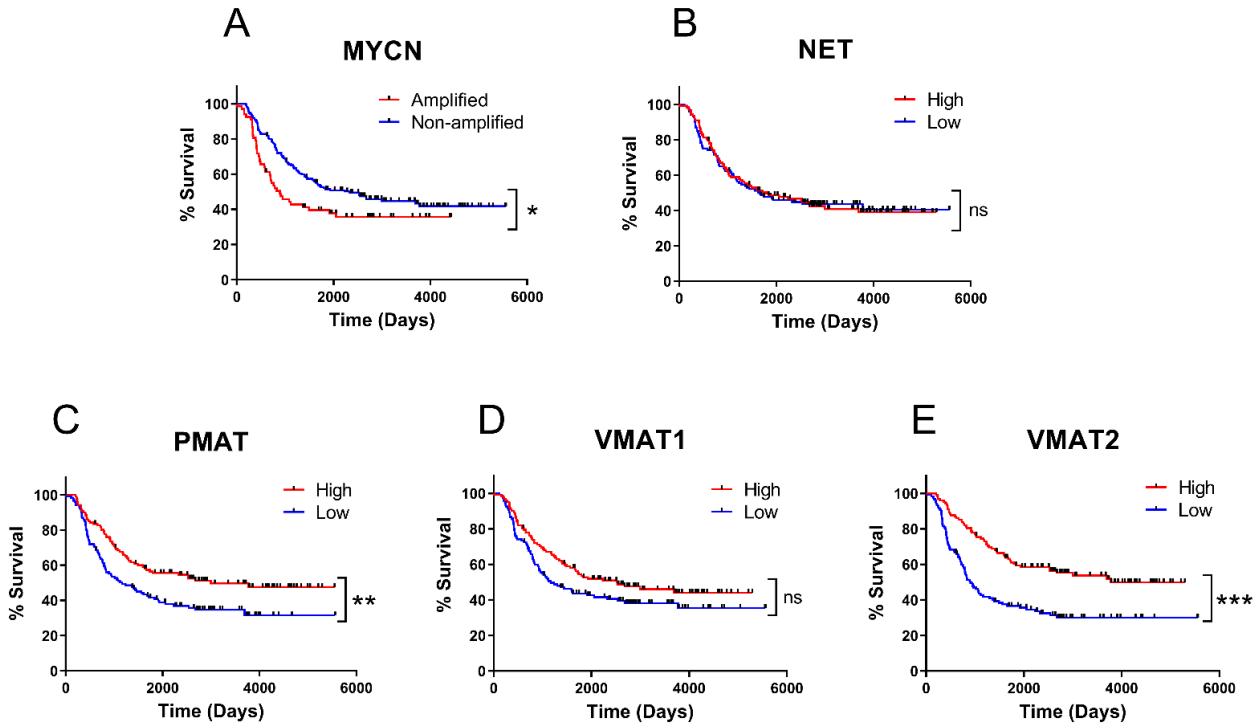

Figure 2.4. Kaplan-Meier Survival Curves of 243 NB patients from TARGET database based on transporter gene expression without stratification of MYCN status.

For selected transporters (B-E), gene expression array data was divided into high and low expression groups (top and bottom 50th percentile respectively), and Kaplan-Meier survival analysis was performed. For survival curve for MYCN (A), the clinically assigned MYCN status was used to divide the patients into MYCN amplified (N=68) or non-amplified (N=175) groups. Statistical significance was determined using the Log-Rank Test (ns – not significant; *P < 0.05; **P < 0.01; ***P < 0.001).

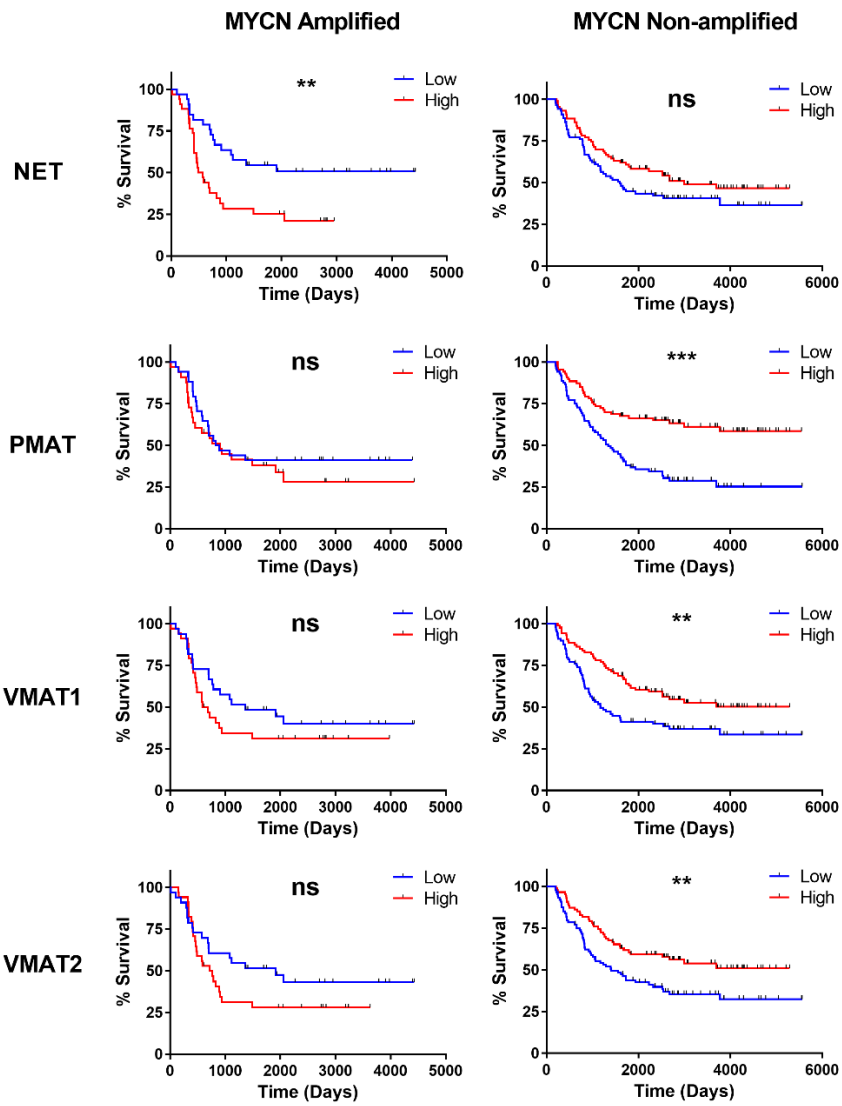

Figure 2.5. Kaplan-Meier survival curves based on transporter gene expression levels after stratification by MYCN amplification status.

Gene expression array data and survival data were acquired from the TARGET database. Patients were divided into MYCN Amplified (N=68) and MYCN Non-amplified (N=175) groups based on their clinically assigned MYCN status. Each group was then divided into high (top 50th percentile – red) and low (bottom 50th percentile – blue) expression levels of NET, PMAT, VMAT1 or VMAT2. Survival between high- and low-expression groups were compared using Log-Rank Test (ns – not significant; *P < 0.05; **P < 0.01; ***P < 0.001).

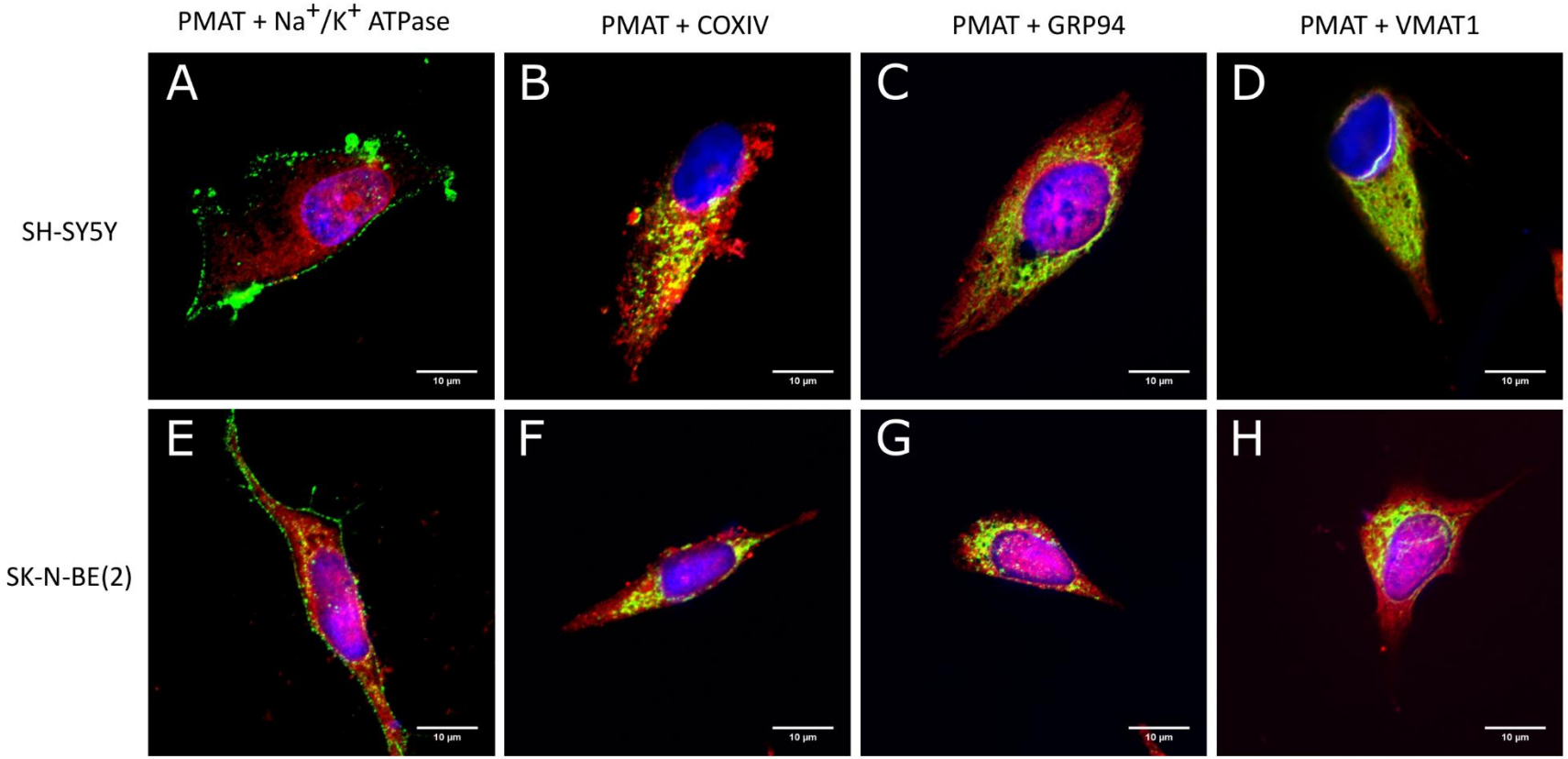

Figure 2.6. PMAT protein localization in NB-derived cell lines determined by immunofluorescence staining.

Co-immunofluorescence was conducted with cultured cell slides of SH-SY5Y (A-D) or SK-N-BE(2) (E-H) cells. The red color in figures indicates the staining of PMAT (A-H), and the green color represents the expression of the plasma membrane marker Na^+/K^+ ATPase (A and E), mitochondrial marker COXIV (B and F), endoplasmic reticulum marker GRP94 (C and G) or vesicular marker VMAT1 (D and H). The nuclei were stained with DAPI and are shown in blue.

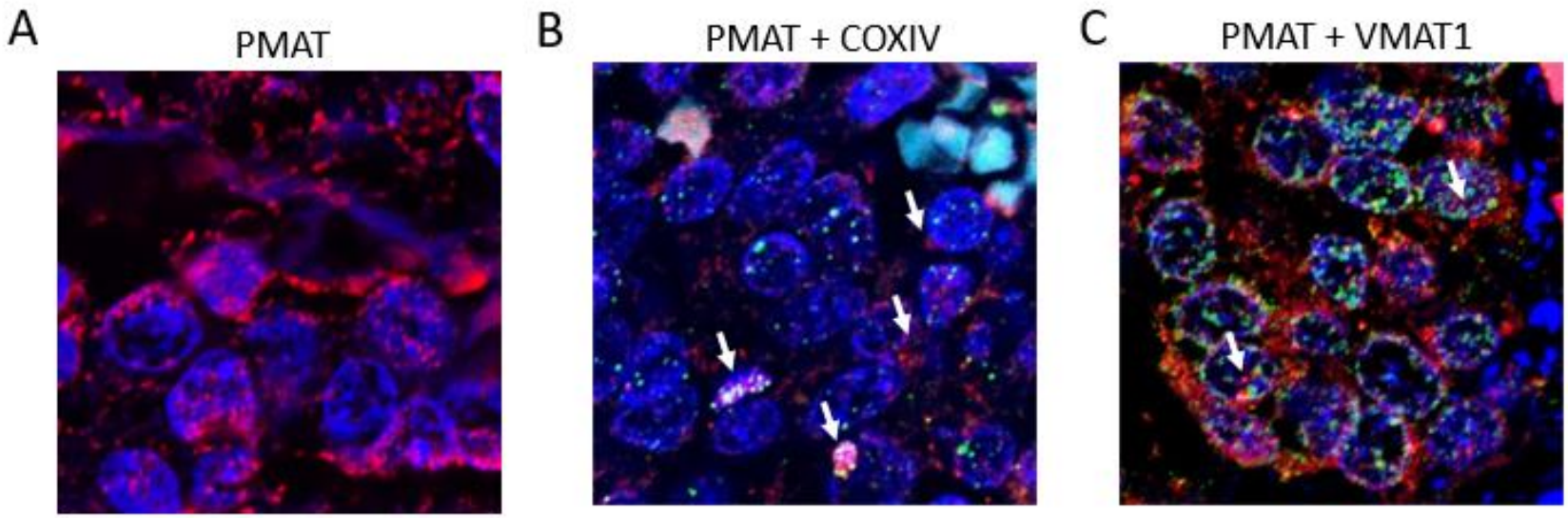

Figure 2.7. PMAT protein expression and localization in local NB patient tissue samples determined by immunofluorescence. Co-immunofluorescence was conducted with patient tissue slides from Seattle Children's Hospital NB tumor samples. The red color in the figures indicates the staining of PMAT (A-C), and the green color represents the expression of the mitochondrial marker COXIV (B) or vesicular marker VMAT1 (C). The nuclei were stained with DAPI and are shown in blue. Arrows indicate areas where co-localization of PMAT with COXIV (B) or VMAT1 (C) was observed.

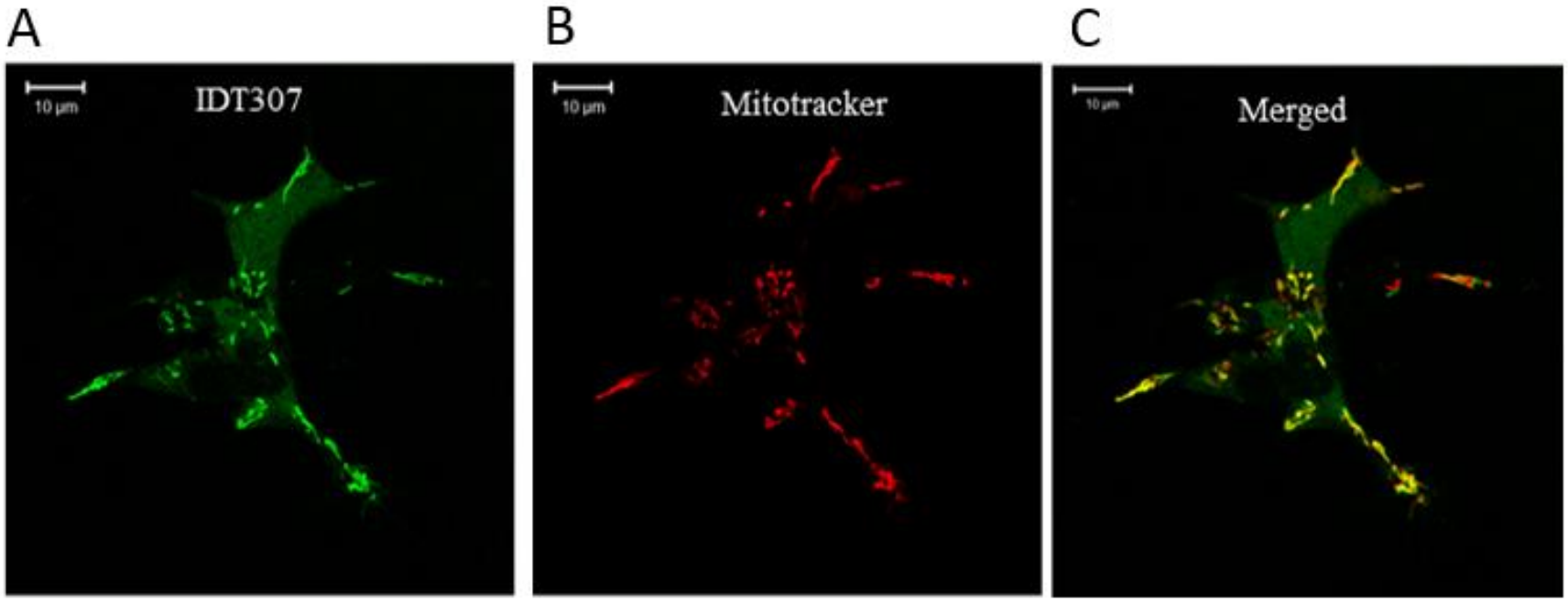

Figure 2.8. Intracellular localization of IDT307 in SH-SY5Y cells.

SH-SY5Y cells were incubated with IDT307 (1 μM) and Mitotracker Deep Red for 30 min. Localization of IDT307 (green, A) and Mitotracker (red, B) was determined by confocal microscopy. Yellow indicates co-localization (C).

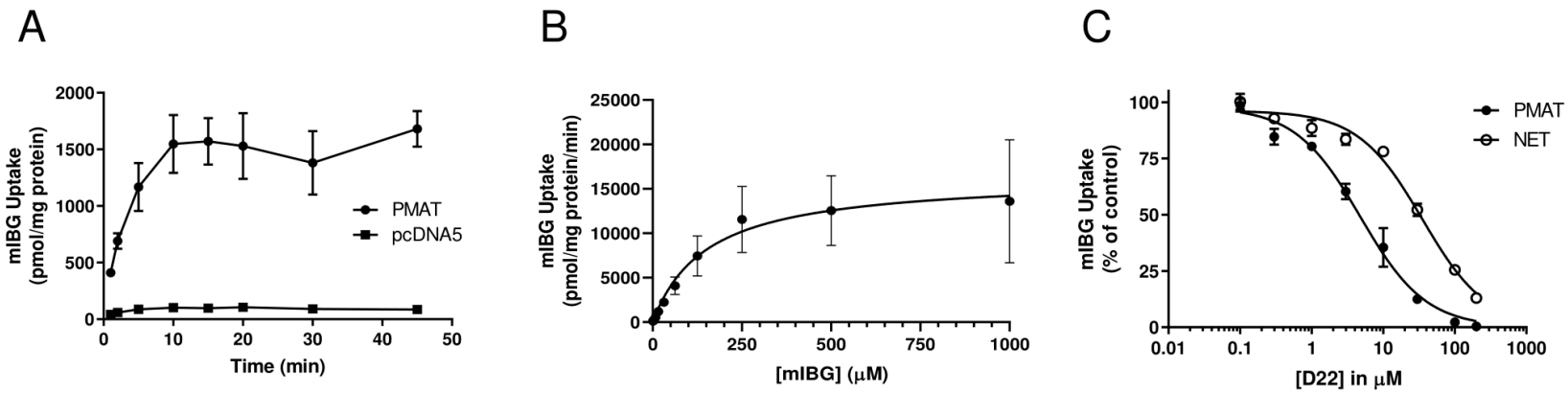

Figure 2.9. Kinetics of mIBG uptake by PMAT and inhibition of PMAT- or NET-mediated mIBG uptake by D22.

(A) Time-dependent uptake of 1μM mIBG was measured at 37°C with pcDNA5 (vector) and PMAT transfected HEK293 cells. (B) Concentration-dependent uptake of PMAT-mediated mIBG transport after a 2-minute incubation. Transporter-specific uptake was calculated by subtracting the activity in vector-transfected cells from the activity in PMAT-expressing cells. (C) Effect of D22 on mIBG (2 μM) uptake mediated by PMAT or NET. Transporter-specific uptake was obtained by subtracting the uptake in vector-transfected cells and data is expressed as a percentage of mIBG uptake in the absence of D22 (control). The IC_{50} values were obtained by fitting the data using non-linear regression. All data points represent the mean ± S.D. from three independent experiments.

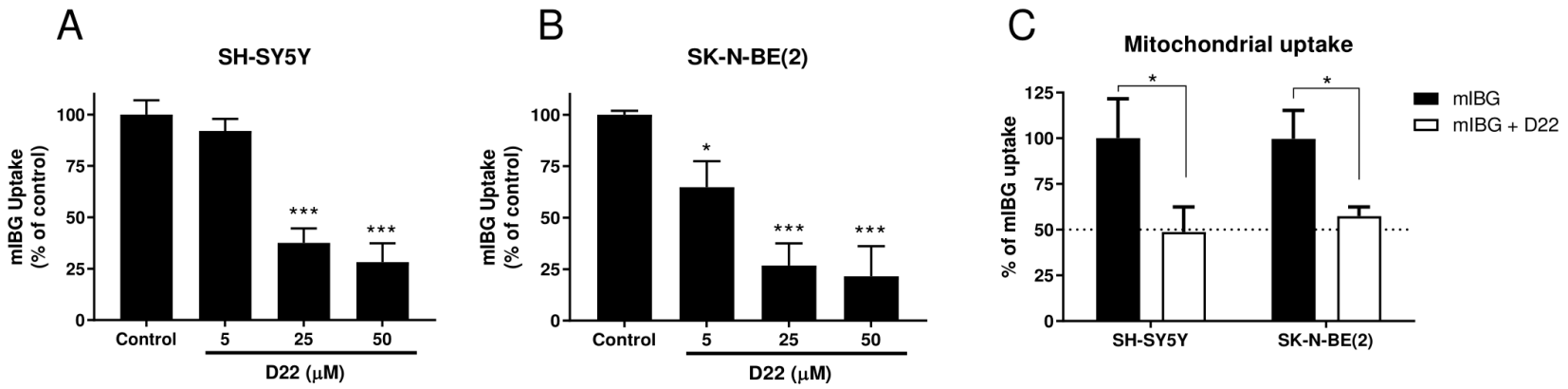

Figure 2.10. Effect of D22 on mIBG uptake in whole cells and in mitochondria isolated from NB-derived cell lines.

Effect of D22 on mIBG (2 μM) uptake by intact SH-SY5Y (A) and SK-N-BE(2) (B) cells. Uptake of mIBG in absence and presence of varying D22 concentrations were compared using one-way ANOVA with the Bonferroni method to correct for multiple comparisons. Mitochondrial uptake of mIBG (2 μM) was measured in the absence or presence of D22 (100 μM) (C). Mitochondrial fractions were isolated from SH-SY5Y or SK-N-BE(2) cells. Data is expressed as a percentage of mIBG uptake relative to uptake in the absence of D22. All data points represent the mean ± S.D. from three independent experiments. Mitochondrial uptake of mIBG in the absence and in the presence of D22 were compared using unpaired Student's t test (*$P < 0.05$, ***$P < 0.001$).

Table 2.1. Demographic and clinical information from 249 patients with gene expression array data available on TARGET Neuroblastoma Database.

		Number of patients (%)
Gender	Male	143 (57.4%)
	Female	106 (42.6%)
Race	American Indian or Alaska Native	1 (0.4%)
	Asian	3 (1.2%)
	Black or African America	31 (12.4%)
	Native Hawaiian or other Pacific Islander	3 (1.2%)
	White	180 (72.4%)
	Unknown	31 (12.4%)
INSS Stage	Stage 1	30 (12.0%)
	Stage 3	1 (0.4%)
	Stage 4	216 (86.8%)
	Unknown	2 (0.8%)
MYCN status	Amplified	68 (27.3%)
	Non-amplified	175 (70.3%)
	Unknown	6 (2.4%)

NOTE. Data collected on 05/13/2020 from TARGET neuroblastoma database – gene expression array and clinical file. Abbreviations: INSS, International Neuroblastoma Staging System.

Chapter 3. INTERACTION AND TRANSPORT OF BENZALKONIUM CHLORIDES (BACS) BY THE ORGANIC CATION AND MULTIDRUG AND TOXIN EXTRUSION TRANSPORTERS

3.1 ABSTRACT

Humans are chronically exposed to benzalkonium chlorides (BACs) from different environmental sources. The FDA has recently called for additional BAC safety data, as these compounds have been reported as cytotoxic and with great potential for biochemical interactions. Biodistribution studies revealed that BACs extensively distribute to many tissues and accumulate at high levels, especially in the kidneys, but the underlying mechanisms are unclear. The goals of this study were to characterize the interactions of BACs of varying alkyl chain length (C8 to C14) with the human organic cation transporters (hOCT1-3) and multidrug and toxin extrusion proteins (hMATE1/2K), with the goal to identify transporters that could be involved in the tissue disposition of BACs. Using transporter-expressing cell lines, we showed that all BACs are inhibitors of hOCT1-3 and hMATE1/2K, with IC_{50} values ranging from 0.83 to 25.8 µM. Further, the short-chain BACs (C8 and C10) were identified as substrates of these transporters. Interestingly, while BAC C8 displayed typical Michaelis-Menten kinetics, C10 demonstrated a more complex substrate-inhibition profile. Transwell studies with transfected Madin-Darby canine kidney cells revealed that intracellular accumulation of basally applied BAC C8 and C10 was substantially higher (8.2- and 3.7-fold, respectively) in hOCT2/hMATE1 double-transfected cells in comparison to vector-transfected cells, supporting a role of these transporters in mediating renal accumulation of these compounds in vivo. Together, our results suggest that BACs interact with hOCT1-3 and hMATE1/2K as both inhibitors and substrates, and that these transporters may

play important roles in tissue distribution and potential toxicity of short-chain BACs. Our findings have important implications for understanding human exposure and susceptibility to BACs due to environmental exposure.

3.2 INTRODUCTION

Benzalkonium chlorides (BACs) are quaternary ammonium compounds (**Figure 3.1**) with alkyl chain lengths ranging from 8 to 18 carbons (C8 to C18). These compounds are cationic surfactants with broad anti-microbial properties and are widely used as disinfectants or preservatives in cleaning products, medical products, and in the food processing industry (Pereira and Tagkopoulos, 2019). Although BACs have been used in consumer products since the 1950's and were believed to be safe, a wide range of cytotoxicity has been reported in various biological systems (Herman and Bass, 1989b; Nałecz-Jawecki *et al.*, 2003b; Sarkar *et al.*, 2012b; Melin *et al.*, 2014; Hrubec *et al.*, 2017; Herron *et al.*, 2021; Arnold *et al.*, 2023), and the US Food and Drug Administration (FDA) has called for additional safety data on its use in healthcare and consumer antiseptic products (FDA, 2015, 2016).

The widespread use of cleaning products containing BACs in hospitals, restaurants, and at home indicates that humans are frequently and chronically exposed to these compounds. Indeed, a study analyzing human serum samples collected before (n = 111) and during (n = 111) the COVID-19 pandemic detected BACs in more than 95% of samples and showed a 174% increase in the median BAC concentration during the pandemic when compared to pre-pandemic levels (Zheng *et al.*, 2021). Moreover, another study found that blood concentrations of BACs (C12, C14 and C16) correlated with toxicological endpoints, such as decreased mitochondrial function, increased inflammatory cytokines, and altered sterol biosynthesis (Hrubec *et al.*, 2021).

Importantly, short-chain BACs were found to be potent inhibitors of cholesterol biosynthesis in cell lines (Herron *et al.*, 2016), suggesting that even low levels of BAC exposure could lead to significant biochemical interactions.

Biodistribution studies in rats have reported that following oral or intravenous administration, BACs are highly distributed to several tissues including the heart, liver, lungs, spleen, and kidneys (Xue *et al.*, 2002, 2004; Kera *et al.*, 2021). The kidneys were identified as a major organ of accumulation, with BAC concentrations much above plasma levels and showing preferential accumulation of shorter alkyl chain BACs (Kera *et al.*, 2021). Additionally, BAC C12 and C16 have been reported to cross the blood-placental barrier and to reach mice neonatal brain (Herron *et al.*, 2019). Although tissue distribution in humans is more difficult to assess, pathological examinations following poisoning cases reported lungs, heart, liver, and kidneys as affected tissues (van Berkel and de Wolff, 1988; Hitosugi *et al.*, 1998; Tambuzzi *et al.*, 2022), suggesting BACs may distribute to these organs. In particular, a case report on a delayed death following suicidal ingestion of Lysoform® – containing BACs as the main constituent – was the first to reveal microscopic pictures of BAC toxicity, showing clear signs of acute kidney injury including foci of tubular necrosis (Tambuzzi *et al.*, 2022). These emerging evidences demonstrate that BACs distribute and accumulate in various human tissues with potential toxicological effects. However, the mechanisms driving the accumulation of BACs in these tissues are poorly understood.

The human polyspecific organic cation transporters are a group of solute carrier transporters that mediate cellular transport of many endogenous and exogenous organic cations, impacting their systemic and tissue-specific disposition (International Transporter Consortium *et al.*, 2010; Wagner *et al.*, 2016; Koepsell, 2020). This group includes the organic cation transporters

1, 2, and 3 (hOCT1, hOCT2 and hOCT3) and the multidrug and toxin extrusion proteins 1 and 2K (hMATE1 and hMATE2K). Interestingly, the tissue distribution of these transporters largely overlaps with tissues in which BAC accumulation has been reported (Kera *et al.*, 2021). For instance, hOCT1 is a major isoform highly expressed in the liver known to mediate uptake of organic cations into hepatocytes, hOCT2 and hMATE1/2K are expressed respectively in the basal and apical membranes of renal proximal tubule cells and mediate renal uptake and tubular secretion of its substrates, and hOCT3 is broadly expressed in several tissues including the heart, skeletal muscle, and placenta, playing an important role in drug transport in these organs (Wagner *et al.*, 2016; Lee *et al.*, 2018). We thus hypothesized that hOCT and hMATE transporters are involved in the tissue disposition of BACs.

Although hOCTs and hMATEs have been previously reported to interact with various quaternary ammonium compounds (Zhang *et al.*, 1999; Dresser *et al.*, 2002; Tanihara, Masuda, Sato, Katsura, Ogawa, and K-I Inui, 2007; Sala-Rabanal *et al.*, 2013), their interaction with BACs has never been investigated. In this study, we characterized the interactions of BACs of varying alkyl chain lengths (C8 to C14) with hOCT1-3 and hMATE1/2K transporters. Compounds were investigated as potential inhibitors and substrates, and detailed kinetic interactions were characterized. The potential impact of hOCT2 and hMATE1 in BAC renal disposition and accumulation was investigated by using an in vitro model of renal transepithelial transport employing hOCT2/hMATE1 double-transfected cells.

3.3 MATERIALS AND METHODS

3.3.1 *Materials*

[^{14}C]Metformin (115 mCi/mmol) was purchased from Moravek Biochemicals, Inc. (Brea, CA). Optima LC−MS grade acetonitrile, water, formic acid, and ammonium formate used in liquid chromatography were purchased from Fisher Scientific (Santa Clara, CA). Lucifer yellow (LY) was from MP Biomedicals (Irvine, CA). Benzalkonium Chlorides (BACs) of various alkyl chain lengths (C8, C10, C12 and C14) were from Sigma-Aldrich (St. Louis, MO). Deuterated (d_7-benzyl) BACs (d_7-C10-BAC, d_7-C12-BAC and d_7-C14-BAC) were synthesized as previously described (Herron *et al.*, 2016). Cell culture media and reagents were purchased from Invitrogen (Carlsbad, CA).

3.3.2 *Cell Lines and Cell Culture*

Flp-In human embryonic kidney (HEK) 293 cells stably transfected with hOCT1, hOCT2, hOCT3, hMATE1, hMATE2K or empty pcDNA5/FRT vector (control) were previously established in our laboratory (Duan and Wang, 2010; Yin *et al.*, 2015). HEK293 cells were maintained in high glucose Dulbecco's modified Eagle's medium supplemented with 10% fetal bovine serum, 2 mM L-glutamine, 100 IU/mL penicillin, 100 µg/mL streptomycin, and 150 µg/mL hygromycin B. The surface of the flasks and plates was coated with 0.1 mg/mL poly-D-lysine in Milli-Q water to improve HEK293 cell attachment. The Madin-Darby Canine Kidney (MDCK) cells double-transfected with hOCT2 and hMATE1 or empty vector were previously generated and validated in our laboratory (Yin *et al.*, 2015) and were maintained in high glucose Dulbecco's modified Eagle's medium supplemented with 15% fetal bovine serum, 500µg/mL G418, and

200µg/mL hygromycin B. All cell lines were cultured in a 37ºC humidified incubator with 5% CO_2.

3.3.3 *Uptake and Inhibition Assays in HEK293 Cells*

Uptake and inhibition assays were performed as previously described (Duan and Wang, 2010; Yin *et al.*, 2015, 2016) with modifications for analysis of BACs by liquid chromatography-tandem mass spectrometry (LC-MS/MS). Briefly, HEK293 cells were seeded in 96-well plates and grown to greater than 90% confluency (1–2 days). Prior to incubation, cells were washed twice with prewarmed Krebs-Ringer-HEPES (KRH) buffer (5.6 mM glucose, 125 mM NaCl, 4.8 mM KCl, 1.2 mM KH_2PO_4, 1.2 mM $CaCl_2$, 1.2 mM $MgSO_4$, and 25 mM HEPES, pH 7.4). Uptake was initiated by the addition of buffer at 37°C containing a substrate with or without inhibitor. For hOCT-transfected cells KRH at pH 7.4 was used, while for hMATE-transfected cells KRH was adjusted to pH 8.0. Uptake was quenched by washing the cells three times with ice-cold KRH buffer. After washing, cells from incubations with BACs were permeabilized with 100 µL of acetonitrile:water (1:1) containing 50 nM internal standard (d_7-BACs) for analysis by LC-MS/MS. Precipitated protein was then solubilized in 100 µL 1 M NaOH at 37ºC for 1 hour, neutralized with 100 µL 1 M HCl, and protein content from each well was measured by the BCA method. For incubations containing radiolabeled substrate (^{14}C-metfomin), cells were directly lysed with 1 M NaOH, neutralized with 1 M HCl, and the lysate was used for protein quantification (BCA method) and for measuring radioactivity by liquid scintillation counting (Tri-Carb, Perkin Elmer, Waltham, MA). For inhibition studies, ^{14}C-metformin was used as the classic substrate at 8.7 µM (1 µCi/mL), well below its reported K_m value for these transporters (Liang and Kathleen M Giacomini, 2017). Experiments were performed within the initial uptake rate period. Transporter-

specific uptake was calculated by subtracting uptake in the vector-transfected cells, and uptake in the presence of inhibitor was normalized to uptake in the absence of inhibitor.

3.3.4 *Trans-stimulation Studies in HEK293 Cells*

In trans-stimulation experiments, pcDNA5 (vector)-transfected and hOCT1-, hOCT2- and hOCT3-transfected cells were preincubated for 15 minutes with KRH buffer at pH 7.4 with or without (control) 1 µM of indicated BAC. Cells were then rinsed two times with ice-cold KRH buffer before incubation at 37°C for 4 minutes in KRH buffer (pH 7.4) containing 8.7 µM (1 µCi/mL) ^{14}C-metformin. Cells were then rinsed three times with ice-cold KRH buffer and lysed with NaOH 1M as described above. Radioactivity and protein content were measured in the lysate. Uptake in the vector-transfected cells was subtracted from transporter-transfected cells to obtain transporter-specific uptake, and metformin uptake after pre-incubation with BACs was normalized to uptake in the control condition.

3.3.5 *Transwell Studies in hOCT2/hMATE1 Double-Transfected MDCK Cells*

Transepithelial flux of BACs across MDCK cell monolayers was determined as previously described with slight modifications (Yin *et al.*, 2015, 2016; López Quiñones *et al.*, 2020). Briefly, empty vector and hOCT2/hMATE1-expressing MDCK cells were seeded at a density of 2 x 10^5 cells/cm^2 on 12-well Corning™ Transwell™ inserts (PET membrane, 0.4 µM pore size). Transport experiments were performed 5 days after seeding. These studies were performed under a pH gradient (basolateral pH 7.4 and apical pH 6.0). An apical pH of 6.0 was chosen based on previously published methods by our and other groups to mimic the average urine pH (Tsuda *et*

al., 2009; Rowland and Tozer, 2010; Müller *et al.*, 2011; Yin *et al.*, 2015). The integrity of the MDCK monolayer and proper formation of tight junctions was verified by measurement of transepithelial flux of lucifer yellow (50 µM). Only data from inserts with less than 5% lucifer yellow transfer over the 2-hour time course were accepted ($P_{app} < 1.6 * 10^{-6}$ cm/s). After removal of cell culture media from both sides of the inserts, cells were carefully washed three times with warm KRH buffer pH 7.4. For apical-to-basal (A-to-B) transport, 1.5 mL of KRH buffer (pH 7.4) was added to the B chamber, and transport was initiated by adding 0.5 mL of KRH (pH 6.0) containing 1µM BAC (C8 or C10) and lucifer yellow (50 µM) to the A chamber. Similarly, for basal-to-apical (B-to-A) transport, 0.5 mL of KRH buffer (pH 6.0) was added to the A chamber, and transport was initiated by adding 1.5 mL of KRH (pH 7.4) containing BAC and lucifer yellow to the B chamber. When pyrimethamine was used, it was added to the A chamber only at 10 µM. To measure transcellular transport, at each time point, 100 µL of sample from the receiving chamber was collected and replaced with the adequate buffer. Fluorescence measurements of lucifer yellow were performed from a top-read position in a Synergy HTX plate reader (Biotek, Winooski, Vermont) using a 420/50 nm excitation and 528/20 nm emission filter set. After fluorescence was measured, 100 µL of acetonitrile containing 100 nM d_7-BACs was added to each sample, followed by centrifugation and quantification of BACs by LC-MS/MS. At the end of the experiment (120 minutes), inserts were washed three times with ice-cold KRH buffer, and cells were permeabilized using acetonitrile containing 100 nM d_7-BACs, diluted 1:1 with KRH buffer and centrifuged before LC-MS/MS analysis. Following permeabilization, the precipitated protein was solubilized with 1 M NaOH and neutralized with 1 M HCl, and protein content was measured by BCA method and used to normalize intracellular accumulation of BACs.

3.3.6 *Quantification of BACs by LC-MS/MS*

Levels of BAC C8, C10, C12 and C14 were quantified using a LC-MS/MS system consisting of a Waters Acquity UPLC system coupled to a Waters Synapt XS quadrupole time-of-flight (QToF) mass spectrometer (Waters Corporation, Milford, MA). Samples were prepared in 50% acetonitrile containing 50 nM individual d_7-BACs as internal standards. The autosampler compartment was maintained at 10°C from which 8 µL sample aliquots were injected to the LC column by a flow-through needle. Reversed-phase analyte separation was performed on a Thermo Hypersil GOLD C_{18} column (100x2.1 mm, 1.9 µm particle size) operated at ambient temperature and 0.4 mL/min flow rate. The initial mobile phase composition of solvent A (water with 0.1% formic acid and 2 mM ammonium formate) and solvent B (acetonitrile) was 80% A and 20% B. Percent B was linearly increased at a rate of 6% per minute out to 10 minutes to reach 80% B. Percent B then increased to 100% to wash the column for 2 minutes before returning to the initial conditions (20% B) to re-equilibrate the column for 2 minutes prior to the next injection. Electrospray ionization in positive ion mode (ESI+) was run under the following source conditions: capillary voltage 2.5 kV, cone voltage 30 V, source offset 10 V, source temperature 150°C, desolvation temperature 500°C, cone gas flow 50 L/hr, desolvation gas flow 1000 L/hr, and nebulizer gas flow 6.5 bar. The mass detector was calibrated to sodium formate cluster ions immediately prior to each run. During data acquisition, leucine-enkephalin lock mass ($[M+H]^+$ 556.2771 m/z) was sampled at regular intervals and applied as the mass correction reference.

Targeted MS/MS detection of BACs was accomplished by isolation of the precursor $[M]^+$ ions in the quadrupole followed by fragmentation in the transfer cell and accurate mass measurement by the time-of-flight mass analyzer. Fragmentation of BAC $[M]^+$ precursor ions produced $[M - benzyl]^+$ and $[benzyl]^+$ as the two major fragment ions for the unlabeled BACs, or

[M - d_7-benzyl]$^+$ and [d_7-benzyl]$^+$ fragment ions for deuterium-labeled d_7-BAC internal standards. The precursor to product mass-to-charge (*m/z*) transitions monitored for each analyte are described in **Table 3.1**. LC-MS/MS chromatograms were accurate mass filtered (±0.020 Da) for the two major fragment ions and the resulting peak areas were integrated using TargetLynx application manager in MassLynx software (Waters Corporation). Analyte peak areas were normalized to the appropriate internal standard peak area where d_7-BAC-C10 served as the internal standard for BAC-C8 and BAC-C10, d_7-BAC-C12 as the internal standard for BAC-C12, and d_7-BAC-C14 as the internal standard for BAC-C14.

3.3.7 *Data Analysis*

Inhibition, uptake, and trans-stimulation studies in HEK293 cells were performed in triplicate and repeated at least three independent times. The concentrations of BACs were corrected based on nonspecific binding to plastic, which was determined by comparison of drug concentration when diluted in organic solvent in comparison to KRH buffer. Transwell studies in MDCK cells were performed in one (A-to-B direction) or two (B-to-A direction) individual apparatuses and were repeated independently at least three times. Data is reported as mean ± SD. Data was plotted and fitted through nonlinear regression using GraphPad Prism 7.0 (GraphPad Software Inc., La Jolla, CA). IC_{50} values were obtained by fitting the following four-parameter dose-dependent inhibition equation to the data:

Equation 3.1: $$V = Bottom + \frac{(Top - Bottom)}{1 + (I/IC_{50})^H}$$

Where V is the rate of uptake in the presence of inhibitor, “Bottom” is the residual non-inhibitable baseline value, “Top” is the rate of uptake in the absence of inhibitor, [I] is the inhibitor

concentration, and H is the Hill coefficient. To obtain graphs and kinetic parameters, the Michaelis-Menten equation was fitted by nonlinear regression to the BAC C8 data:

Equation 3.2: $$v = \frac{V_{max} * [S]}{K_m + [S]}$$

Where v is the uptake velocity, V_{max} is the maximum uptake velocity of the system, K_m is the Michaelis-Menten constant, and [S] is the substrate concentration. A substrate-inhibition kinetic model previously described (Leow and Chan, 2019) was fitted to the BAC C10 transporter-specific uptake data:

Equation 3.3: $$v = \frac{V_{max} * [S]}{K_m + [S] * \left(1 + \frac{[S]}{K_{i,[S]}}\right)}$$

Where $K_{i,[S]}$ is the affinity constant for binding of the substrate to the inhibitory site. For the Transwell experiments, the P_{app} of BAC C8 and C10 were calculated using the following equation:

Equation 3.4: $$P_{app} = (dQ/dt)/(A * C_0)$$

Where dQ/dt is the amount of compound transported over time, A is the insert membrane surface area, and C_0 is the initial compound concentration in the donor chamber. Statistical significance was assessed using one-way ANOVA followed by Dunnett's post hoc test to correct for multiple comparisons or an unpaired student's t-test (with or without Bonferroni post hoc test for multiple comparisons) as specified in the figure legends. A P value less than 0.05 was considered statistically significant.

3.4 RESULTS

3.4.1 *BACs are Strong Inhibitors of the Polyspecific Organic Cation Transporters*

To determine if BACs of varying alkyl chain lengths (C8, C10, C12 and C14) interact with hOCT1, 2, and 3 and hMATE1 and 2K, the uptake of the probe substrate metformin was measured in the absence and presence of varying BAC concentrations. Metformin was used at 8.7 µM, well below its reported K_m value for these transporters (Liang and Kathleen M Giacomini, 2017). All BACs inhibited metformin uptake by hOCT1-3 and hMATE1/2K, displaying dose-dependent inhibition with IC_{50} values ranging from 0.83 to 25.8 µM (**Figure 3.2** and **Table 3.2**). To examine whether BAC chain length impacts inhibition potency, the IC_{50} values towards each transporter were plotted as a function of BAC chain length (**Figure 3.3**). No apparent trend was observed. However, hMATE1 seems to be the most sensitive transporter to BACs, with IC_{50} values consistently lower than other transporters (**Figure 3.3** and **Table 3.2**). Interestingly, a stimulatory effect on hOCT2-mediated metformin uptake was observed for C8 and C10 at low concentrations (**Figure 3.2 A and B**), which was not observed for C12 or C14 (**Figure 3.2 C and D**). This stimulatory effect may be due to trans-stimulation of the transporter. We thus performed trans-stimulation studies in hOCT1-3 transfected HEK293 cells. As shown in **Figure 3.4**, pre-loading hOCT2-transfected HEK293 cells with BAC C8 and C10, but not C12 and C14, led to an enhanced uptake of metformin. No stimulation was observed for hOCT1 or hOCT3; instead, a slight trans-inhibitory effect by C8 and/or C10 was observed (**Figure 3.4**).

3.4.2 *BAC C8 and C10 are Transported by hOCT1-3 and hMATE1/2K*

To determine if BACs are substrates of polyspecific organic cation transporters, we directly measured BAC accumulation in vector- and transporter-transfected HEK293 cells. At a substrate concentration of 1 μM and incubation time of 10 min, C8 significantly accumulated in cells expressing hOCT1, 2, and 3 (~ 13 to 16-fold) and hMATE1/2K (3.4 and 8.3-fold respectively) in comparison to pcDNA5 vector cells (**Figure 3.5**). Similarly, C10 also had significantly higher (~ 2.3 to 3.3-fold) accumulation in transporter-transfected cell lines. In contrast, C12 only displayed a slight uptake (< 1.5-fold) in hOCT1 and hMATE2K-transfected cells, and no significant accumulation was observed for C14 (**Figure 3.5**). These results demonstrate that short-chain BACs (C8 and C10) are substrates for hOCT1-3 and hMATE1/2K whereas longer-chain BACs are poor or not substrates for these transporters.

3.4.3 *Transport Kinetics of BAC C8 and C10 by hOCTs and hMATEs*

The accurate determination of transporter kinetic parameters requires the selection of time points in the initial linear phase of uptake (i.e., initial uptake rates) (Brouwer *et al.*, 2013). Therefore, the time course of C8 and C10 uptake by hOCT1, hOCT2, hOCT3, hMATE1 and hMATE2K was examined to determine the initial uptake rate. The data showed that uptake of C8 and C10 was higher in transporter-expressing cells at all time points tested, and substantial accumulation was achieved after 5- to 10-min incubation in comparison to vector-transfected cells (**Figure 3.6**). Uptake of C8 and C10 by hOCT1-3 was linear up to 7-10 minutes (**Figure 3.6 A and B**) and their uptake by hMATE1/2K was linear up to 4-7 minutes (**Figure 3.6 C and D**). Hence, concentration-dependent studies to determine kinetic parameters were conducted with a 4-

minute incubation time for hOCT1-3 and a 2-minute incubation time for hMATE1/2K. Specific transporter-mediated uptake was obtained by subtracting uptake in vector-transfected cells.

As shown in **Figure 3.7**, hOCT1-, hOCT2-, hOCT3-, hMATE1- and hMATE2K-mediated uptake of C8 displayed saturable kinetics with typical Michaelis-Menten curves, as confirmed by the linear nature of the Eadie-Hofstee plots. The K_m and V_{max} values for each transporter, derived from nonlinear regression fitting to **Equation 3.2**, are summarized in **Table 3.3**. The apparent affinities of the human polyspecific organic cation transporters for C8 are similar, ranging from 6 to 19 μM, which is consistent with their IC_{50} values (ranging from 5 to 14 μM, **Table 3.2**). Interestingly, C10 displayed an atypical transport kinetic profile for all hOCTs and hMATEs, with a hook in the upper left quadrant in the Eadie-Hofstee plot (**Figure 3.8**). These patterns could suggest substrate inhibition kinetics due to substrate binding to multiple sites in these transporters where binding to a secondary site may hinder transport efficiency. We then fit C10 kinetics data using **Equation 3.3**, which includes an affinity constant for binding to the inhibitory site ($K_{i,[s]}$). The K_m, V_{max}, and $K_{i,[s]}$ values calculated for each transporter are presented in **Table 3.3**. The estimated $K_{i.[s]}$ values are 5 to 15-fold higher than the K_m for hOCT1, hOCT2, hMATE1, and hMATE2K, indicating a higher affinity to the binding site that results in substrate translocation. On the other hand, the K_m and $K_{i,[s]}$ for hOCT3 were more comparable, suggesting the affinities to the translocation and the inhibition binding sites are less discernible.

3.4.4 *Transepithelial Transport of BAC C8 and C10 in hOCT2/hMATE1-Transfected MDCK Cells*

The hOCT2 and hMATE1/2K transporters work sequentially to mediate tubular secretion of common substrates and how they function can influence intrarenal accumulation of compounds

(Yin and Wang, 2016). Previous studies have revealed significant renal accumulation of BACs in rats following oral and intravenous dosing, with higher accumulation reported for shorter-chain BACs (Xue *et al.*, 2004; Kera *et al.*, 2021). Our uptake study in HEK293 transporter-transfected cells shows that BAC C8 and C10 are substrates of hOCT2 and hMATE1/2K (**Figure 3.5**). To investigate the potential role of these transporters in renal secretion and intrarenal accumulation of these compounds, transepithelial flux and accumulation of BAC C8 and C10 were assessed in a Transwell system employing vector-transfected and hOCT2/hMATE1-double transfected MDCK cells. As shown in **Figure 3.9** (panels A and B), the B-to-A flux rates of BAC C8 and C10 were constant over the 120-minutes time course, and transport was higher in the double-transfected cells in comparison to vector-transfected cells. The A-to-B transport of BAC C8 and C10 was negligible in both vector- and transporter-transfected cells, with BAC levels in the receiver chamber below our LC-MS/MS limit of quantification. The calculated B-to-A P_{app} of BAC C8 was $17.9 \pm 0.6 \times 10^{-6}$ cm/s, and of C10 was $13.7 \pm 1.0 \times 10^{-6}$ cm/s in hOCT2/hMATE1-transfected cells, which are respectively 4 and 1.5-fold higher than the B-to-A P_{app} in vector cells (**Figure 3.9 C and D**). These results suggest that hOCT2 and hMATE1 in the human kidney can facilitate tubular secretion of these compounds. In vector-transfected MDCK cells, there was detectable transport of BAC C8 and C10 in the B-to-A direction but not in the A-to-B direction. The reason for this observation is unknown but may be due to the expression of endogenous transporters in MDCK cells, such as the canine OCT2 and/or P-glycoprotein (Shu *et al.*, 2001; Goh *et al.*, 2002).

3.4.5 *Intracellular Accumulation of BAC C8 and C10 in hOCT2/hMATE1-Transfected MDCK Cells*

The intracellular accumulation of BAC was measured at the end of the transport study. When BACs were added to the basal chamber, intracellular accumulation in the double-transfected cells was 8.2 and 3.7 times that in vector cells for C8 and C10, respectively (**Figure 3.10 A and B**). This data suggests that hOCT2 facilitates BAC uptake into MDCK cells at a rate significantly higher than their apical efflux rate mediated by hMATE1. Intriguingly, BACs also accumulated when added to the apical chamber in double-transfected cells, with 15- and 5-fold increase for C8 and C10 respectively in comparison to vector cells (**Figure 3.10 A and B**). This data is surprising as it suggests that apical hMATE1 could facilitate BAC uptake into the MDCK cells. To further test this hypothesis, we measured intracellular accumulation of apically added BACs in the absence or presence of the classic hMATE1 inhibitor pyrimethamine. Indeed, in the presence of 10 µM of pyrimethamine added apically, the accumulation of BAC C8 and C10 was significantly reduced (**Figure 3.10 C and D**). Together, these findings strongly suggest that hOCT2 and hMATE1 could play an important role in the intrarenal accumulation of BACs in vivo.

3.5 DISCUSSION

Due to the widespread use of BACs in cleaning products (e.g.: Lysol, Clorox, hand sanitizers and wipes) and in pharmaceutical and personal care products, the general population is exposed to these compounds and BACs have been detected in human blood/serum samples, with increased exposure level observed during the pandemic (Hrubec *et al.*, 2021; Zheng *et al.*, 2021). Studies in rodents have shown that BACs can accumulate in several tissues, with especially high levels in the kidneys (Kera *et al.*, 2021). Although the tissue distribution of BACs overlaps significantly with tissue expression of the polyspecific organic cation transporters, the roles of

these transporters in BAC disposition are currently unknown. In this study, we comprehensively characterized the interaction between BACs C8, C10, C12 and C14 (**Figure 3.1**) with hOCT1-3 and hMATE12K transporters as inhibitors or substrates. The role of hOCT2 and hMATE1 in intrarenal accumulation of short-chain BACs was also investigated using an in vitro model of renal secretion. Findings from our study have important implications for improving our understanding of the mechanisms involved in the disposition and systemic toxicology of BACs.

Our studies showed that all investigated BACs (C8 to C14) are potent hOCT and hMATE inhibitors with IC_{50} values in the high nM to low µM range (**Figure 3.2** and **Table 3.2**). The calculated IC_{50} values are well below the plasma levels reported for these compounds (Zheng *et al.*, 2021), and although the plasma concentrations of BACs are unlikely to elicit meaningful transporter inhibition, the potential involvement of BACs in xenobiotic-drug interactions cannot be ruled out due to their extensive tissue accumulation (Xue *et al.*, 2002, 2004; Kera *et al.*, 2021). We did not observe a relationship between BAC chain length and inhibitory potency towards these transporters (**Figure 3.3**). Previous studies analyzing other quaternary ammonium compounds (i.e.: n-tetraalkylammonium) have reported a relationship between their inhibitory potency and alkyl chain length (Zhang *et al.*, 1999; Dresser *et al.*, 2002). However, the basic structure of BACs is different from n-tetraalkylammonium compounds. Previous pharmacophore studies on the OCTs showed that inhibitors with a positively charged moiety and a hydrophobic aromatic moiety separated by a distance (i.e., the Ar–N distance) around 1-3 carbon length offer the optimal inhibitor binding to the transporter (Zolk *et al.*, 2009). The presence of the positive charge and the benzyl group at 1 carbon length in all BACs may already satisfy these basic pharmacophore features required for the inhibition of these transporters (**Figure 3.1**). Hence, further increasing the alkyl chain lenght.may not have a significant impact on inhibitor potency.

The alkyl chain length does, however, appear to play a role in the substrate-status of these compounds, as our uptake studies revealed BAC C8 and C10, are good substrates of hOCT1-3 and hMATE1/2K (**Figure 3.5**), whereas hOCT/hMATE-mediated uptake seemed less relevant for C12 and C14. Both C8 and C10 are transported by hOCTs and hMATEs with K_m the low μM range (**Table 3.3**). Detailed kinetic analysis showed that while BAC C8 displayed typical Michaelis-Menten kinetics (**Figure 3.7**), C10 demonstrated a more complex substrate-inhibition profile (**Figure 3.8**). hOCT1, hOCT2, hOCT3 and hMATE1 have been reported to have multiple binding sites (Belzer *et al.*, 2013; Harper and Wright, 2013; Martínez-Guerrero and Wright, 2013; Boxberger *et al.*, 2018; Khanppnavar *et al.*, 2022). Our results suggest that at higher concentrations BAC C10 may bind to a second binding region, which may hinder the transport by either an allosteric effect or steric hindrance (Hutzler and Tracy, 2002; Tracy, 2003; Leow and Chan, 2019). Alternatively, BACs are cationic surfactants that could disrupt membrane or cell integrity at higher concentrations, affecting overall cellular accumulation.

The identification of BAC C8 and C10 as substrates of the hOCT1-3 and hMATE1/2K transporters suggests that the polyspecific organic cation transporters could be involved in the tissue-specific disposition of these compounds in humans. The liver is considered a major site of BAC elimination in humans, where these compounds are metabolized via alkyl chain oxidation mediated by the cytochrome P450 (CYP) enzymes in the CYP4F subfamily and CYP2D6 (Seguin *et al.*, 2019). hOCT1 is highly expressed in the sinusoidal membrane of human hepatocytes, and the identification of BAC C8 and C10 as substrates of hOCT1 suggests that this transporter may mediate the uptake of C8 and C10 BACs into hepatocytes, thus facilitating their metabolism by intracellular CYPs. Additionally, fetal exposure to BACs is of special concern in view that short-chain BACs are potent inhibitors of cholesterol biosynthesis (Herron *et al.*, 2016), which is critical

during neurodevelopment (Zhang and Liu, 2015). In fact, rodents exposed to a quaternary ammonium mixture containing BACs have been reported to have decreased fertility and increased incidence of neural tube defects in embryos (Melin *et al.*, 2014, 2016; Hrubec *et al.*, 2017). hOCT3 is highly expressed in the human placenta and could facilitate fetal exposure to organic cation drugs (Lee *et al.*, 2018). Although no data is currently available regarding BAC C8 and C10 fetal accumulation, it is possible that hOCT3 could facilitate the placental transport of BACs, contributing to the deleterious effects observed in embryonic development.

The hOCT2 and hMATE1/2K transporters have been implicated in the renal elimination and accumulation of many organic cations (Yonezawa and Inui, 2011; Yin and Wang, 2016; López Quiñones *et al.*, 2020). The identification of BAC C8 and C10 as substrates of hOCT2 and hMATE1/2K (**Figure 3.5**), and the results from our transepithelial transport and permeability study employing hOCT2/hMATE1 double-transfected cells (**Figure 3.9**) indicate the involvement of these renal transporters in renal disposition of these short-chain BACs. Although no parent BACs have been found in human urine samples (Li *et al.*, 2023), it is possible that C8 and C10 are secreted by hOCT2/hMATEs but undergo complete reabsorption in the nephron tubules, similarly to what has been reported for choline (Wright *et al.*, 1992). Importantly, the kidneys have been consistently reported as a major organ for BAC accumulation in various biodistribution studies in rats. For instance, 30 minutes after a single intravenous dose of BAC mixture (7 mg/kg), the highest level of BAC accumulation was observed in the kidneys, which is ~ 42-fold higher than serum concentrations (Xue *et al.*, 2002). Similarly, 24 hours after oral administration of BACs (250 mg/kg) to rats, kidney concentrations were 15-fold higher than in blood (Xue *et al.*, 2004). Kera et al. (2021) further demonstrated that shorter-chain BACs reached higher concentrations in the kidneys of rats in comparison to longer-chain BACs (C12 > C14 > C16) following IV

administration of a BAC mixture containing equal amounts of each chain length. In contrast, the lungs and spleen preferentially accumulated longer chain BACs (C16 > C14 > C12). In the renal proximal tubule cells, hOCT2 and hMATE1 sequentially mediate the uptake and the efflux of substrates, and the interplay between the two transporters can significantly impact intracellular accumulation of the substrates. If efflux is slower than uptake, compounds will significantly accumulate and potentially lead to nephrotoxicity (Yonezawa and Inui, 2011; Yin and Wang, 2016). The higher accumulation observed in the hOCT2/hMATE1-transfected cells in comparison to vector cells when BACs were applied to the basal chamber suggests that hMATE1-mediated efflux is less efficient than OCT2-mediated uptake (**Figure 3.10**).

Interestingly, we also observed high accumulation of BACs in the hOCT2/hMATE1-transfected cells when BACs were applied to the apical chamber (A-to-B) (**Figure 3.10 A and B**). This may suggest that the initial high BAC concentrations in the apical chamber of our in vitro system may drive hMATE1 to function as an uptake transporter, allowing BACs to accumulate intracellularly. The contribution of hMATE1 to the apical uptake of BAC C8 and C10 was further corroborated by the inhibitory effect of pyrimethamine – a classic hMATE1 inhibitor – which reduced C8 and C10 accumulation by 40% and 35%, respectively, when added apically (**Figure 3.10 C and D**). This is different from what has been previously observed in our laboratory for other hOCT2/hMATE1 substrates such as atenolol, cimetidine and meta-iodobenzylguanidine (Yin *et al.*, 2015, 2016; López Quiñones *et al.*, 2020), for which intracellular accumulation in the A-to-B direction in hOCT2/hMATE1-transfected cells was either comparable or only slightly higher than accumulation in vector-transfected cells. The reason behind this difference is currently unknown. However, in contrast to the other organic cations studied in this double-transfected system, BACs are membrane disruptors, and their addition to the apical side may alter the

microenvironment around the apical membrane of cells and dissipate the proton gradient across the membrane, which could potentially impact the directionality of hMATE1-mediated transport. In conclusion, our Transwell study results demonstrate that the expression of hOCT2 and hMATE1 have substantial impact on the intracellular accumulation of BAC C8 and C10, and thus these transporters may represent a previously unrecognized pathway driving intrarenal accumulation of short-chain BACs in vivo.

In summary, we provide the first evidence that BACs can interact with the polyspecific organic cation transporters both as inhibitors and substrates. Our results showed that BACs C8 to C14 are potent inhibitors towards hOCT1-3 and hMATE1/2K, and that the shorter alkyl chain BACs (C8 and C10) are excellent substrates of these transporters. Our data suggests that hOCT1 and hOCT3 can be determinants in the distribution of BAC C8 and C10 into tissues such as the liver and placenta, whereas hOCT2 and hMATE1 contribute to renal accumulation of these compounds. Our findings provide new insights on the molecular mechanisms driving the tissue-specific disposition of BACs which could have implications for understanding and predicting tissue exposure and organ susceptibility to BAC toxicity in humans as a result of chronic environmental exposure.

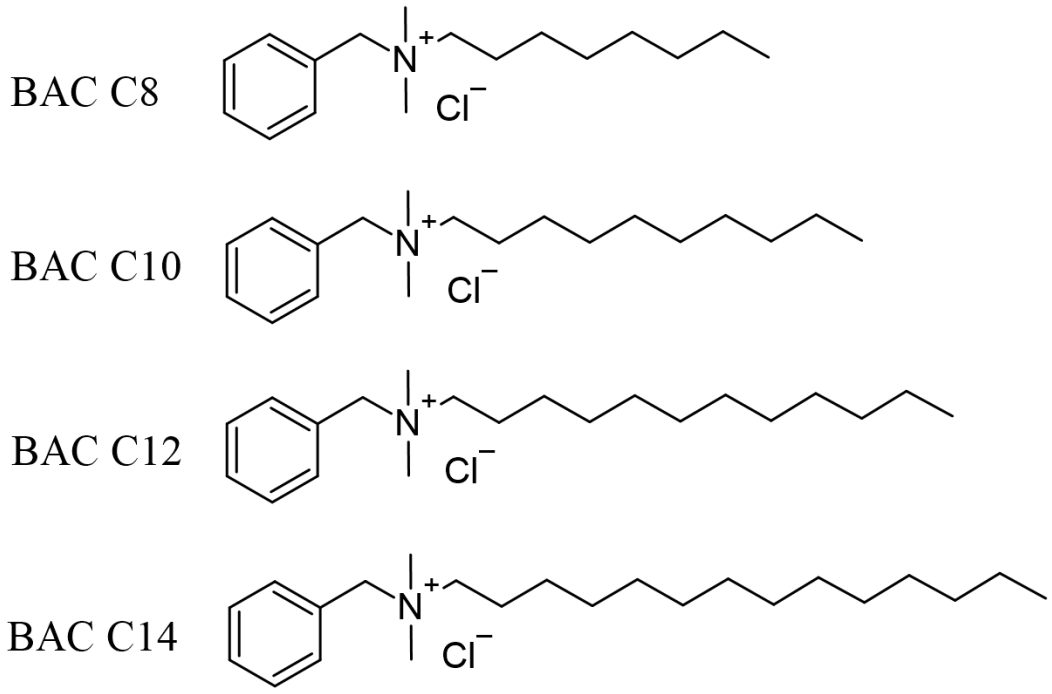

Figure 3.1. Structure of benzalkonium chlorides (BAC) C8, C10, C12 and C14.

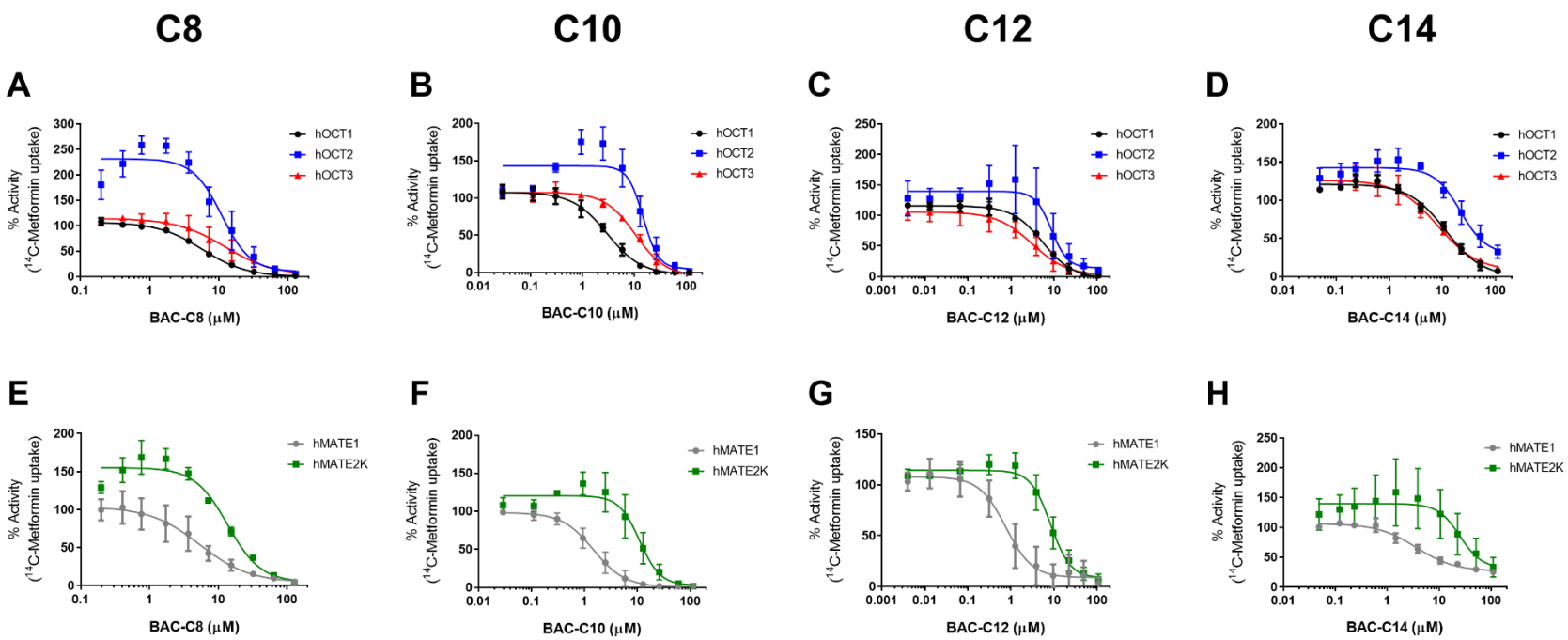

Figure 3.2. Concentration-dependent inhibition of hOCT1, hOCT2, hOCT3, hMATE1, and hMATE2K by BAC C8, C10, C12, and C14.

Uptake of ^{14}C-metformin (8.7 μM) in the absence and presence of BAC C8 (A and E), C10 (B and F), C12 (C and G) and C14 (D and H) was measured in both vector- and transporter-transfected HEK293 cells for 4 minutes at 37ºC. Transporter-specific uptake was obtained by subtracting the activity in vector cells from the activity in transporter-expressing cells, and data is presented as percentage of metformin uptake in the absence of BACs. Each data point represents mean ± SD from at least three independent experiments. IC_{50} values obtained from the dose-dependent inhibition curves are summarized in **Table 3.2**.

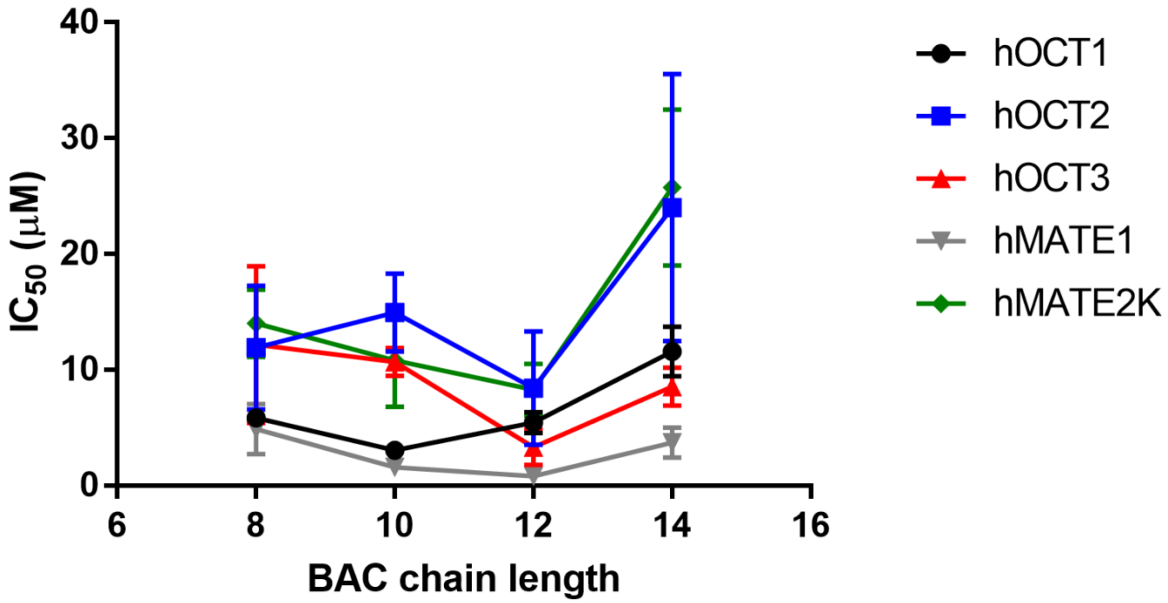

Figure 3.3. Relationship between the alkyl chain length of BACs and their IC_{50} towards hOCT1, hOCT2, hOCT3, hMATE1 and hMATE2K.

Each point represents the mean ± SD IC_{50} value obtained from at least three independent experiments. Although no apparent trend was observed between inhibitory potency and alkyl chain length, BACs appear to be slightly more potent inhibitors of hMATE1.

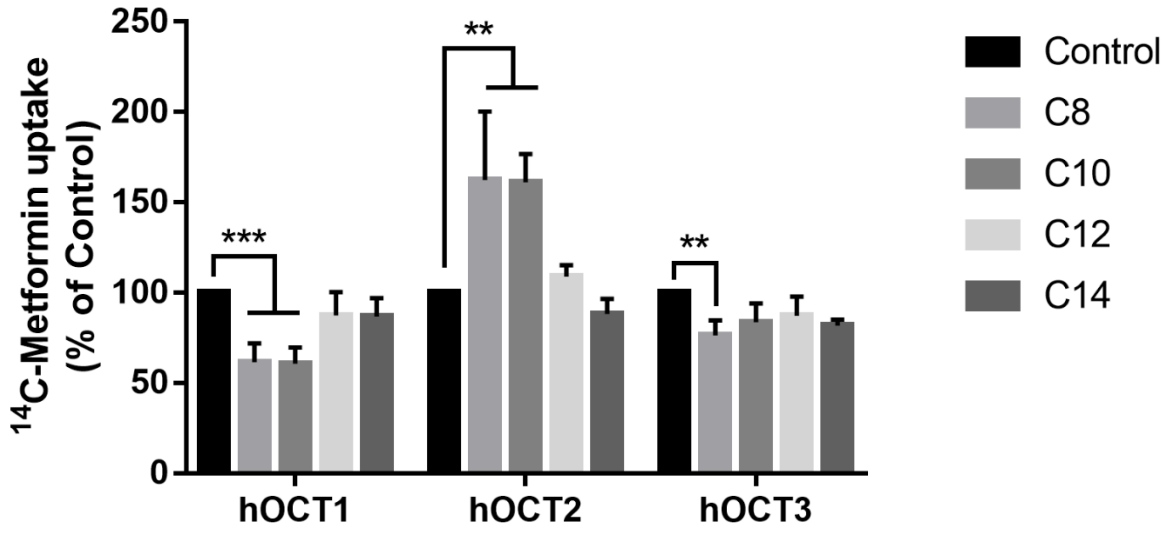

Figure 3.4. Trans-stimulation of ^{14}C-Metformin uptake in hOCT1-, hOCT2-, and hOCT3-expressing HEK293 cells.

Cells were preincubated for 15 minutes at 37°C in the absence (control) or presence of BACs at 1 µM. BACs were removed from extracellular space by washing with ice-cold buffer before cells were incubated for 4 minutes at 37°C with 8.7 µM ^{14}C-Metformin (1 µCi/mL). Transporter-specific uptake was calculated by subtracting uptake in vector-transfected cells subjected to the same conditions, and uptake was normalized to each cell line control. Each bar represents mean ± SD from four independent experiments. The uptake of metformin after preincubation with BACs was compared to the control for each transporter-transfected cell line, and statistical significance was determined by using one-way ANOVA followed by Dunnett's post hoc test (** $P < 0.01$; *** $P < 0.001$).

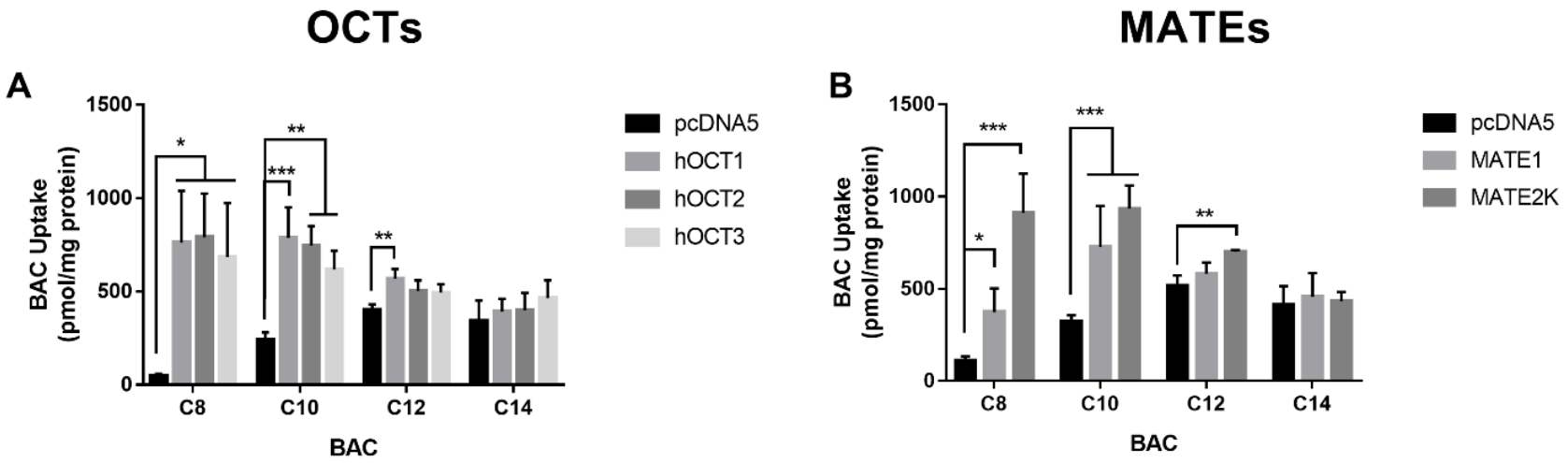

Figure 3.5. Uptake of BAC C8, C10, C12 and C14 by hOCT1-3 (A), and hMATE1/2K (B).

The uptake of 1 µM BAC (C8 to C14) was measured after 10 minutes incubation at 37°C in both pcDNA5 (vector) and transporter expressing HEK293 cells. Data are presented as the means ± SD from three independent experiments. The uptake of each BAC in transporter-expressing cells was compared with that in vector-transfected cells (* $P < 0.05$; ** $P < 0.01$; *** $P < 0.001$). Statistical significance was determined by using one-way ANOVA followed by Dunnett's test.

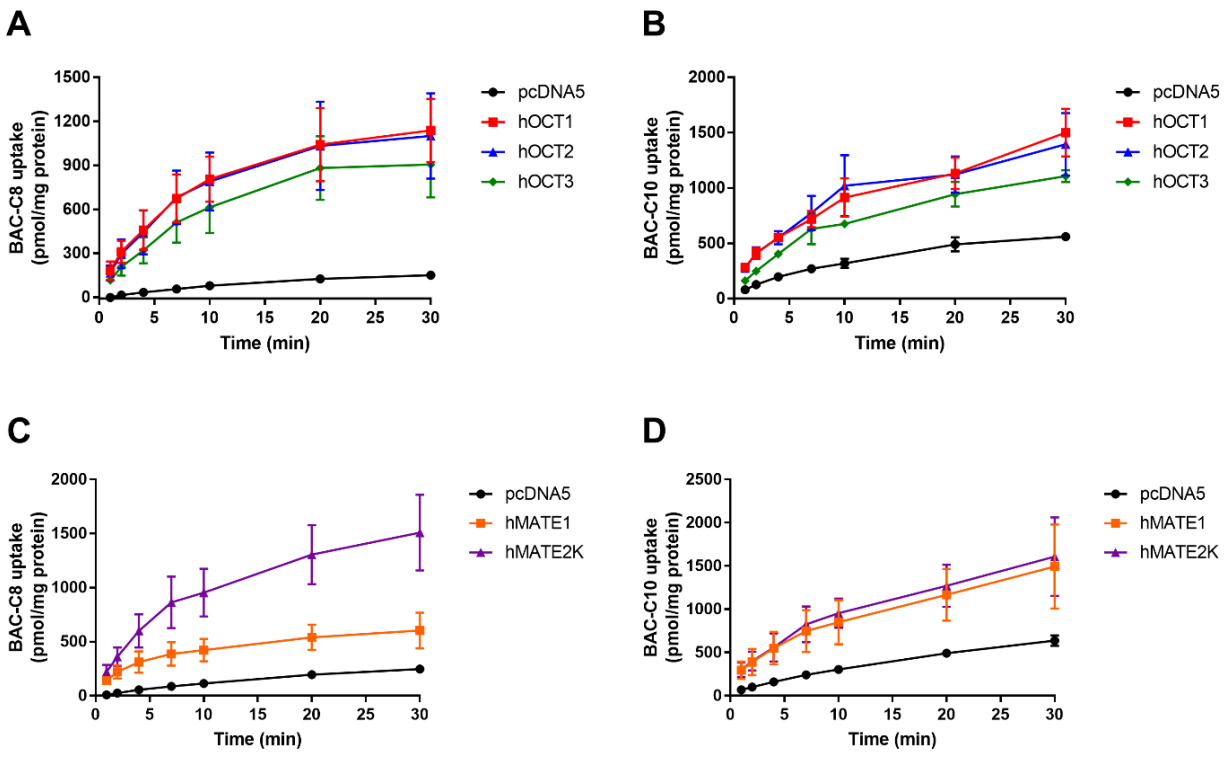

Figure 3.6. Time course of BAC C8 and C10 uptake mediated by hOCT1-3 and hMATE1/2K.

Uptake of 1 µM BAC C8 (A and C) or C10 (B and D) was measured in HEK293 cells expressing pcDNA5 empty vector (black), hOCT1 (red), hOCT2 (blue), hOCT3 (green), hMATE1 (orange) and hMATE2K (purple) at specified time points (1 to 30 minutes) at 37°C. Data points represent the mean ± S.D. from three independent experiments.

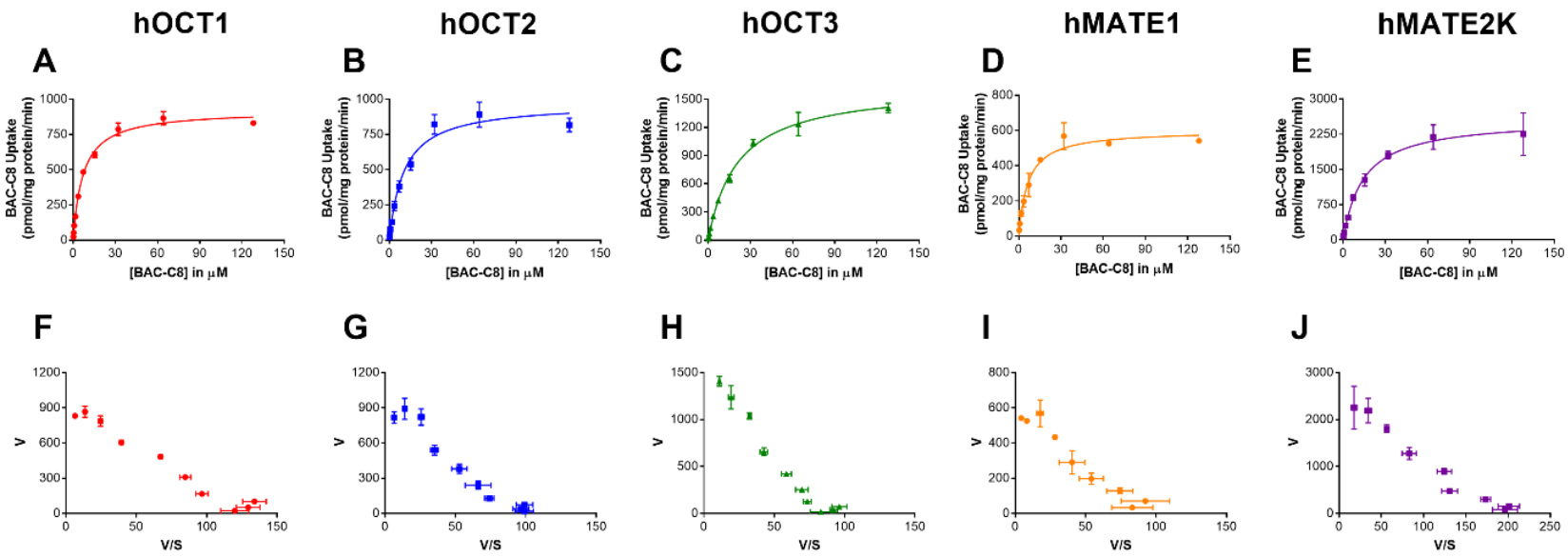

Figure 3.7. BAC C8 uptake kinetics by hOCT1-3 and hMATE1/2K.

Concentration-dependent uptake was measured in both control and transporter-expressing cell lines at 37°C within the linear phase of uptake (4 minutes for hOCT1-3 and 2 minutes for hMATE1/2K). Transporter-specific uptake was obtained by subtracting the uptake in control cells from the uptake in transporter-expressing cells. (A-E) panels display saturation curves (v vs. s) and (F-J) panels show Eadie-Hofstee transformations (v vs. v/s) for the kinetic data. Based on the Eadie-Hofstee plots, the standard Michaelis-Menten equation (**Equation 3.2**) was fitted to the data from hOCT1- (A), hOCT2- (B), hOCT3- (C), hMATE1- (D) and hMATE2K- (E) mediated uptake of BAC C8. Concentration-dependent uptake was performed independently three times for each transporter, and results from one

representative experiment are shown. Data points represent the means ± S.D. in triplicate. The kinetic parameters summarized in **Table 3.3** are the mean ± S.D. of the values from all three independent experiments.

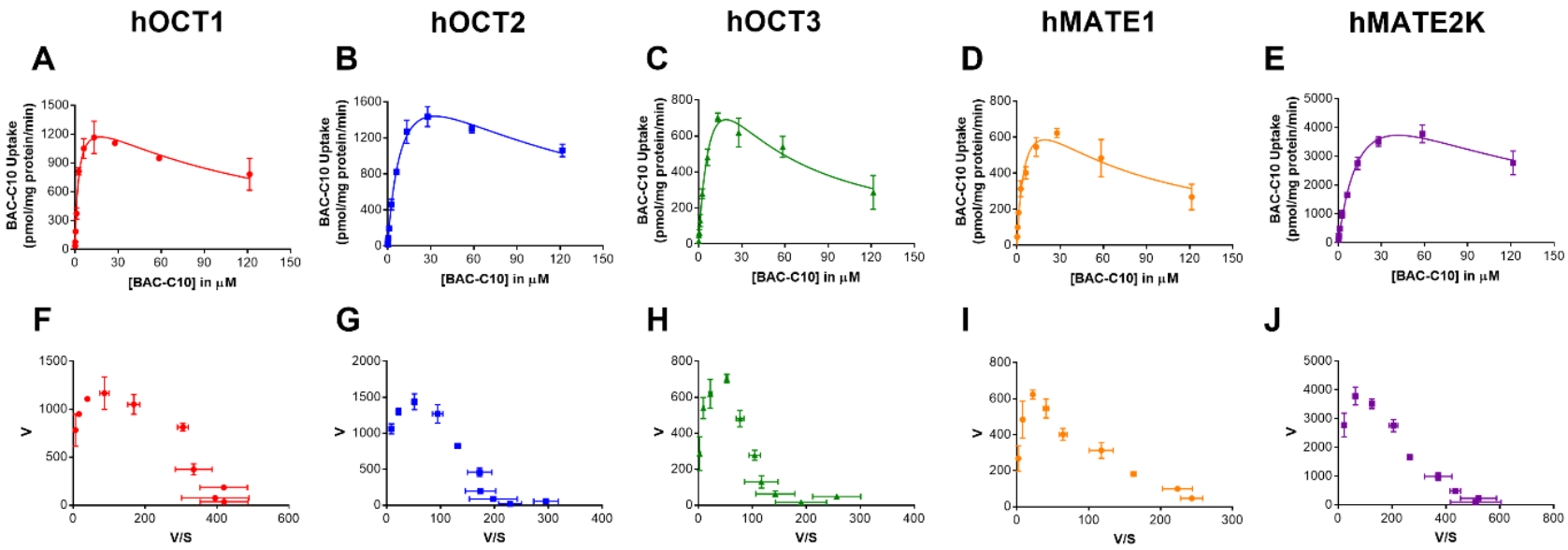

Figure 3.8. BAC C10 uptake kinetics by hOCT1-3 and hMATE1/2K.

Concentration-dependent uptake was measured in both control and transporter-expressing cell lines at 37°C within the linear phase of uptake (4 minutes for hOCT1-3 and 2 minutes for hMATE1/2K). Transporter-specific uptake was obtained by subtracting the uptake in control cells from the uptake in transporter-expressing cells. (A-E) panels display saturation curves (v vs. s) and (F-J) panels show Eadie-Hofstee transformations (v vs. v/s) for the kinetic data. Based on the Eadie-Hofstee plots, a substrate-inhibition kinetic model (**Equation 3.3**) was fitted to the data from hOCT1- (A), hOCT2- (B), hOCT3- (C), hMATE1- (D) and hMATE2K- (E) mediated uptake of BAC C10. Concentration-dependent uptake was performed independently three times for each transporter, and results from one

representative experiment are shown. Data points represent the means ± S.D. in triplicate. The kinetic parameters summarized in **Table 3.3** are the mean ± S.D. of the values from all three independent experiments.

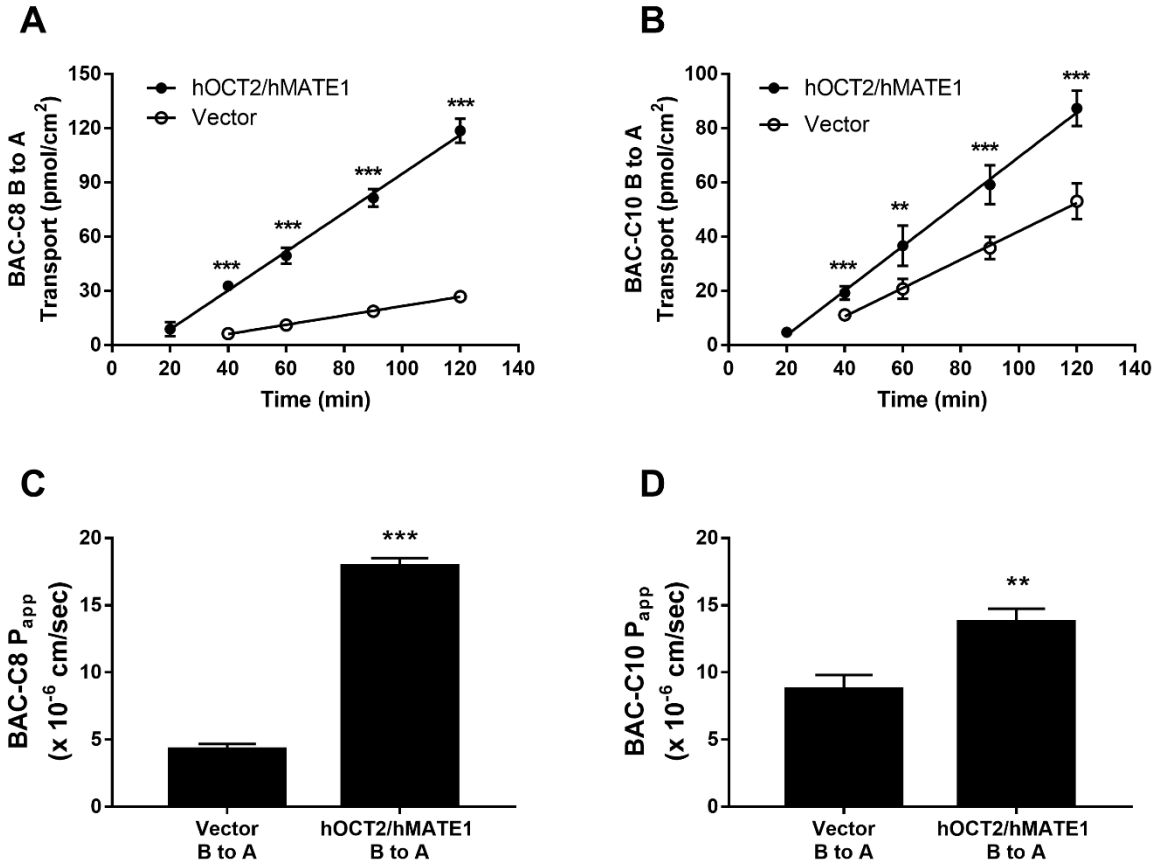

Figure 3.9. Transepithelial transport and apparent permeability (P_{app}) of BAC C8 and C10 in vector-transfected and hOCT2/hMATE1 double-transfected MDCK cells.

Basolateral to apical (B-to-A) transport of BAC C8 (A) or C10 (D) across vector (open circle) and hOCT2/hMATE1-transfected (closed circle) MDCK monolayers. Apical to basolateral (A-to-B) transport of BAC C8 and C10 were below the limit of quantification and thus are not shown. Transport was initiated by adding KRH buffer containing 1 µM BAC to the basal chamber, and a 100 µL aliquot was collected periodically from the apical chamber and replenished with an equal volume of KRH buffer. BAC C8 and C10 in the aliquots were measured by LC-MS/MS. The pH in the apical and basal chamber was 6.0 and 7.4, respectively. B-to-A P_{app} of BAC C8 (C) and BAC C10 (D) was calculated using **Equation 3.4** described in *Materials and Methods*. Transport

and permeability were compared between vector- and OCT2/hMATE1-transfected MDCK cells (** $P < 0.01$; *** $P < 0.001$). Statistical significance was determined by using an unpaired Student's t test with the Bonferroni correction when multiple comparisons were done. Each data point represents the means ± S.D. from three independent experiments.

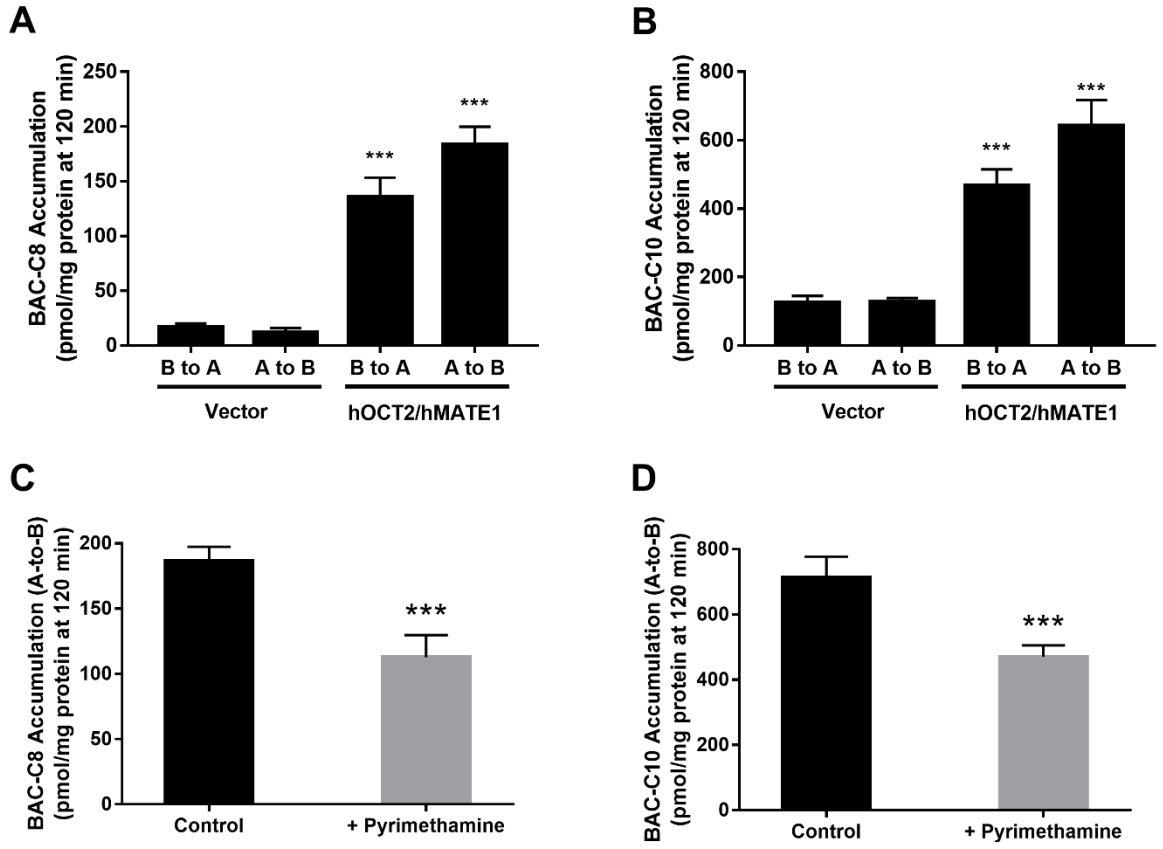

Figure 3.10. Intracellular accumulation of BAC C8 and C10 in vector- and hOCT2/hMATE1 double-transfected MDCK cells.

At the end of the 120-minute transepithelial transport assay, MDCK cells were lysed and the intracellular accumulation of BAC C8 (A) and C10 (B) was measured by LC-MS/MS and normalized to protein content. Intracellular accumulation of C8 and C10 applied basally or apically in hOCT2/hMATE1-transfected cells were compared to their respective accumulation in vector-transfected MDCK cells (*** $P < 0.001$). Additionally, accumulation of C8 (C) and C10 (D) applied apically in hOCT2/hMATE1-transfected cells was measured in the absence (control) or presence of 10 µM pyrimethamine (also applied apically) and values were compared (*** $P < 0.001$). Statistical significance was determined by using an unpaired Student's t test with the

Bonferroni correction when multiple comparisons were done. Each data point represents the means ± S.D. from data obtained from three independent experiments.

Table 3.1. Mass-to-charge (m/z) transitions monitored for BACs and d_7-BACs in targeted MS/MS.

A Waters Synapt XS quadrupole time-of-flight (QToF) mass spectrometer was used. The nominal m/z values are reported for the precursors, while fragments m/z are reported after mass correction based on the leucine-enkephalin lock mass reference.

Analyte	**Precursor *m/z* (nominal)**		**Fragment *m/z* (accurate)**
BAC-C_8	248	→	156.176 / 91.055
BAC-C_{10}	276	→	184.206 / 91.055
BAC-C_{12}	304	→	212.238 / 91.055
BAC-C_{14}	332	→	240.269 / 91.055
d_7-BAC-C_{10}	283	→	184.206 / 98.098
d_7-BAC-C_{12}	311	→	212.238 / 98.098
d_7-BAC-C_{14}	339	→	240.269 / 98.098

Table 3.2. IC_{50} of BAC C8, C10, C12 and C14 of metformin uptake by hOCT1-3 and hMATE1/2K.

Data is presented as mean ± S.D. of the IC_{50} values from three or four independent experiments.

BAC	IC_{50} ± S.D. (μM)				
	hOCT1	**hOCT2**	**hOCT3**	**hMATE1**	**hMATE2K**
C8	5.9 ± 0.6	11.9 ± 5.3	12.2 ± 6.8	4.9 ± 2.2	14.0 ± 2.9
C10	3.0 ± 0.7	14.9 ± 3.4	10.7 ± 1.2	1.6 ± 0.7	10.8 ± 4.0
C12	5.5 ± 0.9	8.4 ± 4.9	3.3 ± 1.5	0.83 ± 0.38	8.3 ± 2.2
C14	11.6 ± 2.1	24.0 ± 11.5	8.6 ± 1.6	3.7 ± 1.3	25.8 ± 6.8

Table 3.3. Kinetic parameters of BAC C8 and BAC C10 uptake by hOCT1-3, and hMATE1/2K.

Models were chosen based on examination of Eadie-Hofstee plots. The standard Michaelis-Menten equation (**Equation 3.2**) was fitted to the BAC C8 data, while a substrate-inhibition model (**Equation 3.3**) was fitted to the BAC C10 uptake kinetics data. Results are represented as mean ± S.D. of the K_m, V_{max} and $K_{i,[s]}$ from three independent experiments.

Transporter	BAC C8		BAC C10		
	K_m (μM)	**V_{max} (pmol/mg protein/min)**	**K_m (μM)**	**V_{max} (pmol/mg protein/min)**	**$K_{i,[s]}$ (μM)**
hOCT1	8.7 ± 2.3	1091 ± 339	6.8 ± 3.8	1480 ± 163	93.1 ± 19.4
hOCT2	10.4 ± 3.9	965 ± 43	19.1 ± 6.8	2673 ± 412	106.5 ± 11.2
hOCT3	18.9 ± 2.4	1716 ± 157	27.4 ± 22.1	2421 ± 1233	37.1 ± 19.3
hMATE1	6.0 ± 0.7	487 ± 206	4.9 ± 1.4	975 ± 49	52.2 ± 16.2
hMATE2K	9.7 ± 4.1	2239 ± 385	19.3 ± 0.3	6102 ± 973	111 ± 27.6

Chapter 4. USE OF A DOUBLE-TRANSFECTED SYSTEM TO PREDICT OCT2/MATE1-MEDIATED RENAL DRUG-DRUG INTERACTIONS

4.1 ABSTRACT

Accurate predictions of renal drug-drug interactions (DDIs) mediated by the human organic cation transporter 2 (hOCT2) and multidrug and toxin extrusion proteins (hMATEs) remain challenging. Current DDI evaluation using plasma maximal unbound inhibitor concentrations ($I_{max,u}$) and IC_{50} values determined in single transporter-transfected cells frequently leads to false or overprediction, especially for hMATE1. Emerging evidence suggests intracellular unbound inhibitor concentration may be more relevant for hMATE1 inhibition in vivo. However, the determination of intrarenal inhibitor concentrations is impractical. Here we explored the use of hOCT2/hMATE1 double-transfected MDCK cells as a new in vitro tool for DDI risk assessment. Our results showed that potent in vitro hMATE1 inhibitors (hydroxychloroquine, brigatinib, and famotidine) failed to inhibit metformin B-to-A flux in the double-transfected system. On the other side, the classical hOCT2/hMATE1 inhibitors, pyrimethamine and cimetidine, dose-dependently inhibited metformin's apparent B-to-A permeability (P_{app}). The different behaviors of these hMATE1 inhibitors in the double-transfected system can be explained by their different ability to gain intracellular access either via passive diffusion or transporter-mediated uptake. A new parameter ($IC_{50,flux}$) was proposed reflecting the inhibitor's potency on overall hOCT2/hMATE1-mediated tubular secretion. The $IC_{50,flux}$ values significantly differ from the IC_{50} values determined in single transporter-transfected cells. Importantly, the $IC_{50,flux}$

accurately predicted in vivo DDIs (within 2-fold) when used in a static model. Our data demonstrated that the $IC_{50,flux}$ approach circumvents the need to measure intracellular inhibitor concentrations and more accurately predicted hOCT2/hMATE1-mediated renal DDIs. This system represents a new approach that could be used for improved DDI assessment during drug development.

4.2 INTRODUCTION

The renal organic cation secretion system, constituted by the organic cation transporter 2 (hOCT2) and multidrug and toxin extrusion proteins 1 and 2K (hMATE1/2K), is a major drug secretion system in the human kidney. Respectively expressed in the basolateral and the apical membrane of renal proximal tubular epithelial cells (PTECs), hOCT2 and hMATEs work sequentially to mediate renal secretion of many cationic drugs such as metformin, atenolol, and cimetidine (Morrissey *et al.*, 2013; Yin and Wang, 2016). Inhibition of hOCT2/hMATEs can lead to drug-drug interactions (DDIs), which may impact not only systemic exposure and pharmacokinetics of substrate drugs but also their intrarenal accumulation, potentially leading to nephrotoxicity (Morrissey *et al.*, 2013; Yin and Wang, 2016). Evaluation of new molecular entities (NMEs) as substrates and inhibitors of renal hOCT2 and hMATE1/2K transporters is recommended by regulatory agencies, including the US Food and Drug Administration (FDA), the European Medicines Agency (EMA) and the Pharmaceuticals and Medical Devices Agency (PMDA).

Current guidelines for initial DDI assessment are based on the inhibitor's maximal unbound plasma concentration ($I_{max,u}$) and its half-maximal inhibitory concentration (IC_{50}) towards a specific transporter determined using single-transfected cell lines (FDA. In vitro DDI guidance,

2020). If the $I_{max,u}/IC_{50}$ value is larger than the regulatory agency's cutoff value (e.g., ≥ 0.1 for hOCT2 or hMATE1 by FDA), the sponsor should consider conducting an in vivo DDI study (FDA. In vitro DDI guidance, 2020). While this approach is widely adopted due to its simplicity and feasibility, there are gaps in translating in vitro data to successfully predict in vivo DDIs, especially for hMATEs. Indeed, many compounds exhibit potent hMATE1 inhibition in vitro with $I_{max,u}/IC_{50}$ surpassing the cutoff value, but this does not translate to DDIs in vivo (Hibma *et al.*, 2016; Mathialagan *et al.*, 2021; Ogasawara *et al.*, 2021; Krishnan *et al.*, 2022). For instance, famotidine has an $I_{max,u}/IC_{50}$ value of 4 for hMATE1 (40-fold above the FDA cutoff value). However, clinical evaluation showed no impact of famotidine on metformin exposure in vivo (Hibma *et al.*, 2016). The high rate of false- or over-prediction for hMATE1-mediated DDIs is concerning as it can lead to costly and unnecessary clinical studies (Mathialagan *et al.*, 2021; Krishnan *et al.*, 2022).

One possible reason contributing to the false- or over-prediction of hMATE1-mediated DDIs is that plasma $I_{max,u}$ is used to predict the degree of hMATE1-inhibition in vivo. Physiologically, hMATE is located at the apical (urine-facing) membrane of PTECs, not in direct contact with the plasma. Although unbound drug is also present in the filtrate, previous evidence suggests that hMATE inhibitors may need to enter PTECs in order to inhibit the transporter (Yin *et al.*, 2016). Thus, unbound intracellular concentration of the inhibitor would be more relevant in predicting hMATE inhibition than $I_{max,u}$, which may significantly differ from unbound intracellular concentrations due to multiple factors, including passive permeability, transporter-mediated uptake/efflux, and intracellular binding or sequestration of the inhibitor (**Figure 4.1**). However, accurate determination or prediction of intracellular concentrations in human PTECs can be challenging and laborious (Guo *et al.*, 2018). Additionally, many inhibitors interact with both hOCT2 and hMATEs with varying inhibition potencies. While tubular secretion is sequentially

mediated by hOCT2 and hMATEs, initial DDI assessment is based on the inhibition of individual transporters, which does not consider the inhibitor's overall impact on the net secretion process and possible interplay between apical and basolateral transporters.

The Transwell system employing transporter-transfected Madin-Darby canine kidney (MDCK) cells is commonly used in drug transporter research. Unlike uptake studies which measure cellular accumulation, the Transwell system allows the measurement of substrate flux across a monolayer of MDCK cells. Single- or double-transfected MDCK cells are typically employed in substrate evaluation for efflux transporters (e.g. P-gp) or assessment of substrate transepithelial transport mediated by multiple transporters (e.g. the hOCT2/hMATE1 pathway) (Sato *et al.*, 2008; König *et al.*, 2011; Yin *et al.*, 2015, 2016; López Quiñones *et al.*, 2020). However, its utility in quantitative assessment of renal DDIs has been largely unexplored. Here, we used hOCT2/hMATE1 double-transfected cells as an in vitro model to assess the inhibitory potential of compounds on the transepithelial flux of the organic cation probe substrate metformin. A new parameter reflecting the inhibition potency of a compound on metformin transepithelial basal-to-apical (B-to-A) flux ($IC_{50,flux}$) is proposed and used to predict the in vivo DDI potential using a static model. Our results showed that this approach can accurately predict hOCT2/hMATE1-mediated renal DDIs without the necessity to measure intracellular inhibitor concentrations.

4.3 Materials and Methods

4.3.1 *Materials*

[^{14}C]Metformin (112 mCi/mmol) was purchased from Moravek Biochemicals, Inc. (Brea, CA). [^{3}H]mannitol (20 Ci/mmol) was purchased from American Radiolabeled Chemicals, Inc. (St.

Louis, MO). Hydroxychloroquine (HCQ) was purchased from Toronto Research Chemicals, Inc. (North York, ON, Canada). Brigatinib (BRI) was purchased from MedChemExpress LLC (Monmouth Junction, NJ). Pyrimethamine (PYR) was purchased from TCI America, Inc. (Portland, OR). Cimetidine (CIM) and famotidine (FAM) were purchased from Sigma Aldrich (St. Louis, MO). All chemicals were analytical grade. Cell culture media and reagents were purchased from Invitrogen (Carlsbad, CA).

4.3.2 *Cell Lines and Cell Culture*

Flp-In human embryonic kidney (HEK) 293 cells stably transfected with hOCT2, hMATE1, or empty pcDNA5/FRT vector (control) were previously established in our laboratory (Duan *et al.*, 2015; Yin *et al.*, 2015). Both control and transporter-expressing HEK293 cells were maintained in high glucose Dulbecco's modified Eagle's medium (DMEM) supplemented with 10% fetal bovine serum, 2 mM L-glutamine, 100 IU/mL penicillin, 100 µg/mL streptomycin, and 150 µg/mL hygromycin B. The surface of the flasks and plates were coated with 0.1 mg/mL poly-D-lysine in Milli-Q water to improve HEK293 cell attachment. The Madin-Darby Canine Kidney (MDCK) cells double-transfected with hOCT2 and hMATE1 or empty vector were previously generated and validated in our laboratory (Yin *et al.*, 2015) and were maintained in DMEM supplemented with 15% fetal bovine serum, 500µg/mL G418, and 200µg/mL hygromycin B. All cell lines were cultured in a 37ºC humidified incubator with 5% CO_2.

4.3.3 *Inhibition Assays in HEK293 Cells*

Inhibition assays were performed as previously described (Duan and Wang, 2010; Yin *et al.*, 2015, 2016) with slight modifications. Briefly, HEK293 cells were seeded in poly-D-lysine

coated 96-well plates and grown to greater than 90% confluency (1–2 days). Cells were washed twice with prewarmed Krebs-Ringer-HEPES (KRH) buffer (5.6 mM glucose, 125 mM NaCl, 4.8 mM KCl, 1.2 mM KH_2PO_4, 1.2 mM $CaCl_2$, 1.2 mM $MgSO_4$, and 25 mM HEPES, pH 7.4). Uptake of ^{14}C-labeled metformin in vector-transfected and transporter expressing HEK293 cells were performed within the linear range of metformin uptake at 37°C in the presence or absence of various inhibitor concentrations. Experiments were conducted at sub-saturating concentration of ^{14}C-metformin (8.9 µM and 1 µCi/mL). For hOCT2-transfected cells uptake was performed using KRH at pH 7.4, while for hMATE1-transfected cells KRH at pH 8.0 was used to generate an outwardly directed proton gradient favoring metformin uptake. Uptake was quenched by washing the cells three times with ice-cold KRH buffer. After washing, cells were solubilized with 100 µL 1M NaOH at 37ºC and neutralized with 100 µL 1M HCl after 1 hour. Radioactivity of 150 µL of the lysates was measured by a Tri-Carb Liquid Scintillation Counter (Perkin Elmer, Waltham, MA). The protein content in the lysates was measured through the BCA method using 20 µL of the lysate, and the uptake in cells was normalized to their total protein content. Transporter-specific uptake was calculated by subtracting the uptake in the vector-transfected cells, and uptake in the presence of inhibitor was normalized to uptake in the absence of inhibitor.

4.3.4 *Transwell Studies in hOCT2/hMATE1 Double-Transfected MDCK Cells*

Transepithelial flux of metformin across MDCK cell monolayers was determined as previously described (Yin *et al.*, 2015, 2016). Briefly, empty vector and hOCT2/hMATE1-expressing MDCK cells were seeded at a density of 2 x 10^5 cells/cm^2 on 12-well Corning™ Transwell™ inserts (PET membrane, 0.4 µM pore size). Transport experiments were performed 5 days after seeding. Integrity of the MDCK monolayer and proper formation of tight junctions

was verified by measurement of transepithelial flux of mannitol as described previously (Yin *et al.*, 2015), and only data from inserts in which mannitol apparent permeability (P_{app}) value was below 1 x 10^{-6} cm/s were accepted. After removal of cell culture media from both sides of the inserts, cells were carefully washed three times with warm KRH buffer pH 7.4. For apical-to-basal (A-to-B) transport, 1.5 mL of KRH buffer (pH 7.4) was added to the B chamber, and transport was initiated by adding 0.5 mL of KRH (pH 6.0) containing [^{14}C]metformin (1µCi/mL, 8.9µM) and [^{3}H]mannitol (1µCi/mL, 50nM) to the A chamber. Similarly, for basal-to-apical (B-to-A) transport, 0.5 mL of KRH buffer (pH 6.0) was added to the A chamber, and transport was initiated by adding 1.5 mL of KRH (pH 7.4) containing radiolabeled metformin and mannitol to the B chamber. An apical pH of 6.0 was used based on previously published methods by our and other groups to mimic the average urine pH (Tsuda *et al.*, 2009; Rowland and Tozer, 2010; Müller *et al.*, 2011; Yin *et al.*, 2015). To measure transcellular transport, at each time point 50 µL of sample from the receiving chamber were collected for metformin and mannitol quantification and replaced with an equal volume of the appropriate KRH buffer. Inhibitors studied (HCQ, BRI, PYR, CIM and FAM) were applied to the basal, apical or both chambers at the start of the Transwell study as specified in the figure legends. At the end of the experiment (120 minutes), inserts were washed three times with ice-cold KRH buffer and cells were lysed using 1M NaOH and then neutralized with 1M HCl after 1 hour. Radioactivity of the cell lysate and buffer aliquots collected during the transcellular transport time course was measured by a Tri-Carb Liquid Scintillation Counter (Perkin Elmer, Waltham, MA). Intracellular accumulation of metformin was normalized to total protein content in cell lysate, which was measured by the BCA method.

4.3.5 *Data Analysis*

Inhibition studies in HEK293 cells were performed in triplicate and repeated at least three times independently. Transwell studies using MDCK cells were performed in two individual apparatuses and were repeated independently at least three times. Data is reported as mean ± SD from at least three independent replicates. Data was plotted and fitted through nonlinear regression using GraphPad Prism 7.0 (GraphPad Software Inc., La Jolla, CA). IC_{50} values were obtained by fitting the following four-parameter dose-dependent inhibition equation to the data:

Equation 4.1: $$V = Bottom + \frac{(Top - Bottom)}{1 + (I/IC_{50})^{H}}$$

where V is the rate of uptake – or apparent permeability (P_{app}) value – in the presence of inhibitor; Bottom is the residual non inhibitable baseline value constrained to values higher or equal to zero; Top is the rate of uptake – or P_{app} value – in the absence of inhibitor; I is the inhibitor concentration; and H is the Hill coefficient. For the Transwell experiments, the P_{app} of metformin was calculated using the following equation:

Equation 4.2: $$P_{app} = (dQ/dt)/(A * C_0)$$

where dQ/dt is the amount of metformin transported over time, A is the insert membrane surface area, and C_0 is the initial metformin concentration in the donor chamber. Statistical significance was assessed using one-way ANOVA followed by Dunnett's post hoc test to correct for multiple comparisons. A P value less than 0.05 was considered statistically significant.

4.3.6 *Prediction of hOCT2 and hMATE1-Mediated DDIs with Metformin*

The effect of inhibition of hOCT2 and hMATE1 on plasma exposure of metformin was assessed using the mechanistic static model previously proposed by Feng et al. (Feng *et al.*, 2013; Feng and Varma, 2016):

Equation 4.3:
$$\mathbf{AUCR} = \mathbf{1} \,/\, \left(\mathbf{1} - \boldsymbol{f_{sec}} * \frac{[I_{u,max}]/IC_{50}}{1+[I_{u,max}]/IC_{50}}\right)$$

where AUCR represents the area under the concentration-time curve ratio in the presence over absence of an inhibitor; $[I_{max,u}]$ represents the plasma maximum inhibitor unbound concentration; IC_{50} represents the concentration of inhibitor necessary to inhibit 50% of either individual transporter activity or transepithelial flux; and f_{sec} represents the fraction of metformin's renal clearance mediated by secretion in the absence of inhibitors. In our calculations, glomerular filtration rate of healthy young adults was assumed to be 120 mL/min, and metformin f_{sec} was calculated as 0.8 considering that metformin is exclusively renally eliminated, has a renal clearance of 600 mL/min (Bristol-Myers Squibb Company. Glucophage (metformin hydrochloride) [package insert], 2017) and is negligibly bound to plasma proteins.

4.3.7 *Estimated Physicochemical Properties of Compounds*

The strongest basic pKa values for tested inhibitors were collected from https://go.drugbank.com/. Calculated LogP values (computed by XLogP3 3.0) were collected from https://pubchem.ncbi.nlm.nih.gov/. LogD at pH 6.0 and 7.4 were calculated using ChemAxon's Calculator Plugins. The percentage of ionization at pH 7.4 was calculated using the Henderson-Hasselbalch equation.

4.4 RESULTS

4.4.1 *Hydroxychloroquine (HCQ) and Brigatinib (BRI) Selectively Inhibit hMATE1.*

In order to evaluate the impact of inhibitor intracellular accessibility on hMATE1 inhibition in the double-transfected system, it is necessary to have compounds that are selective for hMATE1 inhibition. To expand the profile of hMATE1 selective inhibitors, we chose HCQ and BRI based on literature evidence suggesting these compounds may preferentially inhibit hMATEs over hOCT2 (Takeda Pharmaceutical Company Ltd. ALUNBRIG (brigatinib) [package insert], 2020; Yee *et al.*, 2021). Next, we determined IC_{50} values of HCQ and BRI towards hOCT2 and hMATE1 in HEK293 cells expressing a single transporter. Metformin was used as a probe substrate at a concentration well below its apparent affinity (K_m) value (Yin *et al.*, 2016). For hOCT2-expressing cell line, experiments were performed at pH 7.4, and for hMATE1-expressing cell line, experiments were performed at pH 8.0 (Tanihara, Masuda, Sato, Katsura, Ogawa, and K ichi Inui, 2007). Results showed that both HCQ and BRI preferentially inhibit hMATE1 (**Figure 4.2**). HCQ inhibited hMATE1 with a calculated IC_{50} of 2.4 ± 1.3 µM, and no significant inhibition of hOCT2 was observed up to 100 µM, in agreement to what was previously reported by Yee et al., 2021. BRI was found to be approximately 10-fold more potent towards hMATE1 than hOCT2, with IC_{50} values of 0.63 ± 0.24 µM and 6.5 ± 2.3 µM respectively.

4.4.2 *MATE1 Inhibition by HCQ and BRI Does Not Translate to Inhibition of Metformin Flux in hOCT2/hMATE1 Double-Transfected MDCK Cells.*

Next, we tested the inhibitory potential of HCQ and BRI towards the B-to-A transepithelial flux of metformin in a hOCT2/hMATE1 double-transfected MDCK cell system. An HCQ

concentration of 40 µM and a BRI concentration of 6.25 µM were selected for this study. Based on the IC_{50} values determined in single-transfected HEK293 cells, at these concentrations, HCQ was expected to completely inhibit hMATE1, with no impact on hOCT2 transport (**Figure 4.2 A**), and BRI would lead to near complete inhibition of hMATE1 but only partial inhibition of hOCT2 (**Figure 4.2 B**). In addition, due to stronger hMATE1 inhibition, both drugs were expected to lead to an increase in metformin intracellular accumulation. To assess inhibitor accessibility, inhibitors were applied to the apical, basolateral, or to both Transwell chambers. Contrary to the prediction, HCQ had no or minimal impact on metformin B-to-A transepithelial flux regardless of which chamber it was applied to (**Figure 4.3 A**). Similarly, BRI had no or minimal impact on metformin B-to-A flux over the two-hour time course (**Figure 4.3 B**). When P_{app} of metformin was calculated, no inhibitory effect was observed by either HCQ or BRI, except for a small inhibitory effect of HCQ and BRI when applied to the basal chamber (approximately 15% and 25% reduction respectively) (**Figure 4.4 A and B**). The small inhibitory effect observed by basally added BRI is likely due to partial inhibition of basolateral hOCT2. Consistent with the lack of significant hMATE1 inhibition, there were no changes in metformin intracellular accumulation in the presence of either inhibitor (**Figure 4.4 C and D**). These results demonstrate that although HCQ and BRI are potent hMATE1 inhibitors in the single-transfected cell system, these compounds are unable to inhibit hMATE1 in the hOCT2/hMATE1-transfected MDCK monolayer when substrate is added basolaterally.

4.4.3 *Classic MATE/OCT Inhibitors Dose-Dependently Reduced Metformin Transepithelial Flux in Double-Transfected Cells.*

The lack of inhibition by HCQ and BRI observed in the double-transfected system indicates that these compounds are less likely to produce significant DDIs involving hOCT2/hMATE1 in vivo. Clinical metformin DDI studies using these compounds as perpetrators have not yet been reported in the literature. However, clinical DDI studies have been conducted for several classical inhibitors of the renal organic cation secretion system. Therefore, we explored the usefulness of the Transwell system employing hOCT2/hMATE1 double-transfected MDCK cells in the assessment of DDI potential of the classic OCT2 and MATE1 inhibitors pyrimethamine (PYR) and cimetidine (CIM). We also chose to evaluate famotidine (FAM), which is a selective and potent in vitro hMATE1 inhibitor but did not lead to significant clinical DDI with metformin despite reaching plasma $I_{max,u}$ 4-fold higher than its IC_{50} value (**Table 4.1**) (Hibma *et al.*, 2016). We next determined the dose-dependent effect of PYR, CIM, and FAM in metformin transepithelial flux and intracellular accumulation in the double-transfected MDCK system. Inhibitors were applied to both apical and basal chambers simulating the in vivo microenvironment of the nephron where inhibitors are present in both the plasma and the filtrate. As shown in **Figure 4.5**, PYR and CIM dose-dependently inhibited metformin transepithelial flux and increased metformin intracellular accumulation up to 3-fold in comparison to the absence of inhibitor, suggesting predominant inhibition of apical hMATE1. FAM, however, had minimal impact on metformin transepithelial flux, and led to only a marginal increase in metformin intracellular accumulation at the highest concentration tested (40 µM), which is 160-fold above its reported IC_{50} value towards hMATE1 (0.25 µM) (Hibma *et al.*, 2016). These results are consistent with outcomes from clinical DDI studies, in which co-administration of PYR or CIM with metformin

led to a significant increase in metformin AUC, whereas FAM had no impact on metformin exposure (Somogyi *et al.*, 1987; Kusuhara *et al.*, 2011; Hibma *et al.*, 2016).

4.4.4 *Flux IC_{50} ($IC_{50,flux}$) Values Obtained from Transwell Studies More Accurately Predicted in vivo Metformin DDI.*

The results from our Transwell inhibition study suggest that the hOCT2/hMATE1 double-transfected in vitro system has significant predictive value. To further assess if this approach can be used to quantitatively predict the degree of hOCT2/hMATE1 inhibition in vivo, we propose the calculation of a flux IC_{50} ($IC_{50,flux}$) based on the dose-dependent impact of inhibitor on metformin P_{app} values. The $IC_{50,flux}$ takes into consideration the overall impact of the inhibitor on metformin secretion clearance mediated sequentially by hOCT2 and hMATE1. Metformin P_{app} values were calculated using **Equation 4.2** at varying inhibitor concentrations, and $IC_{50,flux}$ values were then estimated from the dose-response curves (**Figure 4.6** and **Table 4.2**). As shown in **Table 4.2**, the $IC_{50,flux}$ values obtained from P_{app} are different from those IC_{50} reported for either transporter using single-transfected HEK293 cells. According to the latest 2020 FDA guidance, an in vivo DDI study is recommended if $I_{max,u}/IC_{50} \geq 0.1$ for either hOCT2 or hMATE1. To determine whether the use of different in vitro systems (e.g., double-transfected cells in Transwell system) leads to different recommendations for in vivo DDI assessment, the $I_{max,u}/IC_{50}$ values of CIM, PYR, and FAM were calculated using IC_{50} values determined from hOCT2-transfected, hMATE1-transfected or hOCT2/hMATE1 double-transfected cell lines (**Table 4.2**). While the use of hOCT2 IC_{50} values led to calculated ratios below 0.1, the use of hMATE1 IC_{50} values resulted in ratios well above the 0.1 cutoff value (1.36, 5.1, and 4.0 for PYR, CIM, and FAM, respectively), leading to recommendations of in vivo DDI studies for all three compounds. In contrast, when using the

$IC_{50,flux}$ values, the calculated ratios resulted in positive DDI prediction for PYR and CIM (0.29 and 0.36 $I_{max,u}/IC_{50,flux}$, respectively), but not for FAM ($I_{max,u}/IC_{50,flux}$ < 0.025). A predicted recommendation based on Transwell inhibition studies matches the results observed in clinical metformin DDI studies (**Table 4.2**). Next, we predicted the percent change in metformin AUC using a static model (**Equation 4.3**). As shown in **Table 4.2**, while the prediction using hOCT2 IC_{50} value for FAM is consistent with in vivo metformin DDI observation, the use of these values for PYR and CIM led to 35-fold and 8-fold underprediction, respectively. For hMATE1, the use of hMATE1 IC_{50} led to overprediction of PYR and CIM-mediated DDIs by 2.4 and 4-fold, respectively, and a complete false prediction for FAM. In contrast, predictions using the $IC_{50,flux}$ values were all within 2-fold of the observed AUC change from in vivo DDI studies (**Table 4.2**). This data suggests that compared to a prediction based on individual transporter IC_{50} values, the use of $IC_{50,flux}$ values obtained from hOCT2/hMATE1 double-transfected cells more accurately predicted in vivo metformin DDI not only in a qualitative manner (based on the $I_{max,u}/IC_{50}$ ratio threshold set by the FDA), but also when used in a static model to predict the percent change to metformin AUC.

4.4.5 *Consideration of Physicochemical Properties, Membrane Permeability, and Substrate Status May Help Explain Inhibition Discrepancies.*

An interesting observation in our study is that the degree to which our $IC_{50,flux}$ values differed from IC_{50} values obtained from hMATE1-transfected cells varied significantly among the inhibitors studied (5-fold for PYR, 14-fold for CIM, and >160-fold for FAM) (**Table 4.2**). Such differences are likely rooted in their different ability to enter the cells, either by passive diffusion or/and carrier-mediated transport, to access the hMATE1 inhibition site (**Figure 4.1**). We thus

examined the physicochemical properties of the inhibitors explored in this study as an indicator of their ability to cross the membrane by passive diffusion (**Table 4.3**). All inhibitors under consideration are weak bases ionized to different degrees under physiological pH. FAM, HCQ, and BRI are highly ionized (>90%), while PYR and CIM are ionized to a lower extent. LogD values were calculated at a physiologically relevant pH of 7.4 (blood) and 6.0 (urine). LogP and LogD values suggest that CIM, FAM, and HCQ are highly hydrophilic, whereas PYR and BRI are more lipophilic. The low molecular weight of PYR, in combination with its high lipophilicity, indicates that PYR may be successful in passively permeating through the membrane and reaching hMATE1 site of inhibition. Despite its high lipophilicity, BRI is a large molecule (molecular weight > 500 g/mol), which could limit its passive permeability (Lipinski *et al.*, 2001) and potentially explain its lack of inhibition in the double-transfected system. In contrast, CIM, FAM, and HCQ are small and highly hydrophilic molecules, which have difficulty crossing the membrane without the assistance of an uptake transporter. This could explain the lack of inhibitory effect of FAM and HCQ in the double-transfected system. CIM is the exception, but it can enter the cells through carrier-mediated uptake, as CIM has been previously reported to be a substrate of hOCT2 and to accumulate in hOCT2/hMATE1-transfected MDCK cells (Yin *et al.*, 2016). Together this data suggests that the ability of the inhibitor to enter cells, either by passive diffusion or carrier-mediated uptake, is an important determinant in its ability to produce clinically significant DDIs through hMATE1 inhibition in vivo.

4.5 DISCUSSION

Accurate prediction of hOCT2/hMATE1-2K-mediated renal DDIs based on in vitro data remains a challenge (Mathialagan *et al.*, 2021; Krishnan *et al.*, 2022). Current DDI risk assessment

relies on the use of plasma $I_{max,u}$ and IC_{50} determined for a single transporter, which frequently leads to false or overprediction for hMATEs. In this study, we explored the use of hOCT2/hMATE1 double-transfected MDCK cells as a new in vitro tool for DDI risk assessment. A new inhibition parameter ($IC_{50,flux}$) reflecting an inhibitor's overall impact on renal secretory clearance was obtained and used to predict in vivo metformin DDIs.

hMATE functions as a proton/organic cation antiporter, with proton binding occurring on the opposite side of substrate binding. For inhibition experiments using hMATE1 single-transfected cells, the extracellular or intracellular pH is modified to create an outwardly directed proton gradient, driving hMATE1 to function as an uptake transporter. In this state, the organic cation binding site is exposed to the extracellular space, allowing IC_{50} determination through conventional uptake studies where substrates and inhibitors are both added to the extracellular side. In PTECs, however, hMATE1 mediates organic cation efflux utilizing the inwardly directed physiologic proton gradient. In this state, organic cation binds from the intracellular side, whereas proton binds from the lumen side. Our previous work suggested that in the natural physiological state, hMATE1 inhibitor binding occurs from the intracellular side (Yin *et al.*, 2016). Our inhibition study with HCQ and BRI further corroborates this observation, as these potent hMATE1 inhibitors (**Figure 4.2**) showed no inhibitory effect on metformin B-to-A flux when applied apically at concentrations much higher than their IC_{50} determined in single-transfected cells (**Figure 4.3** and **Figure 4.4**). Collectively, these data strongly suggest that when hMATE1 functions as an efflux transporter, inhibitors must be present intracellularly, i.e., at the same side with the substrate, to exert an inhibitory effect. The artificial cell models used previously obviate the need for this critical inhibitor disposition characteristic, given that the double-transfected

system takes into consideration the inhibitor's intracellular accessibility, while the single transporter-transfected system lacks attention to the disposition characteristics of the inhibitor.

hMATEs inhibitors can gain intracellular access via passive diffusion or transporter-mediated uptake. Their intracellular concentrations may be additionally influenced by intracellular binding/sequestration and transporter-mediated efflux (**Figure 4.1**). The lack of inhibitory effect of HCQ and BRI on metformin B-to-A flux (**Figure 4.3** and **Figure 4.4**) indicates that they may not reach sufficient intracellular concentration to inhibit hMATE1. HCQ is highly ionized at physiological pH and has a low LogD, limiting its passive membrane permeability. BRI is also highly ionized, and although it has an intermediate LogD, its larger molecular size may also limit its passive permeability (Lipinski *et al.*, 2001) (**Table 4.3**). Neither HCQ nor BRI have been reported as a substrate of the basolateral uptake transporter hOCT2. Instead, both were reported as substrates of the efflux transporter P-glycoprotein (P-gp) present in human kidneys (Li *et al.*, 2018; Weiss *et al.*, 2020) and MDCK cells (Goh *et al.*, 2002). Additionally, HCQ is known to accumulate within lysosomes (Derendorf, 2020). Together, these factors may contribute to low unbound intracellular concentrations resulting in the lack of hMATE1 inhibition in the double-transfected system. These data also suggest that HCQ and BRI may not affect metformin renal secretion in vivo. Unfortunately, no in vivo metformin DDI information is available for HCQ or BRI to corroborate our hypothesis.

PYR and CIM are classic inhibitors of the renal organic cation secretion system known to impact metformin exposure in vivo (Somogyi *et al.*, 1987; Kusuhara *et al.*, 2011). Both PYR and CIM display much higher inhibitory potency towards hMATE1 than for hOCT2 (**Table 4.2**). FAM is also a potent hMATE1 inhibitor (IC_{50} = 0.25 μM) in vitro but has no in vivo effect on metformin exposure (Hibma *et al.*, 2016). When evaluated in our double-transfected Transwell system, PYR

and CIM dose-dependently inhibited metformin P_{app} (**Figure 4.5 A and B**). The observed increase in metformin intracellular accumulation (**Figure 4.5 D and E**) further suggests that the main site of inhibition is hMATE1. In contrast, FAM had minimal impact on metformin transepithelial flux and intracellular accumulation at concentrations up to 40 µM (**Figure 4.5 C and F**), demonstrating a disconnect between inhibition in single- versus double-transfected cell models. These observations are fully consistent with clinical DDI study outcomes, in which co-administration of PYR or CIM with metformin led to a significant increase in metformin AUC, whereas FAM did not (Somogyi *et al.*, 1987; Kusuhara *et al.*, 2011; Hibma *et al.*, 2016).

The different impact of these three inhibitors on metformin flux could be explained by their inherent characteristics impacting intracellular accessibility (**Figure 4.1**). PYR is a small lipophilic molecule only partially ionized at pH 7.4 (**Table 4.3**), and thus more likely to enter cells by passive diffusion. In contrast, FAM is predominantly ionized at physiologic pH, highly hydrophilic ($LogD_{7.4}$ = -2.6), and not a (or a poor) hOCT2 substrate (Motohashi *et al.*, 2004; Tahara *et al.*, 2005). These factors likely contribute to poor FAM intracellular accessibility and lack of hMATE1 inhibition in the Transwell system (**Figure 4.5** and **Figure 4.6**). Although CIM is also a small and highly hydrophilic compound, it is a substrate of hOCT2 (Tahara *et al.*, 2005; Tanihara, Masuda, Sato, Katsura, Ogawa, and K ichi Inui, 2007). Previously, we demonstrated that hOCT2-mediated uptake is crucial for granting CIM intracellular access to inhibit hMATE1 (Yin *et al.*, 2016). Hence, despite CIM's low passive permeability, the presence of hOCT2 in our double-transfected system facilitates CIM intracellular accessibility, resulting in the observed dose-dependent inhibition of metformin P_{app} (**Figure 4.5** and **Figure 4.6**).

Our results suggest that the use of unbound intracellular inhibitor concentrations instead of plasma $I_{max,u}$ could better predict hMATE-mediated clinical DDIs. However, determination of

such concentrations with human PTECs can be challenging and possibly impractical during early drug development. We thus proposed a new approach that accounts for the inhibitor's intracellular accessibility and allows the prediction of DDI potential using plasma inhibitor concentrations. In this approach, a new inhibition parameter ($IC_{50,flux}$) reflecting the inhibitor's potency on overall renal secretory clearance was determined in hOCT2/hMATE1 double-transfected MDCK cells (**Figure 4.6**). The $IC_{50,flux}$ directly links the inhibitory effect on substrate flux with extracellular inhibitor concentrations in the transport buffer, which reflects plasma $I_{max,u}$ (**Figure 4.1**). As shown in **Table 4.2**, the $IC_{50,flux}$ values calculated from metformin P_{app} for PYR, CIM, and FAM were quite different from IC_{50} obtained by uptake studies in single transporter-transfected cells, with the difference being 5-fold for PYR, 14-fold for CIM and >160-fold for FAM for hMATE1. In quantitative prediction of in vivo DDIs using a static prediction model (**Equation 4.3**), the use of $IC_{50,flux}$ performed substantially better than individual transporter IC_{50} values for PYR and CIM (**Table 4.2**). Importantly, it accurately predicted the lack of in vivo DDI for FAM, which would otherwise be incorrectly predicted when using hMATE1 IC_{50}. Therefore, the $IC_{50,flux}$ approach could mitigate the risk of false and over-predictions commonly observed for predicting hMATE1-mediated DDIs, reducing the burden of unnecessary and costly clinical DDI investigations.

The use of hOCT2/hMATE1 double-transfected MDCK cells and the $IC_{50,flux}$ approach have several advantages for predicting renal transporter-mediated DDIs. First, the system is robust for identifying hMATE1 inhibitors that are likely to lead to false DDI prediction as it accounts for inhibitor intracellular accessibility without the need to measure intracellular inhibitor concentrations. Second, it measures the overall inhibitory effect on hOCT2/hMATE1-mediated secretory clearance without assuming a single transporter as the site of interaction. Third, intracellular substrate accumulation can be measured, which could serve as a useful indicator of

intrarenal drug accumulation and drug-induced nephrotoxicity. Lastly, compared to other emerging in vitro platforms such as cultured organoids and microphysiological systems, which require expensive human renal cells and specialized culturing techniques, the double-transfected MDCK system is less complex, cost-effective, and scalable for high throughput screening, which could be incorporated into the current scheme of in vitro DDI assessments during preclinical drug development. A similar concept can be implemented to predict DDIs for other transport pathways, such as hOATP1B/hMRP2 in human hepatocytes.

Our approach nevertheless has limitations. We only considered hMATE1 as the apical efflux transporter. Although recent proteomic studies have reported hMATE2K expression levels are much lower than hMATE1 in human PTECs (Prasad *et al.*, 2016; Kikuchi *et al.*, 2021), we cannot exclude the possibility that hMATE2K may also contribute to renal DDIs. Nevertheless, the concept and approach developed in this study should be applicable to hMATE2K using double- or triple-transfected cell systems expressing hMATE2K. Our model uses a canine-derived cell line (MDCK) that was derived from the distal tubule and also expresses endogenous canine transporters (e.g. P-gp) (Goh *et al.*, 2002). Further, it does not account for the potential role of other human PTEC transporters in the basolateral uptake of hMATE1 inhibitors. Additionally, differences in hOCT2 and hMATE1 expression levels in MDCK-transfected cells in comparison to human PTECs could impact quantitative predictions. Finally, although $IC_{50,flux}$ performed well in our predictions with PYR, CIM, and FAM, this strategy should be further validated with more inhibitors for which clinical DDI information is available.

In summary, our findings highlight the importance of considering inhibitor's accessibility to intracellular space – via passive diffusion or transporter-mediated uptake – for accurate prediction of hMATE1-mediated DDI in vivo. The use of a double-transfected system and $IC_{50,flux}$

has the potential to bridge the gap in the current prediction of hMATE1-mediated DDIs and reduce the burden of unnecessary and costly clinical DDI investigations.

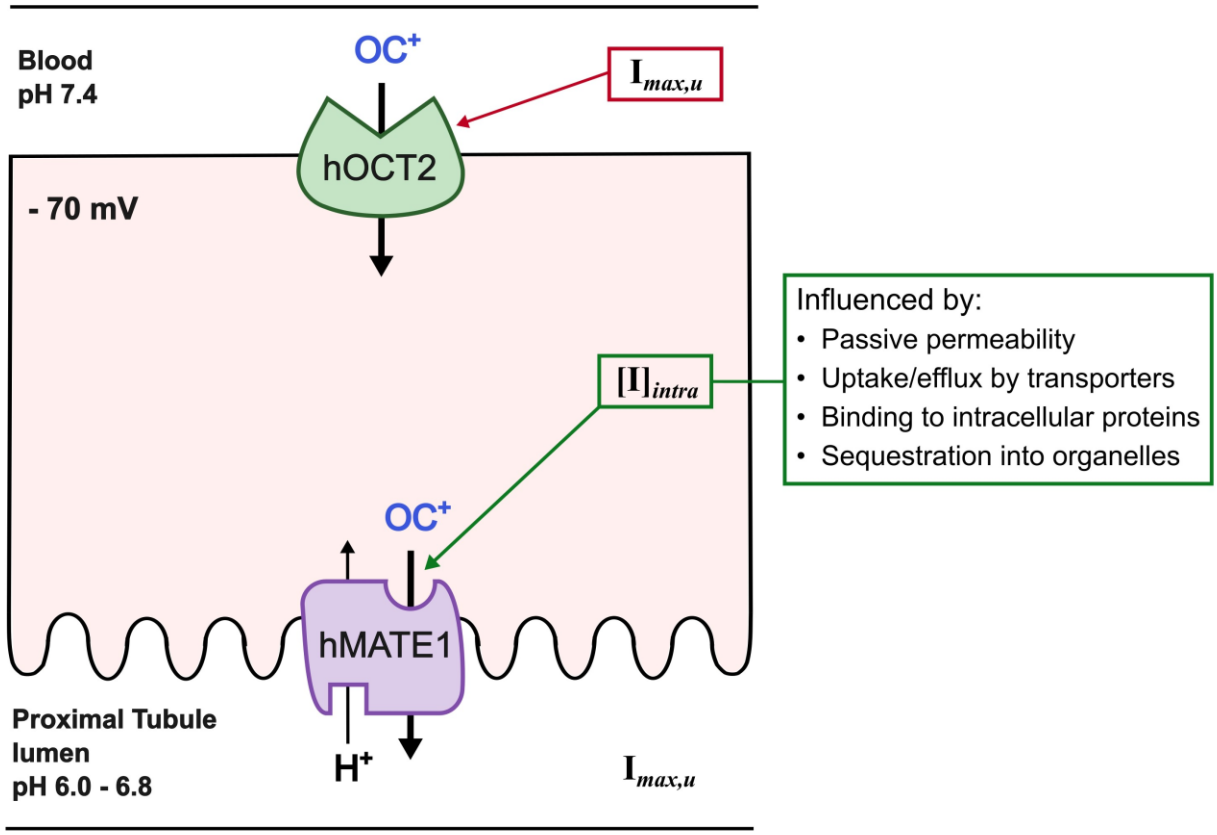

Figure 4.1. Representation of the renal secretion of organic cations (OC^+) sequentially mediated by hOCT2 and hMATE1.

hOCT2 is expressed in basolateral membrane of renal proximal tubule cells and mediates OC^+ uptake driven by the inside-negative membrane potential. hMATE1 is expressed in the apical membrane and functions as a proton/OC^+ exchanger mediating the efflux of OC^+ from intracellular space to the proximal tubule lumen. $I_{max,u}$ denotes the maximal unbound plasma concentration of the inhibitor which also presents in the filtrate due to glomerular filtration. Although $I_{max,u}$ is often used for assessment of DDI potential, intracellular inhibitor concentration ($[I]_{intra}$) may be more relevant for assessment of hMATE1-mediated DDI, which can be influenced by many factors.

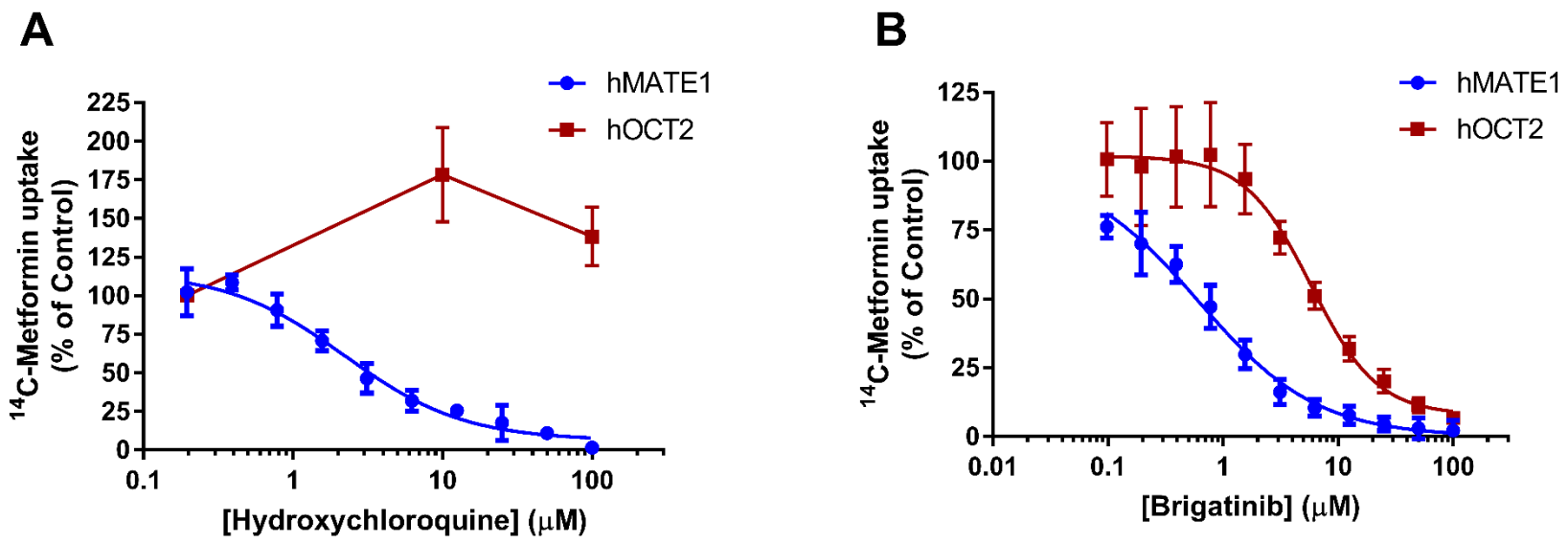

Figure 4.2. Inhibition of hOCT2 and hMATE1 by hydroxychloroquine (A) or brigatinib (B) using metformin as probe substrate. Cells were incubated in KRH buffer containing ^{14}C-labeled metformin (8.9 μM) for 2 minutes in the presence or absence of inhibitor at indicated concentrations. Transporter-specific uptake was calculated by subtracting the uptake in vector-transfected HEK293 cells and data is presented as percentage of the uptake in the absence of inhibitor. A non-linear regression was fit to the data using **Equation 4.1**. Each data point represents mean ± SD from at least three independent experiments.

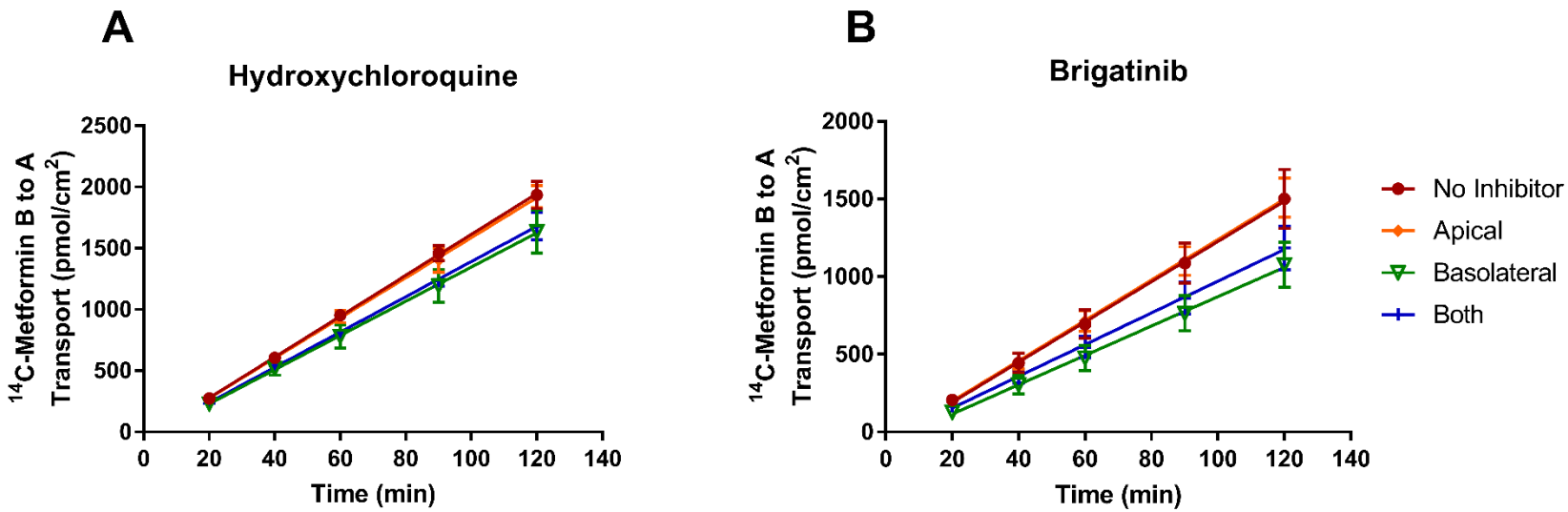

Figure 4.3. Effect of 40 µM hydroxychloroquine (A) or 6.25 µM brigatinib (B) on B-to-A transcellular flux of metformin in hOCT2/hMATE1-expressing MDCK cells.

The pH in the basal and apical chambers were maintained at 7.4 and 6.0, respectively. Cells were incubated in KRH buffer containing ^{14}C-metformin (8.9 µM) in the basal chamber, and B-to-A flux of metformin was measured in the absence or presence of inhibitors added to apical, basolateral or both chambers. An aliquot of buffer from the apical chamber was sampled periodically and replenished with an equal volume of KRH buffer with or without inhibitor. Data is presented as mean ± SD of three independent experiments.

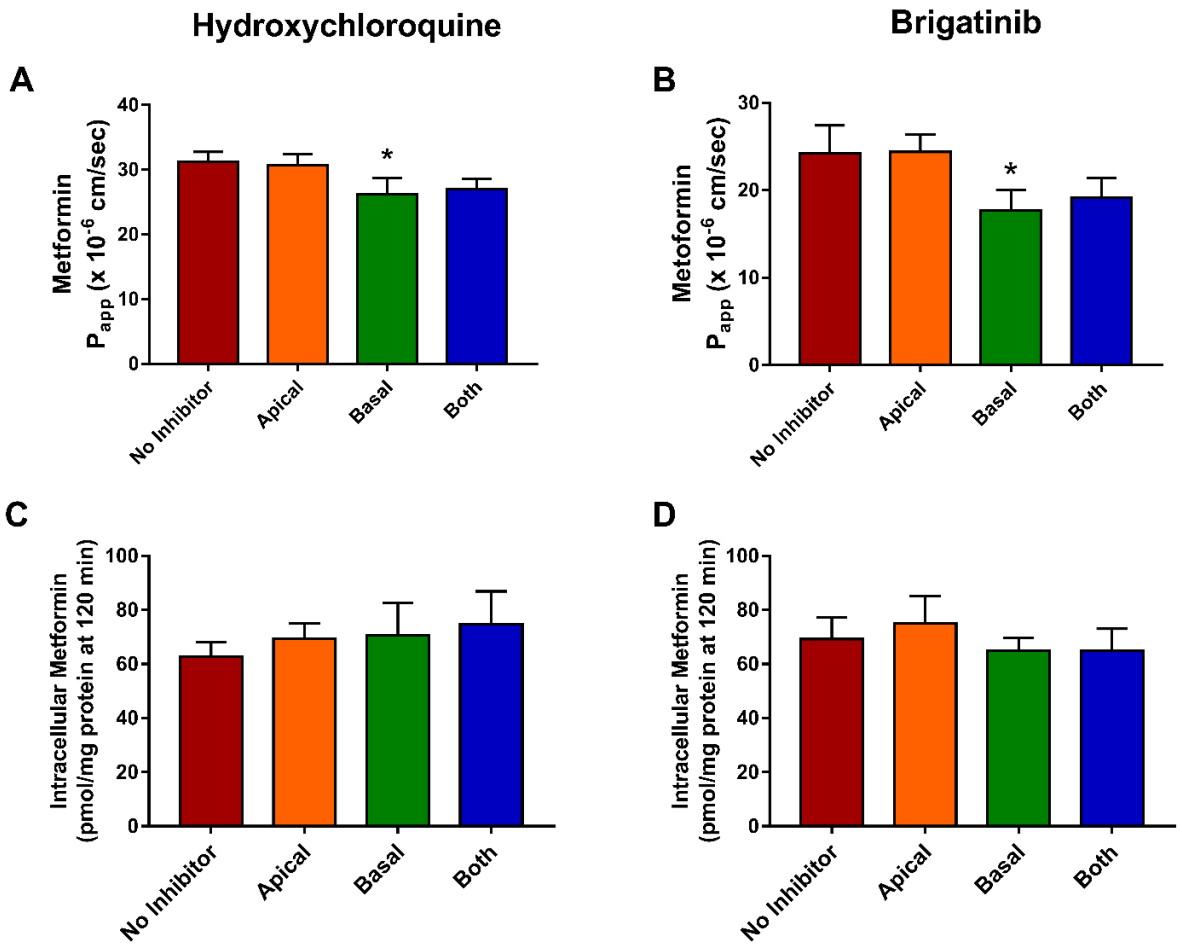

Figure 4.4. Effect of hydroxychloroquine and brigatinib in metformin apparent permeability (P_{app}) and intracellular accumulation in MDCK-hOCT2/hMATE1 cells.

The B-to-A P_{app} value of metformin in the absence or presence of 40µM hydroxychloroquine (A) or 6.25 µM brigatinib (B) was calculated using **Equation 4.2**. Intracellular accumulation of metformin was measured at the end of the Transwell study in the absence and presence of hydroxychloroquine (C) or brigatinib (D). Inhibitors were added to apical, basal or both chambers at the beginning of the Transwell experiment. Permeability and accumulation in the presence of inhibitors was compared to those in absence of inhibitor (* $P < 0.05$). Statistical significance was determined using one-way ANOVA followed by Dunnett's post hoc test to correct for multiple comparisons. Data is presented as mean ± SD of three independent experiments.

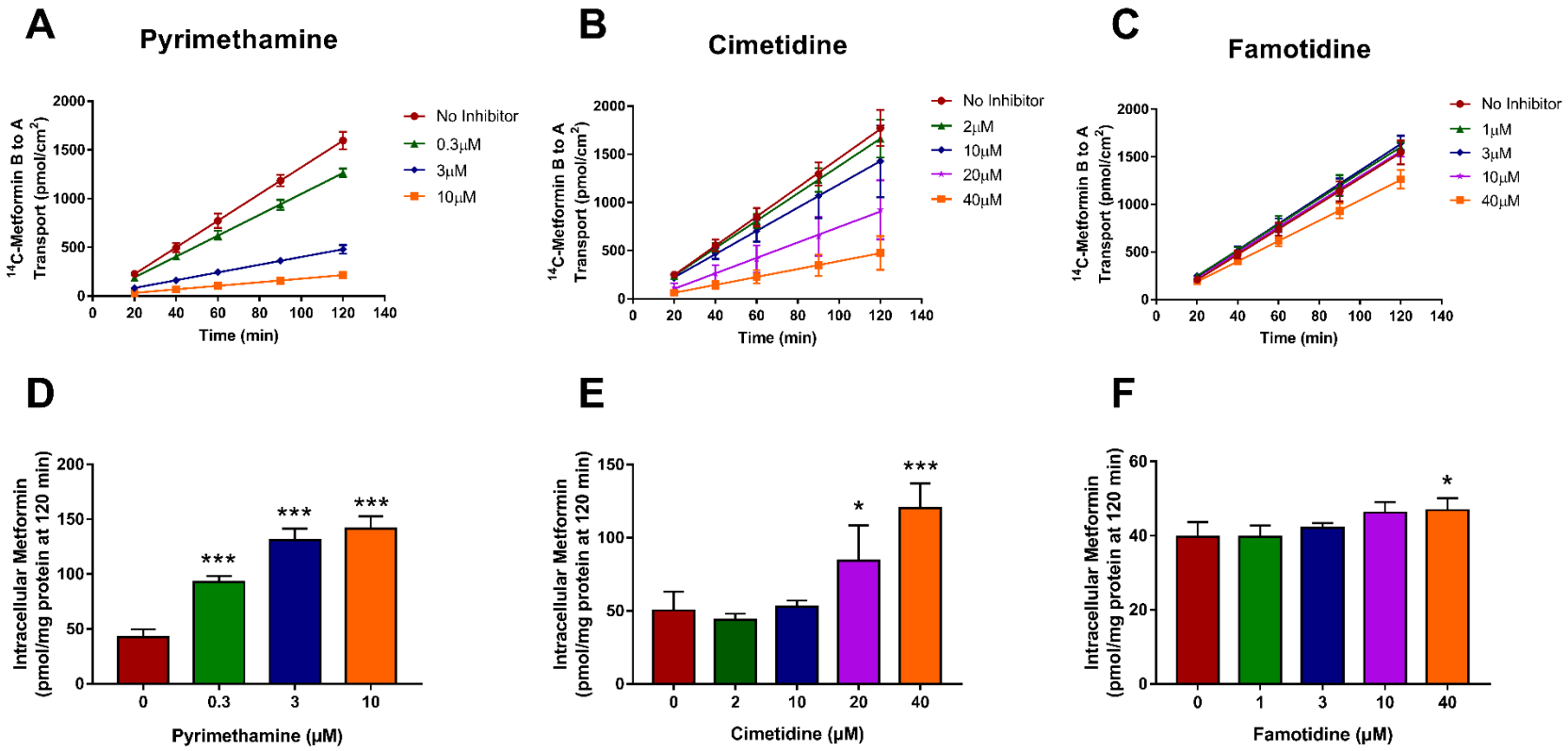

Figure 4.5. Effect of pyrimethamine, cimetidine and famotidine in metformin B-to-A transcellular flux (A, B and C) and intracellular accumulation (D, E and F) in hOCT2/hMATE1-expressing MDCK cells.

The pH in the basal and apical chambers were maintained at 7.4 and 6.0, respectively. Cells were incubated in KRH buffer containing ^{14}C-metformin (8.9 μM) in the basal chamber in the absence or presence of inhibitors. Inhibitors were added to both apical and basal chambers at indicated concentrations. An aliquot of buffer from the apical chamber was sampled periodically up to 120 minutes and B-

to-A flux of metformin was measured in the absence and presence of varying concentrations of pyrimethamine (A), cimetidine (B) and famotidine (C). At the end of the transport experiment, cells were lysed, and intracellular accumulation of metformin was measured in the absence and presence of pyrimethamine (D), cimetidine (E) and famotidine (F). *** $P<0.001$, **$P < 0.01$, *$P < 0.05$ indicates significantly higher accumulation in comparison to control (absence of inhibitor). Statistical significance was determined using one-way ANOVA followed by Dunnett's post hoc test to correct for multiple comparisons. Data is presented as mean ± SD of at least three independent experiments.

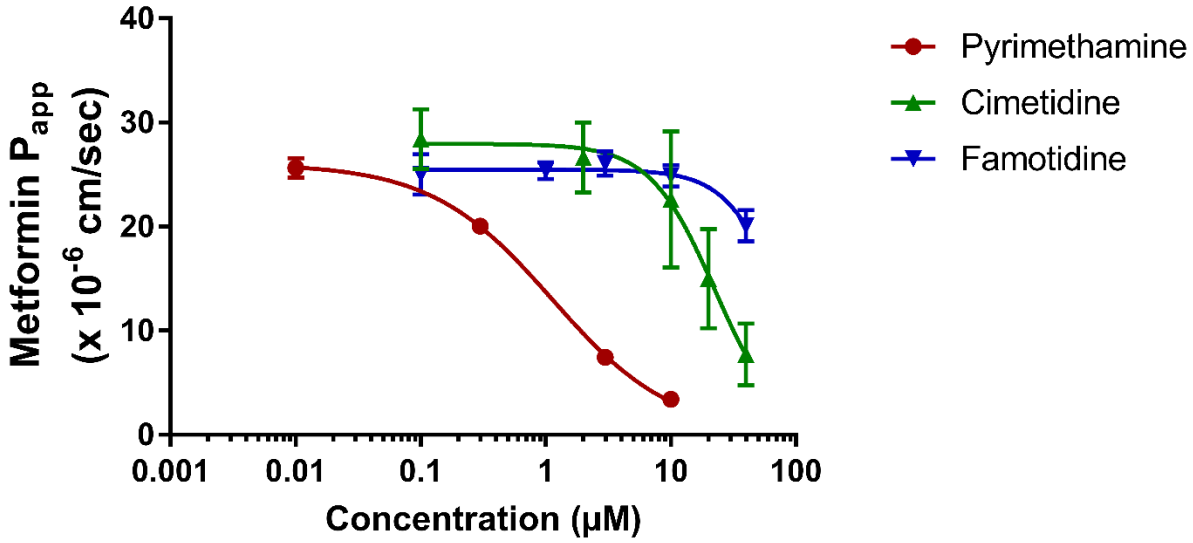

Figure 4.6. Dose-dependent inhibition of metformin B-to-A P_{app} in hOCT2/hMATE1 double-transfected MDCK cells by pyrimethamine, cimetidine and famotidine.

P_{app} values in the absence or presence of varying inhibitor concentrations were calculated using **Equation 4.2.** Inhibitors were added to both basal and apical chambers at the start of the Transwell experiment at indicated concentrations. Each data point represents mean ± SD from three to four independent experiments.

Table 4.1. Assessment of DDI potential and predictivity of static prediction models using $I_{max,u}$ and IC_{50} values collected from literature.

Inhibitor	Dosing	I_{max} (µM)	f_u	$I_{max,u}$ (µM)	IC_{50} (µM)		$I_{max,u}/IC_{50}$		Predicted Change in Metformin AUC (%)		Observed Change in Metformin AUC (%)	Prediction
					OCT2	*MATE1*	*OCT2*	*MATE1*	*OCT2*	*MATE1*		
Fedratinib	600mg [A]	3.8[A]	0.045[A]	0.17[A]	0.78[A]	0.352[A]	0.22	0.49	17	35	-3[A]	FP
Ranitidine	150mg BID, 4 days [B]	1.40[C]	0.85[C]	1.19	15.7[D]	4.04[D]	0.08	0.29	6	22	2.2[B]	FP
Famotidine	800mg (160mg every 4h) [E]	-	-	1.0[E]	66[E]	0.25[E]	0.02	4	1	178	0[E]	FP
Ondansetron	8mg QD, 5 days [F]	0.2[F]	0.25[F]	0.05	3.85[F]	0.035[F]	0.01	1.43	1	89	21[F]	O
Cimetidine	400mg BID, 5 days [G]	9.5[G]	0.8[H]	7.6	93.5[H]	1.5[H]	0.08	5.1	6	202	50[G]	O
Pyrimethamine	50mg [I]	2.29[I]	0.13[I]	0.3	22.9[H]	0.22[H]	0.01	1.36	1	85	35[I]	O
Trimethoprim	200mg BID, 5 days [J]	14.8[J]	0.6[J]	8.9	27.2[J]	6.3[J]	0.32	1.41	24	88	29.5[J]	O

Predicted change in metformin AUC was calculated based on **Equation 4.3**.

FP – false prediction; O – overprediction

[A] Value from Ogasawara et al., 2021

[B] Value from Cho and Chung, 2016

[C] Value from FDA drug label (GlaxoSmithKline. ZANTAC 150 (ranitidine hydrochloride) [package insert], 2004)

[D] Value from Morrissey et al., 2016

[E] Value from Hibma et al., 2016

[F] Value from Li et al., 2016

[G] Value from Somogyi et al., 1987

[H] Value from Yin et al., 2016

[I] Value from Kusuhara et al., 2011

[J] Value from Müller et al., 2015

Table 4.2. Prediction of hOCT2 and hMATE1 mediated DDIs utilizing IC_{50} values determined in single- vs. double-transfected cells ($IC_{50,flux}$).

Data is presented as mean ± SD from three or four independent experiments.

Inhibitor	Transporter assessed	IC_{50} (µM) Substrate: Metformin	$I_{max,u}$ / IC_{50}	Predicted change in Metformin AUC (%)	Observed change in Metformin AUC (%)	Difference from observed
PYR	hOCT2	22.9 [A]	0.01	1	35 [B]	35-fold ↓
	hMATE1	0.22 [A]	1.36	85		2.4-fold ↑
	hOCT2/hMATE1 (Flux)	**1.04 ± 0.15**	**0.29**	**22**		**1.6-fold ↓**
CIM	hOCT2	93.5 [A]	0.08	6	50 [C]	8.3-fold ↓
	hMATE1	1.5 [A]	5.1	202		4-fold ↑
	hOCT2/hMATE1 (Flux)	**21.4 ± 10.0**	**0.36**	**27**		**1.9-fold ↓**
FAM	hOCT2	66 [D]	0.02	1	0 [D]	No difference
	hMATE1	0.25 [D]	4	178		False prediction
	hOCT2/hMATE1 (Flux)	**> 40**	**< 0.025**	**< 2**		**No difference**

$I_{max,u}$ used in calculations for PYR, CIM and FAM are 0.3, 7.6 and 1 µM respectively. Further details of these values can be found in **Table 4.1**. Predicted change in metformin AUC was calculated based on **Equation 4.3**. Overprediction or underprediction are respectively indicated by ↑ or ↓.

[A] Value from Yin et al., 2016.

[B] Value from Kusuhara et al., 2011.

[C] Value from Somogyi et al., 1987.

[D] Value from Hibma et al., 2016

Table 4.3. Physicochemical properties and membrane permeability values of compounds investigated in the present study.

Compound	MW (g/mol)	pKa	% ionized at pH 7.4	LogP (XLogP3 3.0)	LogD (ChemAxon)	
					pH 7.4	pH 6.0
PYR	248.7	7.34	46.6	2.7	2.25	1.19
CIM	252.3	6.91	24.4	0.4	- 0.25	- 0.84
FAM	337.5	8.38	90.5	-0.6	-2.6	- 3.35
HCQ	335.9	9.7	99.5	3.6	0.62	- 3.7
BRI	584.1	8.54	93.2	4.6	2.49	1.1

MW – molecular weight. Only the strongest basic pKa is reported. Percent ionized at pH 7.4 was calculated using the Henderson-Hasselbalch equation.

Chapter 5. CONCLUSIONS AND FUTURE DIRECTIONS

The polyspecific organic cation transporters (pOCTs) are increasingly acknowledged as important determinants in the absorption, distribution, and excretion of many drugs and environmental compounds, impacting pharmacokinetics, pharmacodynamic and toxicological effects of its substrates and representing a potential site for drug interactions (International Transporter Consortium *et al.*, 2010; Wagner *et al.*, 2016; Koepsell, 2020). Although great advances have been made in characterizing substrates and inhibitors of these transporters and in understanding their molecular features and mechanisms of transport, there are still many gaps in our knowledge regarding the role of pOCTs in the disposition and drug interaction of a broader spectrum of chemicals in the human body. This dissertation focused on addressing some of these gaps, and our studies were designed to: (1) elucidate the role of monoamine transporters and pOCTs – especially PMAT – in the disposition of the theranostic agent mIBG in neuroblastoma; (2) investigate the role of pOCTs in the healthy tissue disposition of the environmental chemicals benzalkonium chlorides (BACs); (3) explore the use of a double-transfected system to improve prediction of DDIs mediated by the OCT2/MATE1 renal transporters.

In Chapter 2, we showed that neuroblastoma tumors and cell lines mainly express NET, PMAT, and VMAT1/2, and that the expression of these transporters is significantly reduced when the proto-oncogene MYCN is amplified. We further revealed that PMAT expression is the highest among these transporters, and its expression correlated with improved survival of high-risk neuroblastoma patients without MYCN amplification. We identified that PMAT efficiently transports mIBG, is mainly localized in the mitochondria of neuroblastoma cells, and mediates mitochondrial uptake of mIBG. Our results suggest that PMAT represents a novel risk marker to help predict disease prognosis in neuroblastoma, and that variable expression of PMAT in

neuroblastoma may help explain the interindividual variability in the response to ^{131}I-mIBG therapy. Further studies investigating the protein expression of PMAT in neuroblastoma tumors, and its association with mIBG avidity and retention are important next steps in substantiating our findings. Additionally, investigating the relationship between treatment outcome and tumor expression of PMAT in neuroblastoma patients treated specifically with ^{131}I-mIBG would provide more direct clinical evidence of PMAT's significance in predicting response to ^{131}I-mIBG treatment.

In Chapter 3, we showed that all BACs (C8 to C14) are inhibitors of OCT1-3 and MATE1/2K, and that short-chain BACs (C8 and C10) are also substrates of these transporters. Furthermore, we demonstrated that C8 and C10 are transported across OCT2/MATE1 double-transfected MDCK monolayer and that the expression and function of these transporters significantly impact BAC intracellular accumulation. Our results indicate that transport mediated by OCT2 and MATE1 represents a previously unrecognized pathway driving intrarenal accumulation of BAC C8 and C10, and that OCT1 and OCT3 may play important roles in the tissue distribution of these compounds. The work presented in this dissertation focused on the pOCTs. However, the interaction of BAC with other transporters that take organic cations as substrates (e.g. P-glycoprotein) should also be evaluated and characterized as these transporters could also impact systemic and tissue-specific BAC exposure in humans. Studies in Oct1/2 double knockout mouse models with BAC could further test the significance of these transporters in mediating renal accumulation of these compounds in vivo. Moreover, investigation of BAC accumulation in human proximal tubule epithelial cells, toxicity studies employing a kidney-on-a-chip system, and the assessment of OCT2 and MATE1 inhibitor's impact on BAC accumulation and nephrotoxicity could provide further evidence of the significance of OCT2 and MATE1-

mediated transport in C8 and C10 BAC renal accumulation in humans. Further, given their significant kidney accumulation and their inhibitory potential towards MATE1, the possible involvement of BACs in xenobiotic-drug interactions could be explored in vitro using our OCT2/MATE1 double-transfected renal secretion model. Lastly, because C8 and C10 are usually not the main BAC homologs in commercial products, they are often overlooked in contrast to their longer chain counterparts. However, given that short-chain BACs show potential for biochemical interactions and were identified as potent inhibitors of cholesterol biosynthesis even at nM concentrations (Herron *et al.*, 2016), further in vivo studies focusing on the biodistribution and chronic exposure effect of C8 and C10 BAC would be valuable.

In Chapter 4, we propose a novel strategy using OCT2/MATE1 double-transfected MDCK cells to assess the DDI potential of compounds toward the renal organic cation secretion system. Our results showed that inhibition of MATE1 assessed through simple uptake studies using single-transfected cells does not necessarily translate to inhibition in the double-transfected system. This finding suggests that when MATE1 functions as an efflux transporter (as is the case in the double-transfected system and in vivo) inhibitor accessibility to the intracellular space is crucial for interaction with MATE1. Nevertheless, further studies directly measuring the unbound intracellular concentration of inhibitors in our double-transfected system are necessary to confirm this hypothesis. The double-transfected system allowed us to calculate a new parameter ($IC_{50,flux}$), which reflects the inhibitor's overall impact on OCT2/MATE1-mediated transepithelial flux of substrate and already accounts for the inhibitor's ability to reach the intracellular space. Importantly, the use of $IC_{50,flux}$ in a static DDI prediction model performed better than IC_{50} values determined in single transported-transfected cells when predicting in vivo DDIs involving the OCT2/MATE1 pathway. Our findings indicate that this novel approach has the potential to

identify in vitro MATE1 inhibitors that are unlikely to cause in vivo DDIs, thus reducing the burden of unnecessary and costly clinical DDI investigations. Although we assessed a total of five inhibitors in this study, only three of them had clinical DDI studies available in the literature, and thus a comprehensive study should be done using a larger number of inhibitors, allowing assessment of the positive predictive value and negative predictive value of this novel test strategy. Additionally, although we used metformin as the classic OCT2/MATE1 substrate in our studies, other substrates could be employed in this system to evaluate its usefulness in predicting substrate-dependent inhibition. Finally, a similar concept could be implemented using other double or triple-transporter transfected MDCK cells to predict DDIs involving other transport pathways.

In summary, this dissertation research has greatly contributed to our understanding of the involvement of pOCTs in the systemic and tissue-specific exposure of a broader spectrum of compounds, including a cancer theranostic agent and environmental xenobiotics, and supports a new innovative strategy to improve the prediction of renal DDIs. Specifically, the research revealed that: (1) PMAT is highly expressed intracellularly in neuroblastoma, transports mIBG and thus may represent a major determinant in the therapeutic efficacy of ^{131}I-mIBG; (2) pOCTs transport BAC C8 and C10 and thus can impact tissue accumulation and toxicity of these compounds, having important implications for understanding human exposure and susceptibility to environmental BACs; and (3) the use of OCT2/MATE1 double-transfected MDCK cells and the $IC_{50,flux}$ approach provides a promising strategy to assess the inhibitory potential of compounds towards the renal organic cation secretion system, with the ability to identify in vitro MATE1 inhibitors unlikely to result in in vivo DDIs, thus reducing the burden of unnecessary and costly clinical DDI investigations.

BIBLIOGRAPHY

Ahmed AA, Zhang L, Reddivalla N, and Hetherington M (2017) Neuroblastoma in children: Update on clinicopathologic and genetic prognostic factors. *Pediatr Hematol Oncol* **34**:165–185.

Arakawa H, Omote S, and Tamai I (2017) Inhibitory Effect of Crizotinib on Creatinine Uptake by Renal Secretory Transporter OCT2. *J Pharm Sci* **106**:2899–2903.

Arnold WA, Blum A, Branyan J, Bruton TA, Carignan CC, Cortopassi G, Datta S, DeWitt J, Doherty A-C, Halden RU, Harari H, Hartmann EM, Hrubec TC, Iyer S, Kwiatkowski CF, LaPier J, Li D, Li L, Muñiz Ortiz JG, Salamova A, Schettler T, Seguin RP, Soehl A, Sutton R, Xu L, and Zheng G (2023) Quaternary Ammonium Compounds: A Chemical Class of Emerging Concern. *Environ Sci Technol* **57**:7645–7665.

Barnes K, Dobrzynski H, Foppolo S, Beal PR, Ismat F, Scullion ER, Sun L, Tellez J, Ritzel MWL, Claycomb WC, Cass CE, Young JD, Billeter-Clark R, Boyett MR, and Baldwin SA (2006) Distribution and functional characterization of equilibrative nucleoside transporter-4, a novel cardiac adenosine transporter activated at acidic pH. *Circ Res* **99**:510–519.

Bayer M, Schmitt J, Dittmann H, Handgretinger R, Bruchelt G, and Sauter AW (2016) Improved selectivity of mIBG uptake into neuroblastoma cells in vitro and in vivo by inhibition of organic cation transporter 3 uptake using clinically approved corticosteroids. *Nucl Med Biol* **43**:543–551.

Belzer M, Morales M, Jagadish B, Mash EA, and Wright SH (2013) Substrate-dependent ligand inhibition of the human organic cation transporter OCT2. *J Pharmacol Exp Ther* **346**:300–10.

Blake GM, Lewington VJ, Zivanovic MA, and Ackery DM (1989) Glomerular filtration rate and the kinetics of 123I-metaiodobenzylguanidine. *Eur J Nucl Med* **15**:618–23.

Blanchet EM, Martucci V, and Pacak K (2012) Pheochromocytoma and paraganglioma: Current functional and future molecular imaging. *Front Oncol* **1**:1–9.

Bleeker G, Schoot RA, Caron HN, de Kraker J, Hoefnagel CA, van Eck BL, and Tytgat GA (2013) Toxicity of upfront 131I-metaiodobenzylguanidine (131I-MIBG) therapy in newly diagnosed neuroblastoma patients: a retrospective analysis. *Eur J Nucl Med Mol Imaging* **40**:1711–1717.

Borriello L, Seeger RC, Asgharzadeh S, and DeClerck YA (2016) More than the genes, the tumor microenvironment in neuroblastoma. *Cancer Lett* **380**:304–314.

Bowman MA, Gomez JA, Mitchell NC, Wells AM, Vitela M, Clarke KM, Horton RE, Koek W, and Daws LC (2022) Faster Serotonin Clearance in CA3 Region of Hippocampus and Antidepressant-like Effect of Decynium-22 in Juvenile Mice Are Putatively Linked to Increased Plasma Membrane Monoamine Transporter Function: Implications for Efficacy of Antidepressants in Juven. *Cells* **11**.

Boxberger KH, Hagenbuch B, and Lampe JN (2018) Ligand-dependent modulation of hOCT1 transport reveals discrete ligand binding sites within the substrate translocation channel. *Biochem Pharmacol* **156**:371–384.

Bristol-Myers Squibb Company. Glucophage (metformin hydrochloride) [package insert] (2017) U.S. Food and Drug Administration website. https://www.accessdata.fda.gov/drugsatfda_docs/label/2017/020357s037s039,021202s021s023lbl.pdf. Revised April 2017. Accessed February 2023.

Brouwer KLR, Keppler D, Hoffmaster KA, Bow DAJ, Cheng Y, Lai Y, Palm JE, Stieger B, Evers R, and International Transporter Consortium (2013) In vitro methods to support transporter evaluation in drug discovery and development. *Clin Pharmacol Ther* **94**:95–112.

Bulotta S, Celano M, Costante G, and Russo D (2016) Emerging strategies for managing differentiated thyroid cancers refractory to radioiodine.

Chin BB, Kronauge JF, Femia FJ, Chen J, Maresca KP, Hillier S, Petry NA, James OG, Oldan JD, Armor T, Stubbs JB, Stabin MG, and Babich JW (2014) Phase-1 clinical trial results of high-specific-activity carrier-free 123I-iobenguane. *J Nucl Med* **55**:765–71.

Cho SK, and Chung J-Y (2016) The MATE1 rs2289669 polymorphism affects the renal clearance of metformin following ranitidine treatment. *Int Journal of Clinical Pharmacology and Therapeutics* **54**:253–262.

Coleman RE, Stubbs JB, Barrett JA, de la Guardia M, LaFrance N, and Babich JW (2009) Radiation Dosimetry, Pharmacokinetics, and Safety of Ultratrace^{TM} Iobenguane I-131 in Patients with Malignant Pheochromocytoma/Paraganglioma or Metastatic Carcinoid. *Cancer Biother Radiopharm* **24**:469–475.

Cornelissen J, Wanders RJA, Van den Bogert C, Van Kuilenburg ABP, Elzinga L, Voŭte PA, and Van Gennip AH (1995) Meta-iodobenzylguanidine (MIBG) inhibits malate and succinate driven mitochondrial ATP synthesis in the human neuroblastoma cell line SK-N-BE(2c). *Eur J Cancer* **31**:582–586.

Dahlin A, Xia L, Kong W, Hevner R, and Wang J (2007) Expression and immunolocalization of the plasma membrane monoamine transporter in the brain. *Neuroscience* **146**:1193–1211.

Dasari S, and Tchounwou PB (2014) Cisplatin in cancer therapy: molecular mechanisms of action. *Eur J Pharmacol* **740**:364–78.

Derendorf H (2020) Excessive lysosomal ion-trapping of hydroxychloroquine and azithromycin. *Int J Antimicrob Agents* **55**:106007.

Desai H, Borges-Neto S, and Wong TZ (2019) Molecular Imaging and Therapy for Neuroendocrine Tumors. *Curr Treat Options Oncol* **20**:78.

Dohán O, De La Vieja A, Paroder V, Riedel C, Artani M, Reed M, Ginter CS, and Carrasco N (2003) The sodium/iodide symporter (NIS): Characterization, regulation, and medical significance. *Endocr Rev* **24**:48–77.

Dresser MJ, Xiao G, Leabman MK, Gray AT, and Giacomini KM (2002) Interactions of n-tetraalkylammonium compounds and biguanides with a human renal organic cation transporter (hOCT2). *Pharm Res* **19**:1244–7.

Duan H, Hu T, Foti RS, Pan Y, Swaan PW, and Wang J (2015) Potent and selective inhibition of plasma membrane monoamine transporter by HIV protease inhibitors. *Drug Metabolism and Disposition* **43**:1773–1780.

Duan H, and Wang J (2013) Impaired monoamine and organic cation uptake in choroid plexus in mice with targeted disruption of the plasma membrane monoamine transporter (Slc29a4) gene. *Journal of Biological Chemistry* **288**:3535–3544.

Duan H, and Wang J (2010) Selective transport of monoamine neurotransmitters by human plasma membrane monoamine transporter and organic cation transporter 3. *Journal of Pharmacology and Experimental Therapeutics* **335**:743–753.

DuBois SG, Geier E, Batra V, Yee SW, Neuhaus J, Segal M, Martinez D, Pawel B, Yanik G, Naranjo A, London WB, Kreissman S, Baker D, Attiyeh E, Hogarty MD, Maris JM, Giacomini K, and Matthay KK (2012) Evaluation of Norepinephrine Transporter Expression

and Metaiodobenzylguanidine Avidity in Neuroblastoma: A Report from the Children's Oncology Group. *Int J Mol Imaging* **2012**:1–8.

DuBois SG, Mody R, Naranjo A, Van Ryn C, Russ D, Oldridge D, Kreissman S, Baker DL, Parisi M, Shulkin BL, Bai H, Diskin SJ, Batra V, Maris JM, Park JR, Matthay KK, and Yanik G (2017) MIBG avidity correlates with clinical features, tumor biology, and outcomes in neuroblastoma: A report from the Children's Oncology Group. *Pediatr Blood Cancer* **64**:1–7.

Eisenhofer G (2001) The role of neuronal and extraneuronal plasma membrane transporters in the inactivation of peripheral catecholamines. *Pharmacol Ther* **91**:35–62.

Eisenhofer G, Timmers HJ, Lenders JWM, Bornstein SR, Tiebel O, Mannelli M, King KS, Vocke CD, Linehan WM, Bratslavsky G, and Pacak K (2011) Age at Diagnosis of Pheochromocytoma Differs According to Catecholamine Phenotype and Tumor Location. *J Clin Endocrinol Metab* **96**:375–384.

Engel K, and Wang J (2005) Interaction of organic cations with a newly identified plasma membrane monoamine transporter. *Mol Pharmacol* **68**:1397–1407.

Engel K, Zhou M, and Wang J (2004) Identification and characterization of a novel monoamine transporter in the human brain. *Journal of Biological Chemistry* **279**:50042–50049.

EPA (2006) *Reregistration Eligibility Decision for Alkyl Dimethyl Benzyl Ammonium Chloride (ADBAC)*.

European Medicines Agency (EMA) (2012) Guideline on the investigation of drug interactions.

FDA (2023) Drug Development and Drug Interactions | Table of Substrates, Inhibitors and Inducers. https://www.fda.gov/drugs/drug-interactions-labeling/drug-development-and-drug-interactions-table-substrates-inhibitors-and-inducers (Accessed: 2023/11/02).

Feng B, Hurst S, Lu Y, Varma M v., Rotter CJ, El-Kattan A, Lockwood P, and Corrigan B (2013) Quantitative prediction of renal transporter-mediated clinical drug-drug interactions. *Mol Pharm* **10**:4207–4215.

Feng B, and Varma M v. (2016) Evaluation and Quantitative Prediction of Renal Transporter-Mediated Drug-Drug Interactions. *J Clin Pharmacol* S110–S121.

Filipski KK, Mathijssen RH, Mikkelsen TS, Schinkel AH, and Sparreboom A (2009) Contribution of organic cation transporter 2 (OCT2) to cisplatin-induced nephrotoxicity. *Clin Pharmacol Ther* **86**:396–402.

Gaze MN, Huxham IM, Mairs RJ, and Barrett A (1991) Intracellular localization of metaiodobenzyl guanidine in human neuroblastoma cells by electron spectroscopic imaging. *Int J Cancer* **47**:875–880.

Giacomini KM, and Huang S-M (2013) Transporters in Drug Development and Clinical Pharmacology. *Clin Pharmacol Ther* **94**:3–9.

GlaxoSmithKline. ZANTAC 150 (ranitidine hydrochloride) [package insert] (2004) U.S. Food and Drug Administration website. https://www.accessdata.fda.gov/drugsatfda_docs/label/2005/018703s065,019675s031,020251s016lbl.pdf. Revised October 2004. Accessed March 2023.

Goh L-B, Spears KJ, Yao D, Ayrton A, Morgan P, Roland Wolf C, and Friedberg T (2002) Endogenous drug transporters in in vitro and in vivo models for the prediction of drug disposition in man. *Biochem Pharmacol* **64**:1569–1578.

Govindarajan R, Leung GPH, Zhou M, Tse C-M, Wang J, and Unadkat JD (2009) Facilitated mitochondrial import of antiviral and anticancer nucleoside drugs by human equilibrative nucleoside transporter-3. *Am J Physiol Gastrointest Liver Physiol* **296**:G910-22.

Gu J, Wang L, Li T, Tang S, Wang Y, Zhang W, and Jiang X (2019) Role and mechanism of organic cation transporter 3 in oxaliplatin treatment of colon cancer in vitro and in vivo. *Oncol Rep* **42**:1355–1364.

Guo W, Dong W, Li M, and Shen Y (2019) Mitochondria P-glycoprotein confers paclitaxel resistance on ovarian cancer cells. *Onco Targets Ther* **12**:3881–3891.

Guo Y, Chu X, Parrott NJ, Brouwer KLR, Hsu V, Nagar S, Matsson P, Sharma P, Snoeys J, Sugiyama Y, Tatosian D, Unadkat JD, Huang S-M, Galetin A, and International Transporter Consortium (2018) Advancing Predictions of Tissue and Intracellular Drug Concentrations Using In Vitro, Imaging and Physiologically Based Pharmacokinetic Modeling Approaches. *Clin Pharmacol Ther* **104**:865–889.

Harper JN, and Wright SH (2013) Multiple mechanisms of ligand interaction with the human organic cation transporter, OCT2. *Am J Physiol Renal Physiol* **304**:F56-67.

Herman JR, and Bass P (1989a) Enteric neuronal ablation: structure-activity relationship in a series of alkyldimethylbenzylammonium chlorides. *Fundam Appl Toxicol* **13**:576–84.

Herman JR, and Bass P (1989b) Enteric neuronal ablation: structure-activity relationship in a series of alkyldimethylbenzylammonium chlorides. *Fundam Appl Toxicol* **13**:576–84.

Herron J, Reese RC, Tallman KA, Narayanaswamy R, Porter NA, and Xu L (2016) Identification of Environmental Quaternary Ammonium Compounds as Direct Inhibitors of Cholesterol Biosynthesis. *Toxicological Sciences* **151**:261–270.

Herron JM, Hines KM, Tomita H, Seguin RP, Cui JY, and Xu L (2019) Multiomics Investigation Reveals Benzalkonium Chloride Disinfectants Alter Sterol and Lipid Homeostasis in the Mouse Neonatal Brain. *Toxicol Sci* **171**:32–45.

Herron JM, Tomita H, White CC, Kavanagh TJ, and Xu L (2021) Benzalkonium Chloride Disinfectants Induce Apoptosis, Inhibit Proliferation, and Activate the Integrated Stress Response in a 3-D in Vitro Model of Neurodevelopment. *Chem Res Toxicol* **34**:1265–1274.

Hibma JE, Zur AA, Castro RA, Wittwer MB, Keizer RJ, Yee SW, Goswami S, Stocker SL, Zhang X, Huang Y, Brett CM, Savic RM, and Giacomini KM (2016) The Effect of Famotidine, a MATE1-Selective Inhibitor, on the Pharmacokinetics and Pharmacodynamics of Metformin. *Clin Pharmacokinet* **55**:711–721.

Hines KM, Herron J, and Xu L (2017) Assessment of altered lipid homeostasis by HILIC-ion mobility-mass spectrometry-based lipidomics. *J Lipid Res* **58**:809–819.

Hitosugi M, Maruyama K, and Takatsu A (1998) A case of fatal benzalkonium chloride poisoning. *Int J Legal Med* **111**:265–6.

Hrubec TC, Melin VE, Shea CS, Ferguson EE, Garofola C, Repine CM, Chapman TW, Patel HR, Razvi RM, Sugrue JE, Potineni H, Magnin-Bissel G, and Hunt PA (2017) Ambient and Dosed Exposure to Quaternary Ammonium Disinfectants Causes Neural Tube Defects in Rodents. *Birth Defects Res* **109**:1166–1178.

Hrubec TC, Seguin RP, Xu L, Cortopassi GA, Datta S, Hanlon AL, Lozano AJ, McDonald VA, Healy CA, Anderson TC, Musse NA, and Williams RT (2021) Altered toxicological endpoints in humans from common quaternary ammonium compound disinfectant exposure. *Toxicol Rep* **8**:646–656.

Hsu CL, Chang HY, Chang JY, Hsu WM, Huang HC, and Juan HF (2016) Unveiling MYCN regulatory networks in neuroblastoma via integrative analysis of heterogeneous genomics data. *Oncotarget* **7**:36293–36310.

Hu T, Zha W, Sun A, and Wang J (2022) Live Tissue Imaging Reveals Distinct Transcellular Pathways for Organic Cations and Anions at the Blood-Cerebrospinal Fluid Barrier. *Mol Pharmacol* **101**:334–342.

Huang KM, Zavorka Thomas M, Magdy T, Eisenmann ED, Uddin ME, DiGiacomo DF, Pan A, Keiser M, Otter M, Xia SH, Li Y, Jin Y, Fu Q, Gibson AA, Bonilla IM, Carnes CA, Corps KN, Coppola V, Smith SA, Addison D, Nies AT, Bundschuh R, Chen T, Lustberg MB, Wang J, Oswald S, Campbell MJ, Yan PS, Baker SD, Hu S, Burridge PW, and Sparreboom A (2021) Targeting OCT3 attenuates doxorubicin-induced cardiac injury. *Proc Natl Acad Sci U S A* **118**.

Huang M, and Weiss WA (2013) Neuroblastoma and MYCN. *Cold Spring Harb Perspect Med* **3**.

Hutzler JM, and Tracy TS (2002) Atypical kinetic profiles in drug metabolism reactions. *Drug Metab Dispos* **30**:355–62.

Iavarone A, Lasorella A, Servidei T, Riccardi R, and Mastrangelo R (1993) Uptake and Storage of m-Iodobenzylguanidine Are Frequent Neuronal Functions of Human Neuroblastoma Cell Lines. *Cancer Res* **53**:304–309.

Ilanchezhian M, Jha A, Pacak K, and Del Rivero J (2020) Emerging Treatments for Advanced/Metastatic Pheochromocytoma and Paraganglioma. *Curr Treat Options Oncol* **21**:85.

Inomistova M V., Svergun NM, Khranovska NM, Skachkova O V., Gorbach OI, and Klymnyuk GI (2015) Prognostic significance of MDM2 gene expression in childhood neuroblastoma. *Exp Oncol* **37**:111–115.

International Transporter Consortium, Giacomini KM, Huang S-M, Tweedie DJ, Benet LZ, Brouwer KLR, Chu X, Dahlin A, Evers R, Fischer V, Hillgren KM, Hoffmaster KA, Ishikawa T, Keppler D, Kim RB, Lee CA, Niemi M, Polli JW, Sugiyama Y, Swaan PW, Ware JA, Wright SH, Yee SW, Zamek-Gliszczynski MJ, and Zhang L (2010) Membrane transporters in drug development. *Nat Rev Drug Discov* **9**:215–36.

Irwin MS, and Park JR (2015) Neuroblastoma: Paradigm for precision medicine. *Pediatr Clin North Am* **62**:225–256.

Itagaki S, Ganapathy V, Ho HTB, Zhou M, Babu E, and Wang J (2012) Electrophysiological characterization of the polyspecific organic cation transporter plasma membrane monoamine transporter. *Drug Metabolism and Disposition* **40**:1138–1143.

Jono K, Takayama T, Kuno M, and Higashide E (1986) Effect of alkyl chain length of benzalkonium chloride on the bactericidal activity and binding to organic materials. *Chem Pharm Bull (Tokyo)* **34**:4215–24.

Kamath A, Srinivasamurthy SK, Chowta MN, Ullal SD, Daali Y, and Chakradhara Rao US (2022) Role of Drug Transporters in Elucidating Inter-Individual Variability in Pediatric Chemotherapy-Related Toxicities and Response. *Pharmaceuticals* **15**:990.

Kera H, Fuke C, Usumoto Y, Nasu A, Maeda K, Mukai M, Sato W, Tanabe M, Kuninaka H, and Ihama Y (2021) Kinetics and distribution of benzalkonium compounds with different alkyl chain length following intravenous administration in rats. *Leg Med (Tokyo)* **48**:101821.

Khanppnavar B, Maier J, Herborg F, Gradisch R, Lazzarin E, Luethi D, Yang J-W, Qi C, Holy M, Jäntsch K, Kudlacek O, Schicker K, Werge T, Gether U, Stockner T, Korkhov VM, and Sitte HH (2022) Structural basis of organic cation transporter-3 inhibition. *Nat Commun* **13**:6714.

Kikuchi R, Chiou WJ, Durbin KR, Savaryn JP, Ma J, Emami Riedmaier A, de Morais SM, Jenkins GJ, and Bow DAJ (2021) Quantitation of Plasma Membrane Drug Transporters in Kidney

Tissue and Cell Lines Using a Novel Proteomic Approach Enabled a Prospective Prediction of Metformin Disposition. *Drug Metab Dispos* **49**:938–946.
Kikuchi R, Chiou WJ, Kasai MA, de Morais SM, and Bow DAJ (2019) No Inhibition of MATE1/2K-Mediated Renal Creatinine Secretion Predicted With Ritonavir or Cobicistat. *J Pharm Sci* **108**:3118–3123.
Kikuchi R, Peterkin VC, Chiou WJ, de Morais SM, and Bow DAJ (2017) Validation of a total IC50 method which enables in vitro assessment of transporter inhibition under semi-physiological conditions. *Xenobiotica* **47**:825–832.
Kim M, Weigand MR, Oh S, Hatt JK, Krishnan R, Tezel U, Pavlostathis SG, and Konstantinidis KT (2018) Widely Used Benzalkonium Chloride Disinfectants Can Promote Antibiotic Resistance. *Appl Environ Microbiol* **84**.
Koepsell H (2020) Organic Cation Transporters in Health and Disease. *Pharmacol Rev* **72**:253–319.
Koepsell H (2004) Polyspecific organic cation transporters: Their functions and interactions with drugs.
Koepsell H (2021) Update on drug-drug interaction at organic cation transporters: mechanisms, clinical impact, and proposal for advanced in vitro testing. *Expert Opin Drug Metab Toxicol* **17**:635–653.
König J, Zolk O, Singer K, Hoffmann C, and Fromm M (2011) Double-transfected MDCK cells expressing human OCT1/MATE1 or OCT2/MATE1: determinants of uptake and transcellular translocation of organic cations. *Br J Pharmacol* **163**:546–555.
Krishnan S, Ramsden D, Ferguson D, Stahl SH, Wang J, McGinnity DF, and Hariparsad N (2022) Challenges and Opportunities for Improved Drug-Drug Interaction Predictions for Renal OCT2 and MATE1 / 2-K Transporters. *Clin Pharmacol Ther*, doi: 10.1002/cpt.2666.
Kümmerer K, Eitel A, Braun U, Hubner P, Daschner F, Mascart G, Milandri M, Reinthaler F, and Verhoef J (1997) Analysis of benzalkonium chloride in the effluent from European hospitals by solid-phase extraction and high-performance liquid chromatography with post-column ion-pairing and fluorescence detection. *J Chromatogr A* **774**:281–6.
Kusuhara H, Ito S, Kumagai Y, Jiang M, Shiroshita T, Moriyama Y, Inoue K, Yuasa H, and Sugiyama Y (2011) Effects of a MATE protein inhibitor, pyrimethamine, on the renal elimination of metformin at oral microdose and at therapeutic dose in healthy subjects. *Clin Pharmacol Ther* **89**:837–844.
Lai Y, Tse C-M, and Unadkat JD (2004) Mitochondrial expression of the human equilibrative nucleoside transporter 1 (hENT1) results in enhanced mitochondrial toxicity of antiviral drugs. *J Biol Chem* **279**:4490–7.
Lashford LS, Hancock JP, and Kemshead JT (1991) Meta-Iodobenzylguanidine (mIBG) uptake and storage in the human neuroblastoma cell line SK-N-BE(2C). *Int J Cancer* **47**:105–109.
Lashford LS, Moyes J, Ott R, Fielding S, Babich J, Mellors S, Gordon I, Evans K, and Kemshead JT (1988) The biodistribution and pharmacokinetics of meta-iodobenzylguanidine in childhood neuroblastoma. *Eur J Nucl Med* **13**:574–7.
Lee N, Duan H, Hebert MF, Liang CJ, Rice KM, and Wang J (2014) Taste of a pill: organic cation transporter-3 (OCT3) mediates metformin accumulation and secretion in salivary glands. *J Biol Chem* **289**:27055–27064.
Lee N, Hebert MF, Wagner DJ, Easterling TR, Liang CJ, Rice K, and Wang J (2018) Organic Cation Transporter 3 Facilitates Fetal Exposure to Metformin during Pregnancy. *Mol Pharmacol* **94**:1125–1131.

Leow JWH, and Chan ECY (2019) Atypical Michaelis-Menten kinetics in cytochrome P450 enzymes: A focus on substrate inhibition.

Li H, Smolen GA, Beers LF, Xia L, Gerald W, Wang J, Haber DA, and Lee SB (2008) Adenosine transporter ENT4 is a direct target of EWS/WT1 translocation product and is highly expressed in desmoplastic small round cell tumor. *PLoS One* **3**:e2353.

Li Q, Guo D, Dong Z, Zhang W, Zhang L, Huang S-M, Polli JE, and Shu Y (2013) Ondansetron can enhance cisplatin-induced nephrotoxicity via inhibition of multiple toxin and extrusion proteins (MATEs). *Toxicol Appl Pharmacol* **273**:100–9.

Li Q, and Shu Y (2014) Role of solute carriers in response to anticancer drugs. *Mol Cell Ther* **2**:15.

Li Q, Yang H, Guo D, Zhang T, Polli JE, Zhou H, and Shu Y (2016) Effect of Ondansetron on Metformin Pharmacokinetics and Response in Healthy Subjects. *Drug Metabolism and Disposition* **44**:489–494.

Li W, Sparidans RW, Wang Y, Lebre MC, Beijnen JH, and Schinkel AH (2018) P-glycoprotein and breast cancer resistance protein restrict brigatinib brain accumulation and toxicity, and, alongside CYP3A, limit its oral availability. *Pharmacol Res* **137**:47–55.

Li Z-M, Lakuleswaran M, and Kannan K (2023) LC-MS/MS methods for the determination of 30 quaternary ammonium compounds including benzalkonium and paraquat in human serum and urine. *J Chromatogr B Analyt Technol Biomed Life Sci* **1214**:123562.

Liang X, and Giacomini Kathleen M. (2017) Transporters Involved in Metformin Pharmacokinetics and Treatment Response. *J Pharm Sci* **106**:2245–2250.

Liang X, and Giacomini Kathleen M (2017) Transporters Involved in Metformin Pharmacokinetics and Treatment Response. *J Pharm Sci* **106**:2245–2250.

Lipinski CA, Lombardo F, Dominy BW, and Feeney PJ (2001) *Experimental and computational approaches to estimate solubility and permeability in drug discovery and development q settings*.

Loesberg C, Van Rooij H, Nooijen WJ, Meijer AJ, and Smets LA (1990) Impaired mitochondrial respiration and stimulated glycolysis by m-iodobenzylguanidine (MIBG). *Int J Cancer* **46**:276–81.

López Quiñones AJ, Vieira LS, and Wang J (2022) Clinical Applications and the Roles of Transporters in Disposition, Tumor Targeting, and Tissue Toxicity of meta-Iodobenzylguanidine (mIBG). *Drug Metab Dispos* **50**:1190–1192.

López Quiñones AJ, Wagner DJ, and Wang J (2020) Characterization of meta-iodobenzylguanidine (mIBG) transport by polyspecific organic cation transporters: Implication for mIBG therapy. *Mol Pharmacol* **98**:109–119.

Mairs RJ, Gaze MN, and Barrett A (1991) The uptake and retention of metaiodobenzyl guanidine by the neuroblastoma cell line NB1-G. *Br J Cancer* **64**:293–295.

Makhtar A (2017) Characterization of breast cancer responses to metformin. *Annals of Oncology* **28**:v101.

Martínez-Guerrero LJ, and Wright SH (2013) Substrate-dependent inhibition of human MATE1 by cationic ionic liquids. *J Pharmacol Exp Ther* **346**:495–503.

Masuda S, Terada T, Yonezawa A, Tanihara Y, Kishimoto K, Katsura T, Ogawa O, and Inui K (2006) Identification and Functional Characterization of a New Human Kidney–Specific H+/Organic Cation Antiporter, Kidney-Specific Multidrug and Toxin Extrusion 2. *Journal of the American Society of Nephrology* **17**:2127–2135.

Mathialagan S, Feng B, Rodrigues AD, and Varma MVS (2021) Drug-Drug Interactions Involving Renal OCT2/MATE Transporters: Clinical Risk Assessment May Require Endogenous Biomarker-Informed Approach. *Clin Pharmacol Ther* **110**:855–859.

Melin VE, Melin TE, Dessify BJ, Nguyen CT, Shea CS, and Hrubec TC (2016) Quaternary ammonium disinfectants cause subfertility in mice by targeting both male and female reproductive processes. *Reprod Toxicol* **59**:159–66.

Melin VE, Potineni H, Hunt P, Griswold J, Siems B, Werre SR, and Hrubec TC (2014) Exposure to common quaternary ammonium disinfectants decreases fertility in mice. *Reprod Toxicol* **50**:163–70.

Micali S, Bulotta S, Puppin C, Territo A, Navarra M, Bianchi G, Damante G, Filetti S, and Russo D (2014) Sodium iodide symporter (NIS) in extrathyroidal malignancies: Focus on breast and urological cancer. *BMC Cancer* **14**:1–12.

Modak S, Pandit-Taskar N, Kushner BH, Kramer K, Smith-Jones P, Larson S, and Cheung N-K V (2008) Transient sialoadenitis: a complication of 131I-metaiodobenzylguanidine therapy. *Pediatr Blood Cancer* **50**:1271–3.

Montaldo PG, Lanciotti M, Casalaro A, Cornaglia-Ferraris P, and Ponzoni M (1991) Accumulation of m-Iodobenzylguanidine by Neuroblastoma Cells Results from Independent Uptake and Storage Mechanisms. *Cancer Res* **51**:4342–4346.

Morrissey KM, Stocker SL, Chen EC, Castro RA, Brett CM, and Giacomini KM (2016) The Effect of Nizatidine, a MATE2K Selective Inhibitor, on the Pharmacokinetics and Pharmacodynamics of Metformin in Healthy Volunteers. *Clin Pharmacokinet* **55**:495–506.

Morrissey KM, Stocker SL, Wittwer MB, Xu L, and Giacomini KM (2013) Renal transporters in drug development. *Annu Rev Pharmacol Toxicol* **53**:503–29.

Motohashi H, and Inui K (2013) Organic cation transporter OCTs (SLC22) and MATEs (SLC47) in the human kidney. *AAPS J* **15**:581–8.

Motohashi H, Uwai Y, Hiramoto K, Okuda M, and Inui K-I (2004) Different transport properties between famotidine and cimetidine by human renal organic ion transporters (SLC22A). *Eur J Pharmacol* **503**:25–30.

Müller F, König J, Glaeser H, Schmidt I, Zolk O, Fromm MF, and Maas R (2011) Molecular Mechanism of Renal Tubular Secretion of the Antimalarial Drug Chloroquine. *Antimicrob Agents Chemother* **55**:3091–3098.

Müller F, Pontones CA, Renner B, Mieth M, Hoier E, Auge D, Maas R, Zolk O, and Fromm MF (2015) N1-methylnicotinamide as an endogenous probe for drug interactions by renal cation transporters: studies on the metformin–trimethoprim interaction. *Eur J Clin Pharmacol* **71**:85–94.

Nakajima K, Matsunari I, and Jacobson AF (2018) I-123 metaiodobenzylguanidine innervation imaging as a tool for norepinephrine transporter research: A possible application for genetic analysis in heart failure. *J Nucl Cardiol* **25**:907–910.

Nakamura T, Yonezawa A, Hashimoto S, Katsura T, and Inui K-I (2010) Disruption of multidrug and toxin extrusion MATE1 potentiates cisplatin-induced nephrotoxicity. *Biochem Pharmacol* **80**:1762–7.

Nałecz-Jawecki G, Grabińska-Sota E, and Narkiewicz P (2003a) The toxicity of cationic surfactants in four bioassays. *Ecotoxicol Environ Saf* **54**:87–91.

Nałecz-Jawecki G, Grabińska-Sota E, and Narkiewicz P (2003b) The toxicity of cationic surfactants in four bioassays. *Ecotoxicol Environ Saf* **54**:87–91.

Nancolas B, Guo L, Zhou R, Nath K, Nelson DS, Leeper DB, Blair IA, Glickson JD, and Halestrap AP (2016) The anti-tumour agent lonidamine is a potent inhibitor of the mitochondrial pyruvate carrier and plasma membrane monocarboxylate transporters. *Biochemical Journal* **473**:929–936.

Nies AT, Koepsell H, Damme K, and Schwab M (2011) Organic Cation Transporters (OCTs, MATEs), In Vitro and In Vivo Evidence for the Importance in Drug Therapy, in pp 105–167.

O'Brien SR, and Pryma DA (2022) Neuroendocrine Tumors: Therapy with 131I-MIBG, in *Nuclear Oncology* pp 1461–1480, Springer International Publishing, Cham.

Ogasawara K, Wood-Horrall RN, Thomas Mark, Thomas Michael, Liu L, Liu M, Xue Y, Surapaneni S, Carayannopoulos LN, Zhou S, Palmisano M, and Krishna G (2021) Impact of fedratinib on the pharmacokinetics of transporter probe substrates using a cocktail approach. *Cancer Chemother Pharmacol* **88**:941–952.

Oh JM, and Ahn BC (2021) Molecular mechanisms of radioactive iodine refractoriness in differentiated thyroid cancer: Impaired sodium iodide symporter (NIS) expression owing to altered signaling pathway activity and intracellular localization of NIS. *Theranostics* **11**:6251–6277.

Orentas RJ, Yang JJ, Wen X, Wei JS, Mackall CL, and Khan J (2012) Identification of Cell Surface Proteins as Potential Immunotherapy Targets in 12 Pediatric Cancers. *Front Oncol* **2**:1–16.

Otake K, Uchida K, Ide S, Kobayashi Y, Kobayashi I, and Kusunoki M (2016) Identification of DDX39A as a Potential Biomarker for Unfavorable Neuroblastoma Using a Proteomic Approach. *Pediatr Blood Cancer* **63**:221–227.

Otsuka M, Matsumoto T, Morimoto R, Arioka S, Omote H, and Moriyama Y (2005) A human transporter protein that mediates the final excretion step for toxic organic cations. *Proc Natl Acad Sci U S A* **102**:17923–8.

Otte J, Dyberg C, Pepich A, and Johnsen JI (2021) MYCN Function in Neuroblastoma Development. *Front Oncol* **10**:1–12.

Pabla N, and Dong Z (2008) Cisplatin nephrotoxicity: mechanisms and renoprotective strategies. *Kidney Int* **73**:994–1007.

Parisi MT, Eslamy H, Park JR, Shulkin BL, and Yanik GA (2016) 131I-Metaiodobenzylguanidine Theranostics in Neuroblastoma: Historical Perspectives; Practical Applications. *Semin Nucl Med* **46**:184–202.

Park JR, Bagatell R, London WB, Maris JM, Cohn SL, Mattay KM, and Hogarty M (2013) Children's Oncology Group's 2013 blueprint for research: Neuroblastoma. *Pediatr Blood Cancer* **60**:985–993.

Park JR, Eggert A, and Caron H (2010) Neuroblastoma: Biology, Prognosis, and Treatment. *Hematol Oncol Clin North Am* **24**:65–86.

Pena SA, Salas JG, Gautam N, Ramos AM, and Frantz AL (2023) Sublethal Exposure to Common Benzalkonium Chloride Leads to Antimicrobial Tolerance and Antibiotic Cross-Resistance in Commensal and Opportunistic Bacterial Species. *Appl Microbiol* **3**:580–591.

Pereira BMP, and Tagkopoulos I (2019) Benzalkonium chlorides: Uses, regulatory status, and microbial resistance.

Pharmaceuticals and Medical Devices Agency (PMDA) (2018) Pharmaceuticals and medical devices agency (Japan): drug interaction guideline for drug development and labelling recommendations.

Pharmaceuticals and Medical Devices Agency (PMDA). Pharmaceuticals and medical devices agency (Japan): drug interaction guideline for drug development and labelling recommendations (2018).

Prasad B, Johnson K, Billington S, Lee C, Chung GW, Brown CDA, Kelly EJ, Himmelfarb J, and Unadkat JD (2016) Abundance of Drug Transporters in the Human Kidney Cortex as Quantified by Quantitative Targeted Proteomics. *Drug Metab Dispos* **44**:1920–1924.

Rowland M, and Tozer TN (2010) *Clinical Pharmacokinetics and Pharmacodynamics: Concepts and Applications*, LWW, Baltimore.

Sala-Rabanal M, Li DC, Dake GR, Kurata HT, Inyushin M, Skatchkov SN, and Nichols CG (2013) Polyamine transport by the polyspecific organic cation transporters OCT1, OCT2, and OCT3. *Mol Pharm* **10**:1450–8.

Sarkar J, Chaudhary S, Namavari A, Ozturk O, Chang J-H, Yco L, Sonawane S, Khanolkar V, Hallak J, and Jain S (2012a) Corneal neurotoxicity due to topical benzalkonium chloride. *Invest Ophthalmol Vis Sci* **53**:1792–802.

Sarkar J, Chaudhary S, Namavari A, Ozturk O, Chang J-H, Yco L, Sonawane S, Khanolkar V, Hallak J, and Jain S (2012b) Corneal neurotoxicity due to topical benzalkonium chloride. *Invest Ophthalmol Vis Sci* **53**:1792–802.

Sato T, Masuda S, Yonezawa A, Tanihara Y, Katsura T, and Inui K (2008) Transcellular transport of organic cations in double-transfected MDCK cells expressing human organic cation transporters hOCT1/hMATE1 and hOCT2/hMATE1. *Biochem Pharmacol* **76**:894–903.

Seguin RP, Herron JM, Lopez VA, Dempsey JL, and Xu L (2019) Metabolism of Benzalkonium Chlorides by Human Hepatic Cytochromes P450. *Chem Res Toxicol* **32**:2466–2478.

Shu Y, Bello CL, Mangravite LM, Feng B, and Giacomini KM (2001) Functional characteristics and steroid hormone-mediated regulation of an organic cation transporter in Madin-Darby canine kidney cells. *J Pharmacol Exp Ther* **299**:392–8.

Shu Y, Sheardown SA, Brown C, Owen RP, Zhang S, Castro RA, Ianculescu AG, Yue L, Lo JC, Burchard EG, Brett CM, and Giacomini KM (2007) Effect of genetic variation in the organic cation transporter 1 (OCT1) on metformin action. *Journal of Clinical Investigation* **117**:1422–1431.

Smets LA, Janssen M, Metwally E, and Loesberg C (1990) Extragranular storage of the neuron blocking agent meta-iodobenzylguanidine (MIBG) in human neuroblastoma cells. *Biochem Pharmacol* **39**:1959–1964.

Smith V, and Foster J (2018) High-Risk Neuroblastoma Treatment Review. *Children* **5**:114.

Smith VE, Read ML, Turnell AS, Watkins RJ, Watkinson JC, Lewy GD, Fong JCW, James SR, Eggo MC, Boelaert K, Franklyn JA, and McCabe CJ (2009) A novel mechanism of sodium iodide symporter repression in differentiated thyroid cancer. *J Cell Sci* **122**:3393–3402.

Somogyi A, Stockley C, Keal J, Rolan P, and Bochner F (1987) Reduction of metformin renal tubular secretion by cimetidine in man. *Br J Clin Pharmacol* **23**:545–551.

Song IH, Zong J, Borland J, Jerva F, Wynne B, Zamek-Gliszczynski MJ, Humphreys JE, Bowers GD, and Choukour M (2016) The Effect of Dolutegravir on the Pharmacokinetics of Metformin in Healthy Subjects. *J Acquir Immune Defic Syndr* **72**:400–7.

Streby KA, Shah N, Ranalli MA, Kunkler A, and Cripe TP (2015) Nothing but NET: A review of norepinephrine transporter expression and efficacy of 131 I-mIBG therapy. *Pediatr Blood Cancer* **62**:5–11.

Suh JK, Koh KN, Min SY, Kim YS, Kim H, Im HJ, Namgoong JM, Kim DY, Ahn S Do, Lee JJ, and Seo JJ (2020) Feasibility and effectiveness of treatment strategy of tandem high-dose

chemotherapy and autologous stem cell transplantation in combination with 131I-MIBG therapy for high-risk neuroblastoma. *Pediatr Transplant* **24**:1–8.

Tahara H, Kusuhara H, Endou H, Koepsell H, Imaoka T, Fuse E, and Sugiyama Y (2005) A species difference in the transport activities of H2 receptor antagonists by rat and human renal organic anion and cation transporters. *J Pharmacol Exp Ther* **315**:337–45.

Takeda Pharmaceutical Company Ltd. ALUNBRIG (brigatinib) [package insert] (2020) U.S. Food and Drug Administration website. https://www.accessdata.fda.gov/drugsatfda_docs/label/2020/208772s008lbl.pdf. Revised May 2020. Accessed March 2023.

Tambuzzi S, Gentile G, Andreola S, Migliorini AS, and Zoja R (2022) Visceral Microscopic Pattern From Suicidal Ingestion of Professional Lysoform® With Delayed Death. *Acad Forensic Pathol* **12**:118–125.

Tanihara Y, Masuda S, Sato T, Katsura T, Ogawa O, and Inui K ichi (2007) Substrate specificity of MATE1 and MATE2-K, human multidrug and toxin extrusions/H+-organic cation antiporters. *Biochem Pharmacol* **74**:359–371.

Tanihara Y, Masuda S, Sato T, Katsura T, Ogawa O, and Inui K-I (2007) Substrate specificity of MATE1 and MATE2-K, human multidrug and toxin extrusions/H(+)-organic cation antiporters. *Biochem Pharmacol* **74**:359–71.

Tatsumi S, Matsuoka H, Hashimoto Y, Hatta K, Maeda K, and Kamoshida S (2014) Organic cation transporter 2 and tumor budding as independent prognostic factors in metastatic colorectal cancer patients treated with oxaliplatin-based chemotherapy. *Int J Clin Exp Pathol* **7**:204–12.

Temple W, Mendelsohn L, Kim GE, Nekritz E, Gustafson WC, Lin L, Giacomini K, Naranjo A, Van Ryn C, Yanik GA, Kreissman SG, Hogarty M, Matthay KK, and DuBois SG (2016) Vesicular monoamine transporter protein expression correlates with clinical features, tumor biology, and MIBG avidity in neuroblastoma: a report from the Children's Oncology Group. *Eur J Nucl Med Mol Imaging* **43**:474–481.

Tolbert VP, and Matthay KK (2018) Neuroblastoma: clinical and biological approach to risk stratification and treatment. *Cell Tissue Res* **372**:195–209.

Tracy TS (2003) Atypical Enzyme Kinetics: Their Effect on In Vitro-In Vivo Pharmaco-kinetic Predictions and Drug Interactions. *Curr Drug Metab* **4**.

Tsuda M, Terada T, Ueba M, Sato T, Masuda S, Katsura T, and Inui K (2009) Involvement of Human Multidrug and Toxin Extrusion 1 in the Drug Interaction between Cimetidine and Metformin in Renal Epithelial Cells. *Journal of Pharmacology and Experimental Therapeutics* **329**:185–191.

US FDA (2016) Safety and Effectiveness of Consumer Antiseptics; Topical Antimicrobial Drug Products for Over-the-Counter Human Use; Proposed Amendment of the Tentative Final Monograph; Reopening of Administrative Record. *Federal Register 21 CFR Part 310* **81**:42911–42937.

US FDA (2015) Safety and Effectiveness of Health Care Antiseptics; Topical Antimicrobial Drug Products for Over-the-Counter Human Use; Proposed Amendment of the Tentative Final Monograph; Reopening of Administrative Record. *Federal Register 21 CFR Part 310* **80**:25165–25205.

US Food and Drug Administration (FDA) (2020) In vitro drug interaction studies–cytochrome P450 enzyme-and transporter-mediated drug interaction guidance for industry.

Van Berkel A, Rao JU, Lenders JWM, Pellegata NS, Kusters B, Piscaer I, Hermus ARMM, Plantinga TS, Langenhuijsen JF, Vriens D, Janssen MJR, Gotthardt M, and Timmers HJLM

(2015) Semiquantitative 123I-metaiodobenzylguanidine scintigraphy to distinguish pheochromocytoma and paraganglioma from physiologic adrenal uptake and its correlation with genotype-dependent expression of catecholamine transporters. *Journal of Nuclear Medicine* **56**:839–846.

van Berkel M, and de Wolff FA (1988) Survival after acute benzalkonium chloride poisoning. *Hum Toxicol* **7**:191–3.

Vieira LS, and Wang J (2021) Brain Plasma Membrane Monoamine Transporter in Health and Disease, in *Organic Cation Transporters in the Central Nervous System* (Daws LC ed) p (in press), Handbook of Experimental Pharmacology.

Wagner DJ, Hu T, and Wang J (2016) Polyspecific organic cation transporters and their impact on drug intracellular levels and pharmacodynamics. *Pharmacol Res* **111**:237–246.

Wang J (2016) The plasma membrane monoamine transporter (PMAT): Structure, function, and role in organic cation disposition. *Clin Pharmacol Ther* **100**:489–499.

Wang X, and Li S (2014) Protein mislocalization: Mechanisms, functions and clinical applications in cancer. *Biochim Biophys Acta Rev Cancer* **1846**:13–25.

Wapnir IL, Van De Rijn M, Nowels K, Amenta PS, Walton K, Montgomery K, Greco RS, Dohán O, and Carrasco N (2003) Immunohistochemical profile of the sodium/iodide symporter in thyroid, breast, and other carcinomas using high density tissue microarrays and conventional sections. *Journal of Clinical Endocrinology and Metabolism* **88**:1880–1888.

Weiss J, Bajraktari-Sylejmani G, and Haefeli WE (2020) Interaction of Hydroxychloroquine with Pharmacokinetically Important Drug Transporters. *Pharmaceutics* **12**:919.

Wieland DM, Wu J, Brown LE, Mangner TJ, Swanson DP, and Beierwaltes WH (1980) Radiolabeled adrenergi neuron-blocking agents: adrenomedullary imaging with [131I]iodobenzylguanidine. *J Nucl Med* **21**:349–53.

Wilson JS, Gains JE, Moroz V, Wheatley K, and Gaze MN (2014a) A systematic review of 131I-meta iodobenzylguanidine molecular radiotherapy for neuroblastoma. *Eur J Cancer* **50**:801–815.

Wilson JS, Gains JE, Moroz V, Wheatley K, and Gaze MN (2014b) A systematic review of 131I-meta iodobenzylguanidine molecular radiotherapy for neuroblastoma. *Eur J Cancer* **50**:801–815.

Wright SH, Wunz TM, and Wunz TP (1992) A choline transporter in renal brush-border membrane vesicles: energetics and structural specificity. *J Membr Biol* **126**:51–65.

Xia L, Zhou M, Kalhorn TF, Ho HTB, and Wang J (2009) Podocyte-specific expression of organic cation transporter PMAT: Implication in puromycin aminonucleoside nephrotoxicity. *Am J Physiol Renal Physiol* **296**:1307–1313.

Xu M, Saxena N, Vrana M, Zhang H, Kumar V, Billington S, Khojasteh C, Heyward S, Unadkat JD, and Prasad B (2018) Targeted LC-MS/MS Proteomics-Based Strategy To Characterize in Vitro Models Used in Drug Metabolism and Transport Studies. *Anal Chem* **90**:11873–11882.

Xue Y, Hieda Y, Kimura K, Nishiyama T, and Adachi T (2002) Sensitive determination of benzalkonium chloride in blood and tissues using high-performance liquid chromatography with solid-phase extraction. *Leg Med (Tokyo)* **4**:232–8.

Xue Y, Hieda Y, Saito Y, Nomura T, Fujihara J, Takayama K, Kimura K, and Takeshita H (2004) Distribution and disposition of benzalkonium chloride following various routes of administration in rats. *Toxicol Lett* **148**:113–23.

Yao X, Watkins NH, Brown-Harding H, and Bierbach U (2020) A membrane transporter determines the spectrum of activity of a potent platinum-acridine hybrid anticancer agent. *Sci Rep* **10**:15201.

Yee SW, Vora B, Oskotsky T, Zou L, Jakobsen S, Enogieru OJ, Koleske ML, Kosti I, Rödin M, Sirota M, and Giacomini KM (2021) Drugs in COVID-19 Clinical Trials: Predicting Transporter-Mediated Drug-Drug Interactions Using In Vitro Assays and Real-World Data. *Clin Pharmacol Ther* **110**:108–122.

Yin J, Duan H, Shirasaka Y, Prasad B, and Wang J (2015) Atenolol renal secretion is mediated by human organic cation transporter 2 and multidrug and toxin extrusion proteins. *Drug Metabolism and Disposition* **43**:1872–1881.

Yin J, Duan H, and Wang J (2016) Impact of substrate-dependent inhibition on renal organic cation transporters hOCT2 and hMATE1/2-K-mediated drug transport and intracellular accumulation. *J Pharmacol Exp Ther* **359**:401–410.

Yin J, and Wang J (2016) Renal drug transporters and their significance in drug-drug interactions. *Acta Pharm Sin B* **6**:363–373.

Yokoo S, Masuda S, Yonezawa A, Terada T, Katsura T, and Inui K (2008) Significance of Organic Cation Transporter 3 (SLC22A3) Expression for the Cytotoxic Effect of Oxaliplatin in Colorectal Cancer. *Drug Metabolism and Disposition* **36**:2299–2306.

Yonezawa A, and Inui K-I (2011) Organic cation transporter OCT/SLC22A and H(+)/organic cation antiporter MATE/SLC47A are key molecules for nephrotoxicity of platinum agents. *Biochem Pharmacol* **81**:563–8.

Yonezawa A, Masuda S, Yokoo S, Katsura T, and Inui K-I (2006) Cisplatin and oxaliplatin, but not carboplatin and nedaplatin, are substrates for human organic cation transporters (SLC22A1-3 and multidrug and toxin extrusion family). *J Pharmacol Exp Ther* **319**:879–86.

Yu J, Wang Z, Kinzler KW, Vogelstein B, and Zhang L (2003) PUMA mediates the apoptotic response to p53 in colorectal cancer cells. *Proc Natl Acad Sci U S A* **100**:1931–6.

Zamek-Gliszczynski MJ, Giacomini KM, and Zhang L (2018) Emerging Clinical Importance of Hepatic Organic Cation Transporter 1 (OCT1) in Drug Pharmacokinetics, Dynamics, Pharmacogenetic Variability, and Drug Interactions. *Clin Pharmacol Ther* **103**:758–760.

Zhang D, Hop CECA, Patilea-Vrana G, Gampa G, Seneviratne HK, Unadkat JD, Kenny JR, Nagapudi K, Di L, Zhou L, Zak M, Wright MR, Bumpus NN, Zang R, Liu X, Lai Y, and Khojasteh SC (2019) Drug Concentration Asymmetry in Tissues and Plasma for Small Molecule–Related Therapeutic Modalities. *Drug Metabolism and Disposition* **47**:1122–1135.

Zhang J, and Liu Q (2015) Cholesterol metabolism and homeostasis in the brain. *Protein Cell* **6**:254–64.

Zhang L, Gorset W, Dresser MJ, and Giacomini KM (1999) The interaction of n-tetraalkylammonium compounds with a human organic cation transporter, hOCT1. *J Pharmacol Exp Ther* **288**:1192–8.

Zheng G, Webster TF, and Salamova A (2021) Quaternary Ammonium Compounds: Bioaccumulation Potentials in Humans and Levels in Blood before and during the Covid-19 Pandemic. *Environ Sci Technol* **55**:14689–14698.

Zhou M, Duan H, Engel K, Xia L, and Wang J (2010) Adenosine transport by plasma membrane monoamine transporter: Reinvestigation and comparison with organic cations. *Drug Metabolism and Disposition* **38**:1798–1805.

Zhou M, Xia L, and Wang J (2007) Metformin transport by a newly cloned proton-stimulated organic cation transporter (plasma membrane monoamine transporter) expressed in human intestine. *Drug Metabolism and Disposition* **35**:1956–1962.

Zolk O, Solbach TF, König J, and Fromm MF (2009) Structural determinants of inhibitor interaction with the human organic cation transporter OCT2 (SLC22A2). *Naunyn Schmiedebergs Arch Pharmacol* **379**:337–348.

VITA

Letícia Salvador Vieira was born in the city of Rio Claro (SP) in Brazil. She earned her Bachelor of Science in Pharmacy and Biochemistry from the School of Pharmaceutical Sciences of Ribeirão Preto, at the University of São Paulo.